DEPARTMENT OF PHYSICS, UNIVERSITY OF JYVÄSKYLÄ
RESEARCH REPORT No. 1/1985

EXTENDED PHONON PROJECTION MODEL FOR NUCLEAR COLLECTIVE MOTION

BY
JOUNI SUHONEN

Academic dissertation
for the Degree of
Doctor of Philosophy

To be presented, by permission of the
Faculty of Mathematics and Natural Sciences
of the University of Jyväskylä,
for public examination in Auditorium S-212 of the
University on May 18, 1985 at 12 o'clock noon.

Jyväskylä, Finland
May 1985

URN:ISBN:978-951-39-9467-9
ISBN 978-951-39-9467-9 (PDF)
ISSN 0075-465X

Jyväskylän yliopisto, 2022

ISBN 951-679-228-6
ISSN 0075-465-X

CONTENTS

ABSTRACT

The subject of this work is the formulation and application of a geometrical collective model with comparison to experiment and with other models dealing with low energy nuclear structure. This model, called the EPM(= Extended Phonon-Projection Model) avoids the use of an extensive diagonalization basis in the deformednucleus region by cleverly choosing a three dimensional model space with capability of producing the gross features encountered in moving from spherical vibrator nuclei to almost rigid rotors of deformed shapes.

The use of deformed oriented states calls for angular momentum projection to restore the broken angular momentum conservation in the oriented wavefunctions. After having achieved, in this way, a suitable set of basis states, one obtains the excitation energies by diagonalizing a phenomenological effective boson expansion Hamiltonian in this basis. The diagonalization reproduces the basic feature of the earlier projection model of Lipas et al. , namely the Sakai-Sheline scheme concerning the development of a harmonic vibrator spectrum to a band structure characterized rotor spectrum. The energy spectrum obtained in this way is, however, quite different from the earlier PM(=Projection Model of Lipas et al.).

The E2 transition probabilities have U(5)-characterized selection rules in the limit of small deformations and the Alaga behaviour for large oriented deformations. A distinct feature of the EPM is the violent behaviour of many branching ratios at certain deformations.

Application of the EPM is carried out in the Sm, Gd, Er, and Yb regions where also a comparison with the earlier PM and IBA-1 results is performed.The comparis shows that the 4- and 5-parameter EPM fits are comparable to or better than the 6-parameter IBA-1 fits and produce a systematic parameter behaviour. In contrast to other geometrical models, the low energy transitions are characterized by weak β -to -ground transitions and quite strong γ -to-ground transitions like the IBA. Also a comparison with the CSM(=Coherent State Model of Răduţă et al.) is performed showing a strong similarity between these models in both spectroscopic energies and B(E2) behaviour.

I.PRELIMINARIES

1.Introduction

The complications in treating the nuclear many-body problem have led to the various models and approximation schemes and their truncations. As a basic microscopic background one generally considers the mean-field theory of the shell model upon which one then builds the remaining correlations of the valence nucleons. For certain areas in the chart of nuclides the shell model approach is impossible in spite of the vast variety of possible truncation schemes available. All this is true also for the even-even isotopes which are the topic of this work. Because of the above-mentioned intractability of the shell model for many even-even nuclei, and inspired by the structure of their experimental spectra, a new kind of approach was developed. In this approach the experimentally suggested correlated motion of the nucleons inside the nucleus was phenomenologically described by the collective degrees of freedom of the nuclear system. This approach, based on the theory of classical mechanics, gave birth to a wide class of nuclear collective models. Nowadays, the name "geometrical models" has been attributed to them to distinguish them from the recently developed "algebraic collective models".

In all collective models the most important collective degrees of freedom are the quadrupole and octupole vibrations, rotations of statically deformed nuclear shapes and various density oscillations in the neutron and proton degrees of freedom called giant resonances. The most important geometric models to describe the quadrupole vibrations and (simultaneous) rotations are the vibrator model (or the liquid drop model for spherical equilibrium shapes) and the various rotor models (liquid drop models for deformed equilibrium shapes) like the rotation-vibration model for axially symmetric and the Davydov model for triaxial deformed nuclei. All these collective models restrict the shapes of the nuclei to special small ranges of the quadrupole surface coordinates and thus can not be applied to transitional nuclei and nuclei for which the coexistence of various shapes occur. This lack was cured by the Gneuss-Greiner model which also introduced the concept of collective potential energy surface to describe the development of nuclear shapes from vibrators to almost rigid rotors via the transitional region.

The Gneuss-Greiner model /Gn71/ was one of the first models to describe the interaction between the quasibands (ac-

cording to the Sakai scheme) called the ground, β and γ band. Also other collective models were developed for this purpose, like the extension of the variable moment-of-inertia model /Da70/ the hybridisation of the particle (or quasiparticle) degrees of freedom to the collective motion of the core of the nucleus /Ra83b/, the algebraic approach of the IBA /Ar81/ and the treatment of an effective Hamiltonian within a restricted collective space generated by elementary excitations of a projected coherent state /Li76; Ra83a; Ra84; Su83a; Su84a/.

Among the above models the most popular is nowadays the IBA model, mostly becauce it offers simple and compact expressions for energies in certain limiting situations. These situations are called dynamic symmetries and can be used as a tool in categorizing nuclei having different low energy spectra(in this respect it has the same properties as the Gneuss-Greiner model). An other way to avoid the computational efforts of using (in the deformed region) a large diagonalization basis is to choose a deformed basis and then perform a projection to restore the broken rotational invariance. This is the line of approach chosen in the projection model and in the CSM (=Coherent State Model of Rădu-ţă et al. /Ra83a/). These two models provide a simple way to describe three interacting (quasi)bands within a phonon picture.

In this work I speak about an EPM(=Extended (Phonon) Projection Model),which is an extension of the model of Lipas et al. /Li76/ . Like other geometrical approaches it also gives an intuitive grasp of the problem in terms of the concepts of classical mechanics, but it differs a bit from the famous Bohr- Mottelson approach /Bo75/. Of course, the effective Hamiltonian used in theories of this kind lacks a microscopic background (which is achieved, to some extent in the IBA through the formalism of IBA-2) although, in principle, one could calculate the coefficients of the boson Hamiltonian microscopically by using boson expansion theories, or phenomenologically by using collective potential energy surfaces.

In spite of the lack of a deeper insight into the microscopic foundations of nuclear structure, phenomenological models of this kind serve as a tool in producing ideas and a systematic description of isotopic chains that can be valuable material when striving for a deeper-reaching nuclear structure theories in the future.

I.2.General Theory of Projection

The development of the theory of projection started in the late fifties inspired by the Hartree-Fock calculations for deformed nuclei. It is known that the quantum variational principle for the HF wavefunctions,

$$(I.1.1) \qquad \langle \delta\Phi | \hat{H} - E | \Phi \rangle = 0 \quad ,$$

where the Φ's are single Slater determinants, leads to various symmetry violations both in the resulting HF Hamiltonian h and in the resulting wave functions /Ei76/. The same is true also for other nuclear theories of variational nature, like the HFB, the CHFB etc. /Ri80/. Symmetry violations also occur in theories of non-variational nature, for example in the CSM /Ri80/ and in the projection model. In these theories one imposes the symmetry violation by hand as a starting point of the theory for example in the form of symmetry violating trial functions. In variational theories the symmetry of the trial functions and the iteration process itself determine the degree of symmetry breaking.

The symmetries that are mostly violated are the translational invariance (conservation of linear momentum), rotational invariance (conservation of angular momentum) and rotational invariance in isospace (particle number concervation). Because the above symmetry-imposed conservation laws are a fact of nature, the need of symmetry restoration arises in theories, which try to carry a tidy microscopic appeal. A way to achieve this restoration is the quantum mechanical projection.

In variatinal theories an average conservation of quantities can be attained by using constrained variation. For example the requirement of average conservation of angular momentum in the HF theory can be guaranteed by the constrained variation ($\vec{\omega}$ is the Lagrange multiplier)

$$(I.1.2) \qquad \langle \delta\Phi | \hat{H} - E - \vec{\omega}\,\hat{\vec{J}} | \Phi \rangle = 0$$

requiring wave functions Φ_ω for which

$$(I.1.3) \qquad \langle \Phi_{\omega=J} | \hat{\vec{J}}^2 | \Phi_{\omega=J} \rangle = J(J+1) \quad ,$$

but which are not eigenfunctions of the total angular momentum $\vec{J}$.

The projection of trial wave functions from the original Hilbert space to a more restricted Hilbert space can be performed in variational theories as a projection after variation or before variation /Ei76/ and /Ri80/. The question of superiority of the two methods does not arise in non- variational models like projection model. The recipe for the construction of the projection operators which project out wavefunctions containing the symmetries implied by symmetry groups of the Hamiltonian of the system is very simple /Ei76/: if $|\Phi\rangle$ is a given non-invariant state under a certain symmetry operation, then an invariant state $|\Psi\rangle$ may be constructed from it according to

$$(I.1.4) \qquad |\Psi\rangle = \int d\Omega f(\Omega) U(\Omega) |\Phi\rangle \equiv P_U |\Phi\rangle \quad ,$$

where the weight function $f(\Omega)$ has to be chosen according to a variational principle, ie. by minimization of the expectation value $\langle\Psi|\hat{H}|\Psi\rangle$ of the energy. The operator $U(\Omega)$ is the unitary operator which performs the symmetry operation and Ω denotes the parameters of the symmetry operation.

The practical ways of determining the weight function are many, and in the projection model one uses the results of a classical paper published by Peierls and Yoccoz in 1957 /Pe57/. In this paper the spurious centre-of-mass oscillation, represented by the HF-type shell model wave functions was attacked by projection procedure yielding a formally correct expression for the total energy of the system and translationally invariant wave functions. In the variation adiabatic trial wave functions(wave functions independend of the angular speed ω of the system) were used. However, the lack of Galilean invariance yielded a quantitatively wrong expression for the kinetic energy, but this was corrected by Peierls and Thouless /Pe62/ who used non-adiabatic trial functions in the variation of $f(\Omega)$. The so called generator-coordinate method uses a still wider class of trial functions /Hn66/. In /Pe57/ the restoration of rotation invariance led to the expression

$$(I.1.5) \qquad |\,\alpha\ J\ M\ K\,\rangle = (2J+1)/8\pi^2 \cdot N_{JK} \int d\Omega D^{J\,*}_{MK}(\Omega) U(\Omega) |\,\alpha\ K\rangle ,$$

where Ω now refers to the Euler angles and the $D^{J}_{MK}(\Omega)$ are the Wigner D-functions or rigid rotor eigenfunctions. The state $|\alpha\ K\rangle$ is often referred to as the intrinsic state because of the lack of good angular momentum. The N are normalization constants and α includes all additional quantum numbers.

Because the projection methods do not quarantee the orthogonality of the projected states, an orthogonalization is usually performed, as in ref. /Li76/. Projection may also

lead to overcompleteness. From eq.(I.1.5) one sees that the projection operator P^{J}_{MK} (Which is a true projector only when M=K) can be written as

$$P^{J}_{MK} = (2J+1)/8\pi^2 \cdot \int d\Omega D^{J*}_{MK}(\Omega) U(\Omega) \quad . \tag{I.1.6}$$

In Dirac´s notation it reads /Co71/, /Ho72/

$$P^{J}_{MK} = \sum_{\alpha} |\alpha\ J\ M\rangle\langle\ \alpha\ J\ K| \quad . \tag{I.1.7}$$

II. Basic Concepts of the Projection Model

II.1 The Oriented System

The term oriented system is used here instead of the term intrinsic system to distinguish the BMM freely rotating true intrinsic system (see appendix B) from the system used in the PM. Below it is shown that the model Hamiltonian of the PM corresponds to a system which behaves like BMM intrinsic system that is forced to small vibrations around the laboratory axes with the intrinsic z axis coinciding on the average with the lab. z axis.

The model Hamiltonian H of the PM reads /Ha70/

$$(II.1.1) \qquad H_0 = \tfrac{1}{2} B_0 \sum_m |\dot{\alpha}_m|^2 + \tfrac{1}{2} C_0 \sum_{m\neq 0} |\alpha_m|^2 + \tfrac{1}{2} C_0 (\alpha_0 - \beta_0)^2$$

It may be noted that H_0 in eq. (II.1.1) is an isotropic one (the same mass and stiffness parameter for every magnetic quantum number m) and that it is not a SO(3) scalar (note that it is expressed in laboratory coordinates α_m). So the non-scalarity makes H_0 only a means of generating a suitable set of basis functions. The anisotropic model has been dicussed in /Ho72/. The procedure followed in appendix B leads to the following second quantized form $\hat{H}_0$ of H_0 :

$$(II.1.2) \qquad \hat{H}_0 = \hbar\omega \left[\sum_m (b_m^\dagger b_m + \tfrac{1}{2}) - d(b_0^\dagger + b_0) + d^2 \right] ,$$

where

$$(II.1.2') \qquad d = \beta_0 \sqrt{C_0/2\hbar\omega} ,$$

and $b^\dagger$, b create and destroy usual 5-dimension HO quanta.

To diagonalize the Hamiltonian (II.1.2) a canonical transformation

$$(II.1.3) \qquad \beta_m^\dagger = b_m^\dagger - \delta_{m0} d$$

is needed. Expressed in terms of these 'deformed phonons' H now reads

$$\hat{H}_0 = \hbar\omega \sum_m (\beta_m^\dagger \beta_m + \tfrac{1}{2}) \qquad \text{(II.1.5)}$$

and the condition

$$\beta_m |\tilde{0}\rangle = 0 \qquad \text{(II.1.6)}$$

gives as the 'deformed ground state' $|\tilde{0}\rangle$ a socalled coherent phonon state (unnormalized)

$$|\tilde{0}\rangle = \exp(d b_0^\dagger)|0\rangle \qquad \text{(II.1.7)}$$

The state (II.1.7) is the ground state of the oriented system, and in analogy with the BM intrinsic β and γ state (see appendix B), the oriented β state is $\beta_0^\dagger|0\rangle$ (K=0) and the oriented γ state is $\beta_2^\dagger|0\rangle$ (K=2). It may be noted that because $\hat{H}_0$ is not an SO(3) scalar but only an SO(2) scalar (axial symmetry), the oriented ground, β and γ states are eigenstates of $\hat{L}_3'$ but not $\hat{\vec{L}}^2$ (see appendix B). Furthermore, the oriented states do not have good spherical phonon number as is seen from eg.(II.1.7).

Let us see the meaning of the system represented by H_0 in terms of the BM intrinsic system described in appendix B. The kinetic energy part is the same as in the BM model, (B9), and the potential term can be cast in the form

$$V_0 = \tfrac{1}{2} C_0 \sum_{m\neq 0} |\alpha_m|^2 + \tfrac{1}{2} C_0 (\alpha_0 - \beta_0)^2 =$$

$$= \tfrac{1}{2} C_0 \sum_m |\alpha_m|^2 - C_0 \beta_0 \alpha_0 + \tfrac{1}{2} C_0 \beta_0^2$$

Transforming to the body-fixed system (appendix A2) one gets

$$V_0 \longrightarrow \tfrac{1}{2} C_0 (a_0^2 + 2a_2^2) + \tfrac{1}{2} C_0 \beta_0^2 -$$

$$- C_0 \beta_0 \left[a_0 D_{00}^{2*}(\Omega) + a_2 \left(D_{02}^{2*}(\Omega) + D_{0-2}^{2*}(\Omega) \right) \right]$$

Using the relations (A1.9),(A1.10), (A1.8) and the explicit expressions for spherical harmonics, one get after some manipulations

$$V_0 \longrightarrow V(\beta,\gamma,a_0,a_2,\beta_0) = \tfrac{1}{2}C_0(a_0-\beta_0)^2 + C_0(\beta_0 a_0 + a_2^2)$$

$$-\tfrac{1}{2}C_0\beta_0\left[(3\cos^2\beta-1)a_0 + \sqrt{6}\sin^2\beta\cos 2\gamma\cdot a_2\right] \quad ,$$

where (α,β,γ) are the Euler angles. Because the α_m are parametres of small oscillations, then β and γ are small. Exploiting this one gets

(II.1.9)
$$V_0 \longrightarrow V(\theta,\beta_0,a_0,a_2) \cong \tfrac{1}{2}C_0(a_0-\beta_0)^2 + C_0(\beta_0 a_0 + a_2^2)$$
$$-C_0\beta_0\left(a_0+\sqrt{\tfrac{3}{2}}\theta^2 a_2\right) = \tfrac{1}{2}C_0(a_0-\beta_0)^2 + C_0 a_2^2 - \sqrt{\tfrac{3}{2}}\theta^2 a_2$$

where θ is the polar angle measured from the **z** axis. So one may picture the Hamiltonian $\hat{H}_0$ of the oriented system as

(II.1.10) $$H_0 = H_{BM} + V(\theta) = H_{int}(a_0,a_2) + T_{rot} + V(\theta) \quad ,$$

where

(II.1.11) $$H_{int}(a_0,a_2) = \tfrac{1}{2}B_0(\dot{a}_0^2 + 2\dot{a}_2^2) + \tfrac{1}{2}C_0(a_0-\beta_0)^2 + C_0 a_2^2$$

(II.1.12) $$T_{rot} = \sum_{k=1}^{3} \frac{L'_k}{2\mathcal{I}_k(a_0,a_2)}$$

(II.1.13) $$V(\theta) = -\sqrt{3/2}\,\theta^2 a_2$$

The intrinsic Hamiltonian (II.1.11) is the Bohr-Mottelson Hamiltonian of (B.8) with $C_2=C_0$, and contains two degrees of freedom. The part $T_{rot}+V(\theta)$ includes the rest of the degrees of freedom, namely the three Euler angles. It may be

noted that in $V(\theta)$ the restoring force is harmonic.

The usefulness of the oriented system lies in the fact that the same boson operators are used in the oriented wave functions as in the laboratory Hamiltonian and the transition operators; also the solution of the eigenvalue problem for $\hat{H}$ is easy.

II.2. The Laboratory Hamiltonian

The Hamiltonian $\hat{H}_0$ of the oriented system is used only as a means of generating a suitable set of basis states for the calculations. The energy spectrum of a nucleus is a result of the diagonalization of a rotationally invariant laboratory Hamiltonian $\hat{H}$. In the framework adopted in the PM there is no way of deriving the laboratory Hamiltonian from first principles of a microscopic theory of the nucleus. So the PM is a phenomenological classical collective model where through a suitable parametrization of the theory one gets a set of constants to be determined experimentally.

The starting point of the determination of H are the restrictions imposed on it by the rotational and time reversal invariance and hermiticity. The purpose in this Extended Projection Model (=EPM) is to write down the most general boson (expansion) Hamiltonian satisfying the above requirements (here the word 'expansion' is used without trying to make a connection to the underlying fermion system /Ri80/). This expansion is not a phonon- number conserving one as for example in the IBA, where connection to the underlying fermion number is made through a number-conserving phenomenological Hamiltonian /Ia81/. In this respect the EPM resembles

the model of Gneuss and Greiner /Gn71/ , where this kind of Hamiltonian is used to give insight into nuclear collective potential energy surfaces. There is, however, also a big difference: in the Hamiltonian used by Gneuss and Greiner there was kinetic energy terms only to the lowest order, while they had potential energy terms up to the sixth order. In the EPM the expansion is made in the second-quantized boson operators $b_m^\dagger$ and b_m instead of the collective quadrupole coordinates α_m used by Gneuss and Greiner. This means that the expansion is symmetric in kinetic and potential energy in contrast to the great asymmetry in the Hamiltonian used by G&G (see the discussion in connection with the section III.4).

The most obvious lowest-order Hermitian scalar quantity which can be formed out of the $b^\dagger$'s and b's is the number operator $\hat{N}$ ($b^\dagger$ and $\bar{b}$ both are tensor operators)

$$\hat{N} = b^\dagger \cdot \bar{b} \quad , \quad \bar{b}_m = (-1)^m b_{-m} \tag{II.2.1}$$

This was the only term used in the earlier version of the PM /Li76/, where the deviations from the pure quadrupole phonon limit (the U(5) limit in algebraic language) stemmed merely from the finiteness of the model space. There is also another term of the second order and it is easy to form. Using the above notation it reads (note hermiticity)

$$B_{20} \equiv b^\dagger \cdot b^\dagger + \bar{b} \cdot \bar{b} \quad , \tag{II.2.2}$$

and is seen to be number non-conserving.

There are two kinds of third-order terms, namely B_{21} and B_{30} .The term B_{30} is easy to form because the coupling order in the terms is clearly immaterial. So it is

$$B_{30} = \left[b^\dagger b^\dagger\right]_2 \cdot b^\dagger + \left[\bar{b}\bar{b}\right]_2 \cdot \bar{b} \tag{II.2.3}$$

the term B_{21} is a bit trickier one. In principle it contains 6 different terms, but exploiting the relations

$$\left[b^\dagger b^\dagger\right]_2 \cdot \bar{b} = b^\dagger \cdot \left[b^\dagger \bar{b}\right]_2 \quad ; \quad \left(\left[b^\dagger b^\dagger\right]_2 \cdot \bar{b}\right)^\dagger = b^\dagger \cdot \left[\bar{b}\bar{b}\right]_2 = \left[b^\dagger \bar{b}\right]_2 \cdot \bar{b}$$

$$b^\dagger \cdot \left[\bar{b}\bar{b}\right]_2 = \bar{b} \cdot \left[b^\dagger \bar{b}\right]_2 = \left[\bar{b} b^\dagger\right] \cdot \bar{b} = \left[\bar{b}\bar{b}\right]_2 \cdot b^\dagger = \bar{b} \cdot \left[\bar{b} b^\dagger\right]_2$$

one notices that the coupling order and the mutual order of $b^\dagger$ and $\bar{b}$ are immaterial. So one gets the compact expression

$$B_{21} = \left[b^\dagger b^\dagger\right]_2 \cdot \bar{b} + b^\dagger \cdot \left[\bar{b}\bar{b}\right]_2 \qquad \text{(II.2.4)}$$

Note that the number of terms in B_{21} is immaterial (should be three because there are three ways of coupling the b's) because it is multiplied by a phenomenological constant.

The fourth-order terms need a bit labour, but compact expressions can be achieved on the basis of arguments on uniqueness of the phonon states created on by $b^\dagger$'s. The term B_{40} is again easy:

$$B_{40} = b^\dagger \cdot b^\dagger b^\dagger \cdot b^\dagger + \bar{b} \cdot \bar{b}\bar{b} \cdot \bar{b} \qquad \text{(II.2.5)}$$

This is so because there is only one state $|N=4, J=0\rangle$ (here N is the number of phonons). Because the state $\left[b^\dagger b^\dagger b^\dagger\right]_2|0\rangle$ is unique, the term B_{31} can be written in the form

$$B_{31} = b^\dagger \cdot b^\dagger b^\dagger \cdot \bar{b} + b^\dagger \cdot \bar{b}\bar{b} \cdot \bar{b} \qquad \text{(II.2.6)}$$

The combination of two $b^\dagger$'s and two $\bar{b}$'s gives three linearly independent L=0 objects. These can be written in the form

$$B_{22}^{(L)} = \left[b^\dagger b^\dagger\right]_L \cdot \left[\bar{b}\bar{b}\right]_L \quad , L=0,2,4 \qquad \text{(II.2.7)}$$

Actually, the recoupling of terms of the form $(b^\dagger \cdot \bar{b})(b^\dagger \bar{b})$ gives lower-order terms in addition to the normal-ordered terms in (II.2.7).

It is convenient to note the relation /Ho72/

$$\vec{J}^2 = 6\hat{N} - \sum_L \left[6 - \tfrac{1}{2}L(L+1)\right] B_{22}^{(L)} \quad , \qquad \text{(II.2.8)}$$

which tells that

$$4B_{22}^{(4)} = \vec{J}^2 - 6\hat{N} + 6B_{22}^{(0)} + 3B_{22}^{(2)} \quad . \tag{II.2.9}$$

So, instead of using the term $B_{22}^{(4)}$ in our boson Hamiltonian, one can replace it by the square of the angular momentum, which has much simpler matrix elements between states of good angular momentum. Now we are in a position to write down the boson Hamiltonian up to fourth order:

$$\hat{H} = c_1\hat{N} + c_2B_{20} + c_3B_{21} + c_4B_{30} + c_5B_{40} + \tag{II.2.10}$$

$$c_6B_{31} + c_7B_{22}^{(0)} + c_8B_{22}^{(2)} + c_9\vec{J}^2$$

The number of terms in the Hamiltonian (II.2.10) can be reduced on various grounds. This will be discussed in the next chapter. It may be noted that if only the ground state band would be included in the description, already the Hamiltonian

$$\hat{H}_{eff} = \alpha\hat{N} + \beta\vec{J}^2 \tag{II.2.11}$$

gives all that the Hamiltonian (II.2.10) would give /Ho72/. It is also clear that in our present model the efficiency in reducing anharmonic terms of the Hamiltonian (II.2.10) to a few effective ones is less than in the former projection model because here the diagonalization mixes also β and γ states to the ground state band, whereas in the earlier model the ground state band was chosen to be pure through Schmidt orthogonalization.

The earlier PM already gave good results also for very deformed nuclei although only the harmonic Hamiltonian N was used. This is due to the deformed projected basis states which make the convergence of the boson expansion (II.2.10) faster in the deformed-nucleus region /Ho70/.

II.3.Diagonalization of the Laboratory Hamiltonian

In section II.1 the oriented states $|\tilde{0}\rangle$, $\beta_0^\dagger|\tilde{0}\rangle$ and $\beta_2^\dagger|\tilde{0}\rangle$ were given. However, candidates for the physical states must be eigenstates of the angular momentum In order to achieve this, the theory of projection (section I.2) may be exploited. A simple prescription for the projection is given by the Peierls-Yoccoz projection method. (A nice discussion of the angular momentum content of an oriented state in the light of the uncertainty principle is given in reference /Li72/). Also a Peierls-Thouless method for axially symmetric nuclei could be used, but it is much more complicated and unnecessary for the adiabatic limit. The formula (I.1.5) of section I.2 gives as a result

$$
\begin{aligned}
|g_o\ J\rangle &= N_{go}(J)P^J_{M0}|\tilde{0}\rangle \\
|\beta_o\ J\rangle &= N_{\beta o}(J)P^J_{M0}(b_o^\dagger - d)|\tilde{0}\rangle \\
|\gamma_o\ J\rangle &= N_{\gamma o}(J)P^J_{M2}b_2^\dagger|\tilde{0}\rangle \quad ,
\end{aligned}
\tag{II.3.1}
$$

which correspond to ground state, β and γ bands.

It may be noted that from one oriented state one generates a whole band of states with angular momenta going from a well defined minimum up to infinity. This is analogous to the BMM where each intrinsic state gives a definite band with infinitely many states. The notation is that of section II.2 with N_{g_o} ,N_{β_o} and N_{γ_o} normalization constants given in appendix D2. The non-orthogonality of the basis states $\{|g_o\ J\rangle\ ,\ |\beta_o\ J\rangle\ ,\ |\gamma_o\ J\rangle\}$ implies two ways along which to continue. The first way is to orthogonalize the basis by a Gram-Schmidt procedure and then to diagonalize the laboratory Hamiltonian $\hat{H}$ in this orthogonal basis. This leads to the ordinary eigenvalue problem. In the earlier form of the PM the diagonalization part was left out and the orthogonalization was performed in such a way that it yielded the correct way of evolution of the few low energy levels from pure phonon states (spherical nuclei) to rotor states (deformed nuclei). The correct way of evolution was considered to be the Sakai scheme for quasibands /Li76/.

The second way of dealing with the projected states is to diagonalize $\hat{H}$ directly in this basis yielding a generatized eigenvalue problem (diagonalization in a non-orthogonal basis). The second way was chosen in the EPM because it is more straight forward when standard library routines for computer diagonalization of this kind are available (see section III.1). In appendix C are derived a few important formulas concerning the calculation in Hilbert spaces with non-orthogonal basis states. The basis for the diagonalization is the formula (C.6) where the O_{ij} and the f_{ij} will

form 2×2 matrices for J=0 states (there exists no $|\gamma_o\ 0\rangle$ state) and 3×3 matrices for other J states. Here O_{ij} is now the energy matrix for the laboratory Hamiltonian $\tilde{H}$ to be diagonalized. Writing this down explicitly one gets for J≥2

$$\begin{vmatrix} H^J_{gg}-\alpha & H^J_{g\beta}-\alpha R^J_{g\beta} & H^J_{g\gamma}-\alpha R^J_{g\gamma} \\ H^J_{\beta g}-\alpha R^J_{\beta g} & H^J_{\beta\beta}-\alpha & H^J_{\beta\gamma}-\alpha R^J_{\beta\gamma} \\ H^J_{\gamma g}-\alpha R^J_{\gamma g} & H^J_{\gamma\beta}-\alpha R^J_{\gamma\beta} & H^J_{\gamma\gamma}-\alpha \end{vmatrix} = 0 \qquad \text{(II.3.2)}$$

where

$$H^J_{ij} = \langle i_o\ J|\ \hat{H}\ |\ j_o\ J\rangle$$

$$R^J_{ij} = \langle i_o\ J|\ j_o\ J\rangle \qquad \text{(II.3.3)}$$

, i,j=g,β,γ

As a result of the diagonalization one gets energy eigenvalues and eigenvectors which are to be normalized according to formula (C.10). To be able to carry all this out, one needs to calculate the overlaps R^J_{ij} and the energy matrix elements H^J_{ij}. This requires some special tricks which are discussed for the number operator $\hat{N}$ in reference /Ha70/. The explicit form of P^J_{MK} is not needed in these calculations and the matrix elements of (II 3.2) can be obtained by using general properties of projection operators (see appendix A2). This is a common feature among theories where projection is used.

As a result of the calculation of the R^J_{ij} and the H^J_{ij} one gets ten different complicated integrals which must be calculated numerically (see section III.2). These integrals are tabulated in appendix D1. They are the building blocks of the different energy matrix elements which are tabulated in appendix D2. The appendix D2 do not contain derectly the matrix elements of the different terms in Hamiltonian of eq. (II.2.10) but most of the terms are effective ones and marked with primes. The reason for these 'effective' terms is that in subtracting from the original terms lower-order pieces of the Hamiltonian, one arrives at easier matrix elements, many of them even vanishing. This is completely legal because it has only a renormalizing effect on the phenomenological coefficients C_i. Also the matrix elements of the terms B_{40} and B_{31} are not tabulated because their asymptotic behaviour suggested that they could be left out of the energy fits(i.e. asymptotically their matrix elements become the matrix elements of $\hat{N}$ and B_{20}, see the relations (II.5.11)).

The computationally convenient effective operators are defined as the following linear combinations:

$$B'_{30} \equiv -\sqrt{\tfrac{7}{2}}\,\tfrac{1}{d}B_{30} - B_{20} \quad ; \quad B_{30} = -\sqrt{\tfrac{2}{7}}\,d(B'_{30} + B_{20})$$

$$B'_{21} \equiv -\sqrt{\tfrac{7}{8}}\,\tfrac{1}{d}B_{21} - \hat{N} \quad ; \quad B_{21} = -d\sqrt{\tfrac{8}{7}}(B'_{21} + \hat{N})$$

$$B^{(0)'}_{22} \equiv \tfrac{10}{d^2}B^{(0)}_{22} + \tfrac{\sqrt{14}}{d}B_{30} + B_{20} \; ; \; B^{(0)}_{22} = \tfrac{d^2}{10}\left[B^{(0)'}_{22} + 2B'_{30} + B_{20}\right]$$

(II.3.4)

$$B^{(2)'}_{22} \equiv \tfrac{7}{2d^2}B^{(2)}_{22} + \sqrt{\tfrac{7}{2}}\,\tfrac{1}{d}B_{21} + \hat{N} \; ; \; B^{(2)}_{22} = \tfrac{2d^2}{7}\left[B^{(2)'}_{22} + 2B'_{21} + \hat{N}\right]$$

where d is the deformation/stiffnes parameter of equation (II.1.2´). Thus our effective Hamiltonian gets the form

(II.3.5)
$$\hat{H}_{eff} = c'_1\hat{N} + c'_2B_{20} + c'_3B'_{21} + c'_4B'_{30} + c'_5B^{(0)'}_{22} + c'_6B^{(2)'}_{22} + c'_7\hat{J}^2 \quad ,$$

where

(II.3.6)
$$\begin{aligned} c'_1 &= c_1 - d\sqrt{8/7}\cdot c_3 + 2d^2/7\cdot c_8 \\ c'_2 &= c_2 - d\sqrt{2/7}\cdot c_4 + d^2/10\cdot c_7 \\ c'_3 &= -\sqrt{8/7}\cdot dc_4 + 4d^2/7\cdot c_8 \\ c'_4 &= -\sqrt{2/7}\cdot dc_4 + d^2/5\cdot c_7 \\ c'_5 &= d^2/10\cdot c_7 \\ c'_6 &= 2d^2/7\cdot c_8 \end{aligned}$$

and the terms B_{40} and B_{31} have been left out. The form (II.3.5) can be arrived at by inspection of the asymptotic behaviour of the matrix elements of the different anharmonic terms of the Hamiltonian (see section II.5).

II.4.The Harmonic Limit of EPM

Analytical expressions for the integrals $I_j(J)$, $j=1,\ldots,10$, the overlaps R^J_{ij} and the energy matrix elements H^J_{ij} can be derived in the limit of small and large deformation parameters. The small-d and large-d limits of the $I_j(J)$ are tabulated in appendix E, and it is easy to specialize these formulas for definite J and then use them to calculate special R^J_{ij} and H^J_{ij} analytically. Of course there remains the task of diagonalizing 2×2 or 3×3 matrices by hand ,which is not a very nice job to do. But doing all this one gets hold of the analytical form of eigenvalues and eigenvectors in the two limiting cases of the anharmonic vibrator nucleus (small d) and the rotor nucleus (large d). This is useful in checking the computer program for its correctness and accuracy and also gives some indications of the magnitude of the effects caused by that part of the Hilbert space which was left out of the model space. In this chapter we stick to $\hat{H}=\hat{N}$.

As was mentioned above, the model space in the PM and the EPM is very restricted and causes the spectrum of the number operator to deviate from the pure phonon spectrum at non-zero deformations (d>0). At zero deformation , d=0, the oriented Hamiltonian $\hat{H}$ of eq.(II.1.1) becomes SO(3) invariant and coincides with the laboratory Hamiltonian. This, in turn, should indicate that the harmonic phonon spectrum is recovered for the number operator as laboratory Hamiltonian. But this is not so obvious, because actual calculation for d>0 uses only three oriented states (see chapter II.1) and this would suggest the existence of only the phonon vacuum and the one-phonon state. So one must be careful in extrapolating to zero deformations.

The fact that at small, non-zero d one gets part of the U(5) phonon spectrum (one gets 3 states of each angular momentum and these correspond to the three possible phonon states with that angular momentum in the U(5) spectrum, see fig. 26 on page 100). This is understandable when one makes an expansion of the projected states making use of eqs.(II.1.7) and (II.3.1). So

$$|g_0\, J\, M\rangle = N_{g_0} P^J_{M0} e^{d b_0^\dagger}|0\rangle = N_{g_0} P^J_{M0}(1+ d b_0^\dagger + \\ + \tfrac{1}{2} d^2 b_0^{\dagger 2} + 1/6\cdot d^3 b_0^{\dagger 3} + \ldots)|0\rangle$$

It is easy to derive the relations (A2.14) which may be used now to yield

$$|g_0\ J\ M\rangle = N_{g_0}\Big\{\delta_{J0}|0\rangle + d\,\delta_{J2}b^\dagger_M|0\rangle + \tfrac{1}{2}d^2\sqrt{2J+1}\times$$

(II.4.1) $$\times\begin{pmatrix}2&2&J\\0&0&0\end{pmatrix}[b^\dagger b^\dagger]_{JM}|0\rangle + \tfrac{1}{6}d^3\sqrt{2J+1}\begin{pmatrix}2&2&L\\0&0&0\end{pmatrix}\begin{pmatrix}2&L&J\\0&0&0\end{pmatrix}\times$$

$$\times\left[b^\dagger[b^\dagger b^\dagger]_L\right]_{JM}|0\rangle + \ldots\Big\}$$

Now one clearly sees that at finite d the projected states are a superposition of ordinary U(5) phonon states with different phonon numbers. In the same way one gets

$$|\gamma_0\ J\ M\rangle = N_{\gamma_0}\Big\{\delta_{J2}b^\dagger_M|0\rangle + d\sqrt{2J+1}\begin{pmatrix}2&2&J\\2&0&-2\end{pmatrix}\times$$

(II.4.2) $$\times[b^\dagger b^\dagger]_{JM}|0\rangle + \tfrac{1}{2}d^2\sqrt{2J+1}\sum_{L=0,2,4}\sqrt{2L+1}\begin{pmatrix}2&2&L\\0&0&0\end{pmatrix}\times$$

$$\times\begin{pmatrix}2&L&J\\2&0&-2\end{pmatrix}\left[b^\dagger[b^\dagger b^\dagger]_L\right]_{JM}|0\rangle + \ldots\Big\}$$

$$|\beta_0\ J\ M\rangle = N_{\beta_0}\Big\{-d\,\delta_{J0}|0\rangle + (1-d^2)\,\delta_{J2}b^\dagger_M|0\rangle$$

(II.4.3) $$+ d\sqrt{2J+1}\begin{pmatrix}2&2&J\\0&0&0\end{pmatrix}(1-\tfrac{1}{2}d^2)[b^\dagger b^\dagger]_{JM}|0\rangle +$$

$$+ \tfrac{1}{2}d^2(1-\tfrac{1}{3}d^2)\sqrt{2J+1}\begin{pmatrix}2&2&L\\0&0&0\end{pmatrix}\begin{pmatrix}2&L&J\\0&0&0\end{pmatrix}\left[b^\dagger[b^\dagger b^\dagger]_L\right]_{JM}|0\rangle + \ldots\Big\}$$

To understand the evolution of the low end of the spectrum to the U(5) limit, one may concentrate on J=0 and J=2 states.

Noting that for the two-phonon state in the U(5) limit

(II.4.4) $$|\ n=2\ J\ M\ \rangle = 1/\sqrt{2}\ [b^\dagger b^\dagger]_{JM}|0\rangle$$

one gets

$$|g_0\ 0\ 0\rangle = N_{g_0}\cdot\left[|0\rangle + 1/\sqrt{10}\ d^2\,|\,n=2\ 0\ 0\rangle + \ldots\right]$$

$$|\beta_0\ 0\ 0\rangle = N_{\beta_0}\left[-d|0\rangle + \sqrt{2/5}\,d(1-\tfrac{1}{2}d^2)|n=2\ 0\ 0\rangle + \ldots\right]$$

To be consistent in the power expansion and in calculating the normalization constants N_{g_0}, N_{β_0} one has to use the relation

$$|\ n=3\ J=0\ 0\rangle = 1/\sqrt{6}\,[b^\dagger b^\dagger]_2\cdot b^\dagger|0\rangle$$

and thus arrive at the result

$$|g_0\ 0\ 0\rangle = \left[1+\mathcal{O}(d^4)\right]|0\rangle + d^2/\sqrt{10}\,(1+43d^2/196 + \mathcal{O}(d^4)\ )|n=2\ 0\ 0\rangle + \mathcal{O}(d^3)$$

(II.4.5)
$$|\beta_0\ 0\ 0\rangle = -\sqrt{5/7}\,(1+55d^2/686 + \mathcal{O}(d^4)\ )|0\rangle + \sqrt{2/7}\,(1-275d^2/686 + \mathcal{O}(d^4)\ )|n=2\ 0\ 0\rangle + \mathcal{O}(d^2)$$

$|\gamma_0\ 0\ 0\rangle$ does not exist

Now we come to a critical point: the truncation. The basis $\{|g_0\rangle, |\beta_0\rangle, |\gamma_0\rangle\}$ is a small subset of the complete basis where excitations of any deformed phonon number are included. By truncating the expansions (II.4.5) after the first two terms one gets a two-by-two closed set of basis states, i.e. a one-to-one correspondence between a subspace of the projected states and a subspace of the U(5) states. Strictly speaking, when truncating the above expansions one is not allowed to speak of U(5) states (because they are an infinite series of projected states), but rather quasi U(5) states $|\widetilde{\ }\rangle$ for which

(II.4.6)
$$|\ \widetilde{U(5)}\ \rangle \xrightarrow{d\to 0} |\ U(5)\ \rangle \quad ,$$

because the last terms in (II.4.5) can then be dropped. So

(II.4.5′)
$$|g_0\ 0\ 0\rangle = \left[1+\mathcal{O}(d^4)\right]|\widetilde{0}\rangle + \frac{d^2}{\sqrt{10}}\left[1+\frac{43}{196}d^2+\mathcal{O}(d^4)\right]|\widetilde{2\ 0\ 0}\rangle$$

$$|\beta_0\ 0\ 0\rangle = -\sqrt{\frac{5}{7}}\left[1+\frac{55}{686}d^2+\mathcal{O}(d^4)\right]|\widetilde{0}\rangle + \sqrt{\frac{2}{7}}\left[1-\frac{275}{686}d^2+\mathcal{O}(d^4)\right]|\widetilde{2\ 0\ 0}\rangle$$

Inverting this one gets

$$|\tilde{0}\rangle = [1 - \tfrac{1}{2}d^2 + \mathcal{O}(d^4)]\,|g_0\,0\,0\rangle - \tfrac{1}{2}\sqrt{\tfrac{7}{5}}\,d^2\,|\beta_0\,0\,0\rangle$$

(II.4.7)
$$|\tilde{2}\,0\,0\rangle = \sqrt{\tfrac{5}{2}}\left[1 - \tfrac{3}{28}d^2 + \mathcal{O}(d^4)\right]|g_0\,0\,0\rangle + \\ + \sqrt{\tfrac{7}{2}}\left[1 - \tfrac{43}{196}d^2 + \mathcal{O}(d^4)\right]|\beta_0\,0\,0\rangle$$

The above results can also be obtained by diagonalization in the small-d limit. Using the energy matrix representation (II.3.2), the expressions for the R^J_{ij} and the H^J_{ij} (appendix D2) and the the small-d values for the integrals $I_j(J)$ (appendix E), one arrives at the secular equation

(II.4.8)
$$0 = \begin{vmatrix} \frac{1}{5}d^4 + \frac{1}{35}d^6 - \alpha & \frac{1}{\sqrt{35}}(2d^2 - \frac{17}{49}d^4) + \sqrt{\frac{5}{7}}(1 - \frac{43}{490}d^2)\alpha \\ \frac{1}{\sqrt{35}}(2d^2 - \frac{17}{49}d^4) + \sqrt{\frac{5}{7}}(1 - \frac{43}{490}d^2)\alpha & \frac{1}{7}(4 - \frac{89}{49}d^2) - \alpha \end{vmatrix}$$

$$\Longleftrightarrow \quad (490+215d^2)\alpha^2 - (980+535d^2)\alpha + 7d^6 = 0 \quad ,$$

which gives in addition to the normalized eigenvectors (II.4.7) (identification with the U(5) limit is made on the basis of corresponding eigenvalues) gives as the eigenvalues

(II.4.9)
$$\alpha_1 = 0 + \mathcal{O}(d^3) \quad ; \quad \alpha_2 = 2(1+105d^2/980) + \mathcal{O}(d^3)$$

From eqs.(II.4.5′) and (II.4.9) one can see that when d goes to zero, the projected ground state goes over to the U(5) vacuum and the lowest β state to a mixture of the U(5) vacuum and the U(5) two phonon state of zero angular momentum. This mixture is given in this zero-d limit (strictly speaking the limiting value is out of the model space) by

(II.4.10)
$$|\beta_0\,0\,0\rangle = -\sqrt{5/7}\,|0\rangle + \sqrt{2}/7\,|n{=}2\;0\;0\rangle \quad ,$$

with the vacuum component dominating! Note, that according to eq. (II.4.7) in the zero-d limit the EPM as also the PM ground state go to the pure U(5) vacuum

The process above can be performed also on J=2 states.

This is more tedious because now we have a three-by-three system and the U(5) three-phonon states come into the play. The expansion now reads (see(II.4.1,2,3))

$$|g_0\,2\,M\rangle = N_{g_0}\Big\{ d|n=1\;2\;M\rangle - \frac{d^2}{\sqrt{7}}|n=2\;2\;M\rangle + \\ + \frac{\sqrt{5}}{6} d^3 \sum_{L=0,2,4} \sqrt{2L+1} \begin{pmatrix} 2 & 2 & L \\ 0 & 0 & 0 \end{pmatrix}^2 [b^+[b^+b^+]_L]_{2M}|0\rangle + \mathcal{O}(d^4)\Big\}$$

$$|\gamma_0\,2\,M\rangle = N_{\gamma_0}\Big\{|n=1\;2\;M\rangle + \frac{2d}{\sqrt{7}}|n=2\;2\;M\rangle + \\ + \frac{\sqrt{5}}{2} d^2 \sum_{L=0,2,4} \sqrt{2L+1} \begin{pmatrix} 2 & 2 & L \\ 0 & 0 & 0 \end{pmatrix} \begin{pmatrix} 2 & L & 2 \\ 2 & 0 & -2 \end{pmatrix} [b^+[b^+b^+]_L]_{2M}|0\rangle + \mathcal{O}(d^3)\Big\}$$

$$|\beta_0\,2\,M\rangle = N_{\beta_0}\Big\{(1-d^2)|n=1\;2\;M\rangle - \frac{2d}{\sqrt{7}}(1-\tfrac{1}{2}d^2)|n=2\;2\;M\rangle + \\ + \frac{\sqrt{5}}{2} d^2 \Big(1-\frac{d^2}{3}\Big) \sum_{L=0,2,4} \sqrt{2L+1} \begin{pmatrix} 2 & 2 & L \\ 0 & 0 & 0 \end{pmatrix}^2 [b^+[b^+b^+]_L]_{2M}|0\rangle + \mathcal{O}(d^3)\Big\}$$

The 3-phonon states are now introduced by the use of formulas /Li66/

$$(II.4.11)\qquad N(\lambda\lambda(j')\lambda\, j) = \Big[2 + 4\hat{j}^2 \begin{Bmatrix} \lambda & \lambda & j' \\ j & \lambda & j' \end{Bmatrix}\Big]^{-1/2}$$

$$(II.4.12)\qquad \langle \lambda\lambda(j')\lambda\, j m|\lambda\lambda(j'')\lambda\, j m\rangle = N(\lambda\lambda(j')\lambda\, j) \times \\ \times N(\lambda\lambda(j'')\lambda j)\Big[2\delta_{j'j''} + 4\hat{j}'\hat{j}'' \begin{Bmatrix} \lambda & \lambda & j' \\ j & \lambda & j'' \end{Bmatrix}\Big] \;,$$

where $\hat{j} \equiv \sqrt{2j+1}$, $|\lambda\lambda(j')\lambda jm\rangle$ is an unnormalized three-phonon state with the intermediate coupling indicated (see (II.4.14))) and the $N(\lambda\lambda(j')\lambda j)$ are the corresponding normalization constants. Use of the above formulas indicates that (magnetic quantum numbers left out)

$$(II.4.13)\qquad \sqrt{5/14}|(0)\rangle = \sqrt{7/8}|(2)\rangle = \sqrt{35/72}|(4)\rangle = |\,n=3\;L=2\rangle \;,$$

where

$$(II.4.14) \qquad |(L)\rangle \equiv \left[b^{\dagger}\left[b^{\dagger}b^{\dagger}\right]_2\right]_L|0\rangle = |22(L)22\rangle \ .$$

This is obvious because the 3-phonon J=2 state is unique.

Inserting (II.4.13) in the expansions of the previous page, calculating the norms and truncating one gets

$$(II.4.15) \qquad \begin{aligned}
|g_0\,2\,M\rangle &= \left[1-\tfrac{d^2}{14}+\mathcal{O}(d^4)\right]|\widetilde{1\,2\,M}\rangle - \tfrac{d}{\sqrt{7}}\left[1-\tfrac{d^2}{14}+\right.\\
&\left.+\mathcal{O}(d^4)\right]|\widetilde{2\,2\,M}\rangle + \tfrac{d^2}{\sqrt{14}}\left[1-\tfrac{d^2}{14}+\mathcal{O}(d^4)\right]|\widetilde{3\,2\,M}\rangle\\
|\beta_0\,2\,M\rangle &= \left[1-\tfrac{3}{7}d^2+\mathcal{O}(d^4)\right]|\widetilde{1\,2\,M}\rangle - \tfrac{2d}{7}\left[1+\tfrac{3d^2}{14}+\right.\\
&\left.+\mathcal{O}(d^4)\right]|\widetilde{2\,2\,M}\rangle + \tfrac{3d^2}{\sqrt{14}}\left[1+\tfrac{8d^2}{21}+\mathcal{O}(d^4)\right]|\widetilde{3\,2\,M}\rangle\\
|\gamma_0\,2\,M\rangle &= \left[1-\tfrac{3}{7}d^2+\mathcal{O}(d^4)\right]|\widetilde{1\,2\,M}\rangle + \tfrac{2d}{\sqrt{7}}\left[1-\tfrac{2d^2}{7}+\right.\\
&\left.+\mathcal{O}(d^4)\right]|\widetilde{2\,2\,M}\rangle + \tfrac{d^2}{\sqrt{14}}\left[1-\tfrac{2d^2}{7}+\mathcal{O}(d^4)\right]|\widetilde{3\,2\,M}\rangle
\end{aligned}$$

Inverting, one obtains

$$(II.4.16) \qquad \begin{aligned}
|\widetilde{1\,2\,M}\rangle &= \tfrac{1}{6}\left\{\left[8-\tfrac{9}{7}d^2+\mathcal{O}(d^4)\right]|g_0\,2\,M\rangle - \left[3-\tfrac{15}{7}d^2+\right.\right.\\
&\left.\left.+\mathcal{O}(d^4)\right]|\beta_0\,2\,M\rangle + \left[1-\tfrac{6}{7}d^2+\mathcal{O}(d^4)\right]|\gamma_0\,2\,M\rangle\right\}\\
|\widetilde{2\,2\,M}\rangle &= \tfrac{\sqrt{7}}{3d}\left\{-\left[1+\tfrac{d^2}{14}+\mathcal{O}(d^4)\right]|g_0\,2\,M\rangle + \right.\\
&\left.+\left[1+\tfrac{2}{7}d^2+\mathcal{O}(d^4)\right]|\gamma_0\,2\,M\rangle\right\}\\
|\widetilde{3\,2\,M}\rangle &= \tfrac{\sqrt{14}}{6d^2}\left\{-\left[4-\tfrac{11}{7}d^2+\mathcal{O}(d^4)\right]|g_0\,2\,M\rangle+\left[3-\tfrac{15}{7}d^2+\right.\right.\\
&\left.\left.+\mathcal{O}(d^4)\right]|\beta_0\,2\,M\rangle + \left[1+\tfrac{10}{7}d^2+\mathcal{O}(d^4)\right]|\gamma_0\,2\,M\rangle\right\}
\end{aligned}$$

Diagonalization would give as eigenvectors the states (II.4.16) and as eigenvalues the one-, two- and three-phonon energies. So calling the right sides of eq. (II.4.16) as $|g\ 2\ M\rangle$, $|\gamma\ 2\ M\rangle$, $|\beta\ 2\ M\rangle$ one recovers the Sakai scheme that also underlied the earlier PM, ref. /Li76/ (see also figure 2 on p. 76).

In fig. 1 there are plotted the overlaps for various angular momentum values. It may be seen, that when d approaches zero, the value for the only J=0 overlap, $\langle g_0|\beta_0\rangle$,

goes to $-\sqrt{5/7}$, as could also be seen from eq. (II.4.5'). For the other angular momenta all the overlaps go to unity when d goes to zero. This is readily seen for J=2 from eq. (II.4.15). The asymptotic limit for the overlaps is discussed in section II.5.

In fig. 26 there is shown the relevant part of the U(5) spectrum with total set of quantum numbers and E2 transition probabilities up to phonon number 4. This is an exact limit which the EPM must approach when d decreases, so this is a good check for the computer code. Another limit where the code may be checked is the asymptotic limit discussed in section II.5.

So, the line of argument leading to the use of a very restricted model space is that in this way one can transfer some of the dynamics of the Hamiltonian to (deformed) wave functions, thus allowing a pure harmonic Hamiltonian to generate anharmonic and rotational spectra. This basis is intimately connected to the ellipsoidal form of the rotating nucleus and so even after the truncation in the number of the basis states, this basis is believed to describe rather well nuclear low-spin structure. Enlarging the number of basis states will lead in the case of the harmonic laboratory Hamiltonian closer to the harmonic spectrum, and the restoration of the anharmonic and rotational features in the spectrum will then demand a laboratory Hamiltonian going beyond the harmonic approximation.

II.5. The Asymptotic Limit of the EPM

Let us do the same as in the previous chapter (i.e. examine the structure of J=0 and J=2 states for $\hat{H}=\hat{N}$) now in the case of a large deformation parameter referred to as the asymptotic limit. First examine the case of J=0. Using appendix E for the integrals and appendix D2 for the matrix elements, one obtains the secular equation

$$\begin{vmatrix} d^2-1-3d^{-2}-\alpha & 2/3\cdot d^{-1}+\alpha d^{-1}(1-1/6\cdot d^{-2}) \\ 2/3\cdot d^{-1}+\alpha d^{-1}(1-1/6\cdot d^{-2}) & d^2-2-\alpha \end{vmatrix} = 0$$

$$\left[1-d^{-2}+1/3d^4+\mathcal{O}(d^{-6})\right]\alpha^2+\left[-2d^2+3-d^{-2}+\mathcal{O}(d^{-4})\right]\alpha+$$
$$+\left[d^4-3d^2+5/3+\mathcal{O}(d^{-2})\right]=0$$

Solving this, one gets the eigenenergies

$$(II.5.1)\quad \alpha_1 = d^2-d-1/2+\mathcal{O}(d^{-1}) \;;\; \alpha_2 = d^2+d-1/2+\mathcal{O}(d^{-1})$$

and the corresponding eigenvectors

$$|0_g\rangle = 1/\sqrt{2}\left[1-3/4\cdot d^{-1}+\mathcal{O}(d^{-2})\right]|g_0\ 0\rangle -$$
$$-1/\sqrt{2}\left[1-1/4\cdot d^{-1}+\mathcal{O}(d^{-2})\right]|\beta_0\ 0\rangle$$

$(II.5.2)$

$$|0_\beta\rangle = 1/\sqrt{2}\left[1+3/4\cdot d^{-1}+\mathcal{O}(d^{-2})\right]|g_0\ 0\rangle +$$
$$+\ 1/\sqrt{2}\left[1+1/4\cdot d^{-1}+\mathcal{O}(d^{-2})\right]|\beta_0\ 0\rangle$$

where $|0_\beta\rangle$ is a state of angular momentum J=0 belonging to the β band (E_β>E(ground) ,M's dropped), and g stands for the ground state band).

For J=2 one has the secular equation

$$\begin{vmatrix} d^2 - 1 + \frac{2}{3}\frac{1}{d^2} - \alpha & \frac{5}{3}\frac{1}{d} + \alpha\cdot\frac{1}{d}\left(1 - \frac{7}{6}\frac{1}{d^2}\right) & \frac{\sqrt{2}}{3}\frac{1}{d} + \frac{4\sqrt{2}}{9}\frac{1}{d^3} - \alpha\cdot\frac{\sqrt{2}}{3}\frac{1}{d^3} \\ \frac{5}{3}\frac{1}{d} + \alpha\cdot\frac{1}{d}\left(1 - \frac{7}{6d^2}\right) & d^2 - 2 - \alpha & \frac{2\sqrt{2}}{3}\frac{1}{d^2} \\ \frac{\sqrt{2}}{3}\frac{1}{d} - \alpha\cdot\frac{\sqrt{2}}{3}\frac{1}{d^3} & \frac{2\sqrt{2}}{3}\frac{1}{d^2} & d^2 - \alpha \end{vmatrix} = 0$$

Solving this, one obtains the eigenenergies

$$\begin{aligned} \alpha_1 &= d^2 - d - 1/2 + \mathcal{O}(1/d) \\ \alpha_2 &= d^2 + \mathcal{O}(1/d) \\ \alpha_3 &= d^2 + d - 1/2 + \mathcal{O}(1/d) \end{aligned} \qquad \text{(II.5.3)}$$

and the corresponding eigenvectors

$$\begin{aligned} |2_g\rangle &= 1/\sqrt{2}\left[1+\mathcal{O}(1/d)\right]|g_0\ 2\rangle - 1/\sqrt{2}\left[1+\mathcal{O}(1/d)\right]|\beta_0\ 2\rangle \\ |2_\gamma\rangle &= \left[1+\mathcal{O}(1/d)\right]|\gamma_0\ 2\rangle \qquad \text{(II.5.4)} \\ |2_\beta\rangle &= 1/\sqrt{2}\left[1+\mathcal{O}(1/d)\right]|g_0\ 2\rangle + 1/\sqrt{2}\left[1+\mathcal{O}(1/d)\right]|\beta_0\ 2\rangle \end{aligned}$$

From eq. (II.5.4) one sees that in the asymptotic limit the eigenstate $|J_\gamma\rangle$ begins to decouple from the other eigenstates $|J_\beta\rangle$ and $|J_g\rangle$ and to have only one component, the $|\gamma_0\ J\rangle$ component. This is in contrast to the earlier PM, where the ground state was chosen to be pure, ie

$$|J_g\rangle_{PM} = |g_0\ J\rangle \qquad \text{(II.5.5)}$$

and the β and γ states had the Gram-Schmidt form /Li76/

$$\begin{aligned} |J_\gamma\rangle_{PM} &= N_\gamma\left(1 - |g_0\ J\rangle\langle g_0\ J|\right)|\gamma_0\ J\rangle \\ |J_\beta\rangle_{PM} &= N_\beta\left(1 - |g_0\ J\rangle\langle g_0\ J| - |\gamma_0\ J\rangle\langle\gamma_0\ J|\right)|\beta_0\ J\rangle\ . \end{aligned} \qquad \text{(II.5.6)}$$

There are also big differences in asymptotic energies between the PM and the EPM. From eq. (II.5.3) one sees that

the asymptotic energy differences between states of the same J but belonging to different bands are in the EPM (with obvious notation)

$$\Delta(J)_{\beta g} = E_J^{\beta} - E_J^{g} = 2d + \mathcal{O}(1/d)$$

$$\Delta(J)_{\gamma g} = E_J^{\gamma} - E_J^{g} = d + 1/2 + \mathcal{O}(1/d) \quad , \tag{II.5.7}$$

$$\Delta(J)_{\beta\gamma} = E_J^{\beta} - E_J^{\gamma} = d - 1/2 + \mathcal{O}(1/d)$$

while in the PM the corresponding asymptotic differences are /Li76/, fig.8

$$\Delta(J)^{PM}_{\beta g} = 1 + \mathcal{O}(1/d^2)$$

$$\Delta(J)^{PM}_{\gamma g} = 1 + \mathcal{O}(1/d^2) \tag{II.5.8}$$

$$\Delta(J)^{PM}_{\beta\gamma} = 0 + \mathcal{O}(1/d^2) \quad .$$

So the differences are really drastic and imply a greater β/γ flexibility for the EPM when anharmonic terms in the Hamiltonian are used. Here one sees clearly the effect of diagonalization as the best means of creating an orthonormal basis, the 'optimal' Gram-Schmidt basis. Here the diagonalization lowers the ground state much more than the Schmidt scheme used in the PM. The asymptotic behaviour of energies in the EPM is shown in fig.2 .

Fig.1 shows the overlaps as a function of d. As was mentioned in section II.4 , all the overlaps tend to unity when d goes to zero, except the overlap $\langle g_0\ 0|\beta_0\ 0\rangle$ which behaves like

$$\langle g_0\ 0|\beta_0\ 0\rangle \overset{d\sim 0}{=} -\sqrt{5/7}\left[1-43d^2/490+\mathcal{O}(d^4)\right] \quad . \tag{II.5.9}$$

In the asymptotic limit the behaviour, for example for the J=0 and J=2 states, is

$$\langle g_0\ 0|\beta_0\ 0\rangle \sim -d^{-1}(1+1/6\cdot d^{-2}) + \mathcal{O}(d^{-4})$$

$$\langle g_0\ 2|\beta_0\ 2\rangle \sim -d^{-1}(1-7/6\cdot d^{-2}) + \mathcal{O}(d^{-4})$$

$$\langle g_0\ 2|\gamma_0\ 2\rangle \sim \sqrt{2}/3\cdot d^{-3} + \mathcal{O}(d^{-4}) \tag{II.5.10}$$

$$\langle \beta_0\ 2|\gamma_0\ 2\rangle \sim \mathcal{O}(d^{-4})$$

Comparison with fig.4 of ref. /Li76/ indicates that the overlaps there are wrong and the diminishing of the absolute values of the overlaps $\langle g_0 J | \beta_0 J \rangle$ should occur as $1/d$. The other overlaps go much faster to zero, which indicates the decoupling of the γ band from the others.

An interesting thing is the behaviour of the matrix elements of the anharmonic terms of the Hamiltonian (II.2.10). This asymptotic behaviour leads to the identification of the effective Hamiltonian of eq. (II.3.5). The rules (II.3.4) stem from the facts that asymptotically

$$
\begin{aligned}
&\langle i_0 | B_{30} | j_0 \rangle \sim -\sqrt{2/7}\, d \langle i_0 | B_{20} | j_0 \rangle \\
&\langle i_0 | B_{21} | j_0 \rangle \sim -\sqrt{8/7}\, d \langle i_0 | \hat{N} | j_0 \rangle \\
&\langle i_0 | B_{40} | j_0 \rangle \sim -\sqrt{7/2}\, d \langle i_0 | B_{30} | j_0 \rangle \sim d^2 \langle i_0 | B_{20} | j_0 \rangle \\
&\langle i_0 | B_{31} | j_0 \rangle \sim -\sqrt{7/2}\, d \langle i_0 | B_{21} | j_0 \rangle \sim 2d^2 \langle i_0 | \hat{N} | j_0 \rangle \\
&\langle i_0 | B_{22}^{(0)} | j_0 \rangle \sim 1/10 \cdot d^2 \langle i_0 | B_{20} | j_0 \rangle \\
&\langle i_0 | B_{22}^{(2)} | j_0 \rangle \sim 2/7 \cdot d^2 \langle i_0 | \hat{N} | j_0 \rangle \quad .
\end{aligned}
\tag{II.5.11}
$$

As is easy to see, the higher the order of the anharmonic term, the larger its matrix elements. This is not, however, a proof of the importance of the higher-order terms in the Hamiltonian because their asymptotic behaviour resembles that of $\hat{N}$ and B_{20} . A discussion on these matters is further pursued in section III.2.

II.6. E2 Transition Probabilities and Quadrupole Moments

To be able to discuss transition probabilities, one first needs knowledge of the quantum mechanical operator, the transition operator that is involved. In the liquid drop picture the electric quadrupole operator is written as

$$T_m^{(E2)} = \int \rho r^2 Y_{2m}^* d\tau = \rho_o \int r^2 Y_{2m}^* d\tau \quad , \tag{II.6.1}$$

when uniform density distribution

$$\rho_o = 3Ze/4\pi R_o^3 \tag{II.6.2}$$

is assumed. Assuming the quadrupole deformed shape (B.1) of the liquid drop, the integration of (II.6.1) over the volume bounded by this surface yields /Li66/

$$T_m^{(E2)} = 3ZeR_o^2/4\pi \left\{ \hat{\alpha}_{2m} + 2\sum_{\lambda\lambda'} (-1)^{\lambda-\lambda'} \times \right.$$
$$\left. \times \sqrt{(2\lambda+1)(2\lambda'+1)/4\pi} \begin{pmatrix} \lambda & \lambda' & 2 \\ 0 & 0 & 0 \end{pmatrix} \left[\hat{\alpha}_\lambda \hat{\alpha}_{\lambda'} \right]_{2m} \right\} + \mathcal{O}(\hat{\alpha}_2^3) \tag{II.6.3}$$

Sticking now to the lowest-order operator as in the earlier PM and transforming the first-quantized collective coordinates $\hat{\alpha}_{2m}$ to second- quantized boson operators according to eq. (B.4), one obtains

$$T_m^{(E2)} = e^* (b_m^\dagger + \bar{b}_m) \quad , \tag{II.6.4}$$

where

$$\bar{b}_m = (-1)^m b_{-m} \quad ; \quad e^* = 3ZeR_o^2/4\pi\sqrt{\hbar\omega/2C_o} \tag{II.6.5}$$

Here, as also in the earlier PM, the coefficient e^* is

used as an effective charge parameter and is obtained by fixing the value of one transition probability, which is here chosen to be the 2g-->0g transition.

The above transition operator can now be used to calculate E2-transition probabilities defined in the standard way /Sh63/ as

$$B(E2;\nu J \rightarrow \mu J') = (2J+1)^{-1} |(\mu J' \| T^{(E2)} \| \nu J)|^2 =$$

$$(2J'+1)/(2J+1) \cdot \langle \mu\ J'\ 0 \mid T^{(E2)}_{-M_0} \mid \nu\ J\ M_0 \rangle^2 \times \tag{II.6.6}$$

$$\times (2\ -M_0\ J\ M_0 \mid J'\ 0)^{-2} \quad ,$$

where $\mu,\nu = g,\beta,\gamma$. In the same way the static quadrupole moment is defined as

$$eQ(\mu,J) = \sqrt{\frac{16\pi}{5}} \begin{pmatrix} J & 2 & J \\ -J & 0 & J \end{pmatrix} (\mu\ J \| T^{(E2)} \| \mu\ J) =$$

$$= \sqrt{\frac{16\pi}{5}} \frac{\begin{pmatrix} J & 2 & J \\ -J & 0 & J \end{pmatrix}}{\begin{pmatrix} J & 2 & J \\ 0 & 0 & 0 \end{pmatrix}} \langle \mu\ J\ 0 \mid T^{(E2)}_0 \mid \mu\ J\ 0 \rangle \tag{II.6.7}$$

Here ($\|\ \|$) is a reduced matrix element. We can use $M_0 = 0$ if both J and J' are even or odd and $M_0 = 2$ if either of J and J' is odd. Because the ground, β and γ states are a result of diagonalization in the basis $\{g_0, \beta_0, \gamma_0\}$, they can be written as (except for the states $|\gamma\ J=\text{odd}\rangle$ which are of pure γ character

$$\begin{pmatrix} |g\ J\rangle \\ |\beta\ J\rangle \\ |\gamma\ J\rangle \end{pmatrix} = \begin{pmatrix} \alpha_J(g,g) & \alpha_J(g,\beta) & \alpha_J(g,\gamma) \\ \alpha_J(\beta,g) & \alpha_J(\beta,\beta) & \alpha_J(\beta,\gamma) \\ \alpha_J(\gamma,g) & \alpha_J(\gamma,\beta) & \alpha_J(\gamma,\gamma) \end{pmatrix} \begin{pmatrix} |g_0\ J\rangle \\ |\beta_0\ J\rangle \\ |\gamma_0\ J\rangle \end{pmatrix} \tag{II.6.8}$$

where the $\alpha_J(\mu,\nu)$, $\mu,\nu = g,\beta,\gamma$, are the components of the μ:th eigenvector in the basis $\{|g_0\rangle, |\beta_0\rangle, |\gamma_0\rangle\}$ for each J. The above decomposition of states leads also to the following decomposition in eqs.(II.6.6&7):

$$\langle \mu\ J'\ 0 \mid T^{(E2)}_{-M_0} \mid \nu\ J\ M_0 \rangle = \sum_{i,k} \alpha_J(\nu,i)\alpha_{J'}(\mu,k) \times$$

(II.6.9)

$$\times \langle k_0\ J'\ 0 \mid T^{(E2)}_{-M_0} \mid i_0\ J\ M_0 \rangle \quad ,$$

where $k_0, i_0 \in \{g_0, \beta_0, \gamma_0\}$. The various basic transition matrix elements $\langle k_0\ J'\ 0 \mid T^{(E2)}_{-M_0} \mid i_0\ J\ M_0 \rangle$ can be calculated following the lines of calculation of the matrix elements of the Hamiltonian, examples are to be found in ref. /Ha70/. All the matrix elements needed in eq. (II.6.9) are tabulated in appendix F.

Checking of the computer program and the derivation of analytical expansions for the transition probabilities can be performed in two different limits: the small-d and large-d limit. These limits correspond in the language of the classical theories to the spherical U(5) phonon limit, and to the adiabatic rigid-rotor limit; these limits were already discussed in sections II.4. and II.5. in connection with the energies. Figure 26 shows part of the U(5) phonon spectrum with allowed transitions included. For a transition operator of the form (II.6.4) the transition probabilities are easily calculated, because the matrix elements of operators b and b between spherical phonon states are proportional to boson cfp coefficients /Sh63/.

The asymptotic limit is more interesting and connects to the adiabatic rotor model. When d is very large, a small angular velocity will be enough to attain a given angular momentum J. This is easy to see from the semiclassical formula for a rigid rotor

$$J(J+1) = \mathcal{J}^2\omega^2 \quad , \quad [J] = \hbar$$

where $\mathcal{J}$ is the nuclear moment of inertia, which increases with increasing deformation. So the low angular momentum part of the nuclear spectrum is free from the effects of the Coriolis interaction and thus the rotational motion does not excite additional intrinsic degrees of freedom. (The non-adiabaticity of the system sets in when systems with high angular momenta or small deformations are considered. Then additional features caused by Coriolis and centrifugal interactions must be considered, for example in the form of K mixing). This total separation of intrinsic and collective rotatinal excitations is called the adiabatic limit, and it is also realized in the case of the wobbling oriented system of the EPM. This means spectroscopically a rotational band built on top of every intrinsic exitation. The deviation from this law is customarily caracterized by an expansion in powers of J(J+1), where the magnitude of the coefficient in front of each term indicares the relative importance of this term /Bo75/

The effect of adiabatic rotation is seen in the so-called Alaga rules /Al55/, in which the geometry solely dictates

the values of certain branching ratios of transition probabilities. Denoting by K the projection of J along the intrinsic symmetry axis, one has

$$\text{(II.6.10)} \qquad \frac{B(E2; J\,K \longrightarrow J'K')}{B(E2; J\,K \longrightarrow J''K')} = \frac{(J\,K\,2\,K'-K \mid J'\,K')^2}{(J\,K\,2\,K'-K \mid J''\,K')^2} ,$$

which gives in the special case of the ground state band

$$\frac{B(E2; J_g \longrightarrow J'_g)}{B(E2; J_g \longrightarrow J''_g)} = \frac{(J\,0\,2\,0 \mid J'\,0)^2}{(J\,0\,2\,0 \mid J''\,0)^2} .$$

Measuring everything with respect to the transition 2g-->0g, one gets a useful formula

$$\text{(II.6.11)} \qquad \frac{B(E2; J_g \rightarrow J'_g)}{B(E2; 2_g \rightarrow 0_g)} = \frac{B(E2; J_\beta \rightarrow J'_\beta)}{B(E2; 2_\beta \rightarrow 0_\beta)} = 5(2J'+1)\begin{pmatrix} J & 2 & J' \\ 0 & 0 & 0 \end{pmatrix}^2 ,$$

which can be compared with computer results (also the other possible Alaga rules have been compared to computer calculations). For the quadrupole moments one obtains in the case of the ground state band

$$\text{(II.6.12)} \qquad \frac{[eQ(g,J)]^2}{B(E2; 2_g \rightarrow 0_g)} = 16\pi(2J+1)^2\begin{pmatrix} J & 2 & J \\ 0 & 0 & 0 \end{pmatrix}^2\begin{pmatrix} J & 2 & J \\ -J & 0 & J \end{pmatrix}^2 .$$

These can be compared with large-d numerical results.

An other way of checking the numerical results in the large-d limit is by calculating analytical expansions for the above transitions. The α-matrices of eq. (II.6.9) are obtained from expressions (II.5.2) and (II.5.4), and the asymptotic expressions for the basic transition matrix elements are obtained by the use of appendices F and E. Here are some results (in the units of B(E2;2g-->0g)) :

$$B(E2;2\beta \rightarrow 0\beta) \sim 1 + 2/d + \mathcal{O}(1/d^2) \quad ,$$

$$B(E2;2\beta \rightarrow 0g) \sim 25/256 \cdot d^{-4}\left[1 + \mathcal{O}(1/d)\right] \quad ,$$

$$B(E2;2\beta \rightarrow 2g) \sim 5/56 \cdot d^{-4} + \mathcal{O}(1/d^5) \quad ,$$

$$B(E2;3\gamma \rightarrow 2g) \sim 25/56 \cdot d^{-2}\left[1 + 3/2d + \mathcal{O}(1/d^2)\right] \quad ,$$

$$B(E2;3\gamma \rightarrow 2\beta) \sim 25/56 \cdot d^{-2}\left[1 + 1/2d + \mathcal{O}(1/d^2)\right] \quad ,$$

$$\left[eQ(g,2)\right]^2 \sim -8\sqrt{\pi}/7\left[1 + \mathcal{O}(1/d^2)\right] \quad ,$$

$$\left[eQ(\beta,2)\right]^2 \sim -8\sqrt{\pi}/7\left[1 + 1/d + \mathcal{O}(1/d^2)\right] \quad .$$

One more thing to be noted is the geometrical relation (B.17), which seems to hold true also for the asymptotic limit of the EPM (the same kind of relation for absolute values comes out directly from Alaga rules). This has been computer verified and is discussed in section III.3. It is worth noting that in the EPM eQ_0 is d-depended and different for every band in order to fulfill eq. (B.17). This feature is built in the model in contrast to the BMM, where the same eQ_0 describes every band, unless new degrees of freedom are introduced in the model by making the eQ_0´s parameters to be fixed by experimental data.

III. NUMERICAL TESTING OF THE MODEL

III.1. Numerical Solution

Here a brief outline is given of the numerical methods used in solving the numerical problem. As was explained in section II.3, the projected states (II.3.1) yielded a generalized eigenvalue problem of the Hamiltonian matrix and the corresponding secular equation is depicted in eq.(II.3.2). The calculation of the matrix elements of the Hamiltonian matrix H^J_{ij} and the overlap matrix R^J_{ij} yields eleven different integrals, $I_i(J)$, tabulated in appendix D1.

Because the integrals are quite complicated, i.e. they become very small in the small-d limit (see the discussion in the beginning of appendix E1) and quite large asymptotically and contain an exponential that increases at d>1 very rapidly, ordinary integration techniques are not accurate and fast enough. Because fitting to experimental data calls for an optimization routine, the integrals need to be calculated several times during one computer run. Also, because one needs to handle many D functions during each integration, a method that uses as few integration points as possible is needed (this excludes the usual Simpsonian techniques and others like it). The solution to this problem is a numerical integration technique that is tailor-made to this kind of problem. These special integration techniques use orthogonal polynomials to expand the integrand inside the integration interval. A suitable integration technique to carry out the integrals $I_i(J)$ is the so-called Gauss-Legendre integration /Ab65, Sc68/. Here a 32-point Gauss-Legendre procedure was used with 20 subintervals, and as a consequence the integrals were written in the form

$$I_i(J) = 1/20 \sum_{k=1}^{20} \sum_{j=1}^{32} A_j F_i^J(x_{jk}) \quad , \tag{III.1.1}$$

where

$$(III.1.2) \qquad I_i(J) = \int_{-1}^{1} F_i^J(x)dx \quad ,$$

$$(III.1.3) \qquad x_{jk} = (x_j + 2k - 21)/20$$

and A_i and x_i are the Gauss-Legendre ordinates and abscissas taken from /Ab65/.

The fastest and most accurate way of calculating the Wigner D-functions contained in the integrals is by recursion using Jacobi-polynomials /Ab65, Ba77/ according to formulas (A1.19) and (A1.20) of appendix A1. These D functions are calculated at all the points (III.1.3) and tabulated in a direct access file to be used during the computer run, thus avoiding a continuous calculation of them.

After computing the integrals and thereby the different matrix elements , the task of solving the eigenvalue problem remains. This is dealt with by a library routine that uses canonical transformation techniques /Mo73/. As a result the energy eigenvalues and the (unnormalized) eigenvectors in the projected-state basis $\{|g_0 J\rangle , |\beta_0 J\rangle , |\gamma_0 J\rangle\}$ are obtained. The normalization of the eigenvectors according to formula (C.10) yields the states $\{|g\ J\rangle , |\beta\ J\rangle , |\gamma\ J\rangle\}$ and the eigenamplitudes $\alpha_j(i,j), i,j \in \{g,\beta,\gamma\}$ connected by formula (II.6.8) of section II.6.

During this mathematical process a physical question arises concerning the identification of the spectroscopic quasi bands /Sa82/ of real nuclei. One guiding tool is to observe the behaviour of the band structure produced by the harmonic Hamiltonian $\hat{N}$. This was done in the earlier PM by choosing the order of orthogonalization in the Schmidt procedure in such a way as to yield the Sakai Scheme /Li76/. Here the problem is more difficult to solve because of the large mixing of the eigenamplitudes in certain regions of the spectrum (this is especially true for the Hamiltonians containing also anharmonic terms).

The ground state band is easy to handle by assuming it to be always the yrast band, i.e. its states lying the lowest in energy for each angular momentum This is justified because the EPM is tailor made for describing low-lying collective excitations and thus it does not have any internal degrees of freedom to describe band crossing and back-bending phenomena, which are believed to be connected either to the single-particle aspects (nucleon pair breaking /St72/) or to shape transitions. To describe the collective shape-phase transition in the framework of the EPM, one need a way of introducing two deformation parameters into the calculations and a mechanism of mixing the two bands described by these two parameters. This is certainly outside the scope of this model and so the above treatment of the g band is well founded.

The recognition of the quasi-β and quasi-γ bands is much more difficult because of the large mixing of the projected states in those parts of nuclear spectra where their

energies are close to each other. As a guideline one could use the same arguments as in the earlier PM and obtain the Sakai scheme in the small-d limit using the harmonic Hamiltonian. Then eq.(II.4.16) would give an indication of the recognition procedure. This, however, must also be consistent with the large-d limit, eq.(II.5.4). The procedure which would appear natural is to assign to the γ band the states having the γ component dominant, while the remaining states would belong to the β band. In the actual program a recognition method is used which is developed by collecting data from diagonalizations of different (anharmonic) Hamiltonians and thus the method is 'experimentally' discovered. It also yields the scheme described above in the case of the harmonic Hamiltonian (this is very clearly seen from the energies of fig.2). In addition to this eigenvector-based recognition scheme, a scheme based on experimental energies can be optionally used in actual fits. In this procedure the experimentally known order of the ground, β and γ energies helps in the identification of the bands (this is the scheme followed in most more extensive codes where a legion of different states with the same J are produced).

After having completed the calculation of energies for a chosen set of Hamiltonian coefficients C'_i of eq.(II.3.5) there remains the problem of optimizing the parameters C'_i with respect to the existing spectroscopic data. There exists a great many optimization methods dealing with multi parameter surfaces /Ku73.Ja75/. The best of these proved to be a library routine /IM89/ using a quasi-Newton method /FI72/. This code seems to be the most accurate in discovering small inclinations of 'ditches' on the parameter surface and thus yields a result that reaches nearest to the correct result. The other aspect, however, which must be borne in mind here is that the calculation of the functional to be minimized is less accurate at small deformation parameters, and thus the minimization is rendered more difficult by the noise in the numerical values of the functional. The functional to be minimized in the EPM is a weighted chi squared function

$$\text{(III.1.4)} \qquad f(\{c_i\}) = \sum_{\alpha} \left(\frac{E^{\alpha}_{th}(\{c_i\}) - E^{\alpha}_{exp}}{E^{\alpha}_{exp}} \right)^2 ,$$

where $\alpha \equiv (i,J), i=g,\beta,\gamma$ and the sum includes all the states that one wants to take into the fit. The curly parentheses indicate functional dependence on several variables C_i (coefficients of the Hamiltonian expansion). The weighting here assures the improvement of the fit at low energies at the expense of higher energies, which is in accordance with the philosofy of the model (in earlier days this was also due to the more inaccurate experimental energies in the higher-energy part of the level schemes).

The E2 transition probabilities and static quadrupole moments are calculated from the standard formulas (II.6.6) and (II.6.7). The effective charge, e^*, appearing in the

transition operator is determined by fixing the transition probability B(E2;2g-->0g) to the corresponding experimental value. The SO(3) Clebsch-Gordan (or 3j) coefficients appearing in the explicit expressions for the basic matrix elements (appendix F) are calculated from their explicit formulas /Sh63,We78/.

The output of the program includes the fitted theoretical energy spectrum as printout and as a drawn level scheme (see figs. 27 to 31) In addition, the final values of the parameters C'_i are printed, and certain information is given concerning the success of the fitting (number of functional evaluations, numb. of significant digits and information on the final gradient values at the minimum). Because the functional evaluation takes some time, this first part of the program is not very quick to perform. On the other hand the transition probabilities and quadrupole moments are quickly calculated and printed out after the minimization.

III.2. The Effective Hamiltonian and Its Spectrum

III.2.A The Effective Hamiltonian

The number of free parameters in the effective Hamiltonian (II.3.5) is seven and it includes all important terms up to fourth order. The terms B_{40} and B_{31} were left out because their matrix elements behave asymptotically according to eq. (II.5.11) , where the link $\langle B_{30} \rangle \sim$ constant$\cdot\langle B_{20} \rangle$ is valid already at such small values as $d \sim 2$. This has been found by numerical testing of real nuclei, namely the Gadolinium isotopes $^{150-160}$Gd /Ve83/. There the renormalization character of the B_{30} term was proved by fitting each Gd isotope twice, with term B_{30} included and excluded. Because these Gd isotopes cover the range from spherical to well-deformed nuclei, the omission of the B_{30} term from further fits is well founded (on the other hand, B_{21} remains effective).

The exclusion of the terms B_{30}, B_{40} and B_{31} leaves us an effective Hamiltonian with six parameters. Further investigations of the importance of the various terms in the effective Hamiltonian can be performed by looking at their influence on the odd-J γ-band states. Because the odd-J γ states are decoupled from the rest of the spectrum (no diagonalization needed for the odd-J states because only γ states can have odd angular momenta) it is hard to influence their spacing in the band. Calculation of the Hamiltonian between the states $|\gamma_0$ J=odd$\rangle$ reveals that the only terms that give a non-trivial (non-renormalizing) contribution are $\hat{N}$, $\hat{\vec{J}}^2$ and $B_{22}^{(2)\prime}$. So by this criterion dropping the terms B_{31} and B_{40} is justified. The term $B_{22}^{(2)\prime}$ seems to be more important than the term $B_{22}^{(0)\prime}$ in two ways. First, as mentioned above, the effect of the term $B_{22}^{(0)\prime}$ on the odd-J members of the γ band is 'trivial' whereas the term $B_{22}^{(2)\prime}$ remains effective, i.e. brings in a J dependence to the odd-J γ-band energies. Second, as can be seen from appendix D2, $B_{22}^{(2)\prime}$ has more effective matrix elements than $B_{22}^{(0)\prime}$. So the EPM would predict the phenomenological quadrupole-quadrupole force to be the dominant one at non-zero deformations.

So, summing up, if one takes into account the numerical tests, i.e. the effects on odd-J γ-band members and the magnitude of the matrix elements of the different terms in actual fits, one is left with an effective Hamiltonian with five parameters,

$$\text{(III.2.1)} \qquad \hat{H}_{eff} = c_1'\hat{N} + c_2'B_{20} + c_3'B_{21}' + c_6'B_{22}^{(2)\prime} + c_7'\hat{\vec{J}}^2 \ .$$

In the actual systematic fitting (see chapter IV) the trivial term J^2 is also left out in order to cut down the number of fitting parameters and to investigate the ability of the other anharmonic terms to reproduce rotor spectra. Following the notation used in the computer code one can express the final form of the effective Hamiltonian used in systematic fitting as

$$\text{(III.2.2)} \qquad \hat{H} = c_0\hat{N} + c_1B_{20} + c_2B_{21}' + c_5B_{22}^{(2)\prime} \ .$$

The total Hamiltonian that is allowed in the fits by the computer code, however, reads

$$\text{(III.2.3)} \qquad \hat{H} = c_0\hat{N} + c_1B_{20} + c_2B_{21}' + c_3B_{30}' + c_4B_{22}^{(0)\prime} + c_5B_{22}^{(2)\prime} + c_6\hat{\vec{J}}^2$$

and includes seven parameters. This makes altogether eight parameters with the deformation/softness parameter d which describes the deformation of the projected basis states and thus may be thought to have a connection with the intrinsic shape of the nucleus.

III.2.B. The Effect of the Different Parameters on the Energy Spectrum

The effects of the parameters d, C_0, C_1 and C_2 on the energy spectrum produced by the Hamiltonian (III.2.2) was investigated in /Ve83/. Here I give a short description of the main effects on the band heads and on the internal structure of the bands. By the internal structure of a band I mean here the spectroscopic moment of inertia $\mathcal{J}_{g,\beta,\gamma}$ which may be determined from the energy differences within the bands. The initial spectrum is chosen to have realistic parameter values (from the Gd region) and the evolution of the spectrum was observed as a function of the deviation of the parameters from these initial values.

The increase in d causes the moment of inertia of the band to increase which means pictorially that the band shrinks or contracts and all energy levels become closer to each other. This is easy to understand the basis of the rigid-rotor relation

$$\Delta E_J \equiv E_{J+2} - E_J = (2J+3)/\mathcal{J} \quad . \tag{III.2.4}$$

This shrinking of the spectrum may be counter-acted by increasing the other parameters linearly, i.e. increasing the overall scale of the Hamiltonian. This increase in the moment of inertia with increasing d is quite natural if one imagines a relation of d with the intrinsic shape of the rotating nucleus (originally d described the shape of the oriented system). Then the increase in $\mathcal{J}$ means that the nucleus is becoming more prolate which in turn means increasing d. So the variation of d causes the spectrum to evolve from a spherical (anharmonic) vibrator to an almost rigid rotor. For small d one may also obtain ground-state band spectra which resemble shell model two-valence-particle spectra (with pairing included), other bands may look like vibrational or rotational at the same time. Also vibrator- rotator co-existence may occur[1]. The γ-band head is practically independent of the magnitude of d and only a very small effect on the relative β-γ-band position is observed.

The parameter C_1 does not affect the β- and γ-band moments of inertia, but affects quite strongly their relative positions, i.e. the difference between the locations of

1) see fig. 31 .

their band heads. Also the parameter C_2 has the above effects on the spectrum but to a somewhat lesser extent. The look of the spectrum seems to depend only on the absolute value of the parameter C_3 . It affects the relative β and γ positions in the same way as C_2 but the increase in its magnitude also makes δ_γ increase and δ_β decrease .

Figures 2-7 show the eigenspectrum of each term in the Hamiltonian (III.2.3), exept the spectrum of $\hat{J}^2$ which is trivial. From the pictures it is easy to see that the only terms that bring J dependence to odd-J γ-band energies are $\hat{N}$ and $B_{22}^{(2)'}$. Also one can see that the ground state band is not affected by the fourth-order terms $B_{22}^{(0)'}$ and $B_{22}^{(2)'}$,which has already been discussed in the case of the earlier PM in ref. /Ha70/ . The most interesting behaviour is carried by the harmonic term $\hat{N}$, whose eigenspectrum is shown in fig.2. This should be compared with the results of the earlier PM represented in ref. /Li76/, figures 5 and 8. As already discussed in section II.5, the diagonalization has a drastic effect on the β and γ bands while the ground state band remains almost unchanged. The picture clearly tells that in the small-d limit the Sakai scheme is recovered, whereas asymptotically the rigid rotor spectrum will follow. As already mentioned in section II.5. comparison of figs. 1 and 4 of /Li76/ reveals a mistake in ref./Li76/, which, however, is only due to some error in drawing and does not affect the code used in the earlier PM, /Li83/. The fact that asymptotically

$$\langle g_o | \beta_o \rangle \sim 1/d \quad ,$$

i.e. this overlap diminishes very slowly, causes some special effects on asymptotic transition probabilities and quadrupole moments (see section III.3).

III.3 E2 Transitions and Quadrupole Moments in the EPM

The general features of transition probabilities in the EPM can very well be studied by using only the harmonic Hamiltonian. This facilitates comparison with the earlier PM and the classical collective model of Bohr and Mottelson. So in this chapter the number operator $\hat{N}$ is used as the laboratory Hamiltonian. The diagonalization introduces quite surprising results for some measurable quantities, and this is where the EPM differs from the other classical collective theories. On the other hand, most of the results agree with the earlier models and the usual vibrator and Alaga limits are recovered (this was discussed already earlier in section II.6.).

Figs. 8-10 show some intraband transitions for each of the ground, β and γ bands (the normalization B(E2;2g-->0g)=1, $\forall$ d, was used). The usual U(5) phonon and Alaga limits are recovered and the continuous increase in transition probability with increasing angular momentum is a direct consequence of boson-number non- conservation in the theory. This is in contrast to the algebraic approach of the IBA, where boson-number conservation and the use of only lowest-order bosons yield low-energy spectra where the bands terminate and produce diminishing transition probabilities at the upper end of the band. The only non-trivial thing in figs. 8-10 are the 'bumps' in the curves around the deformations d=1-2. Fig.8 should be compared with figure 12 of ref./Li76/ (almost the same)

The interband transition probabilities in figs. 11-13 are much more interesting (the normalization is B(E2;2g-->0g)=1). In the asymptotic limit all the interband transitions go to zero which indicates the adiabatic separation of intrinsic and rotational motion and the evolution of the projected states towards orthogonality (diminishing overlaps). In the small-d limit the B(E2) values go to the U(5) values of fig. 26 which indicates that the transition probabilities $B(E2;J_\beta \rightarrow J_g)$ should go to zero in this limit (phonon number selection rule). There are also non-trivial bumps in these curves, especially in the curves $B(E2;J_\beta \rightarrow J_\gamma)$, each of which has a pronounced maximum between deformation 2 and 3. The curve for J=2 has also a local minimum around d=1.5 (introducing thereby a local maximum near d=1). This complex behaviour of some B(E2)'s introduces also quite complex branching ratios discussed somewhat later below.

Very interesting curves are depicted in fig. 14, namely the interband B(E2)'s from J=2 to J=0 (the same normalization as above). The curves all go to zero in the small-d limit because of the phonon number selection rules, and asymptotically they approach zero. In the middle region the curves all have atleast one maximum and two of them also have quite an unpredictible minimum of magnitude zero. The most interesting thing about these transition probabilities is that they provide the best way of making comparison (in the region of rotor nuclei) between experimental B(E2)'s, classical collective model predictions and the algebraic IBA

predictions, because these B(E2)'s are experimentally always the best known. The comparison is most conveniently done in the figure below, in which the spectrum of a prolate (or oblate , d<0) symmetric rotor is drawn with the above B(E2)'s included as given in the framework of the EPM, IBA and BMM (the earlier PM gives the classical BMM results /Li83a/). The experimental values seem to be mostly in accordance with the EPM and IBA results, as one can see in chapter IV.

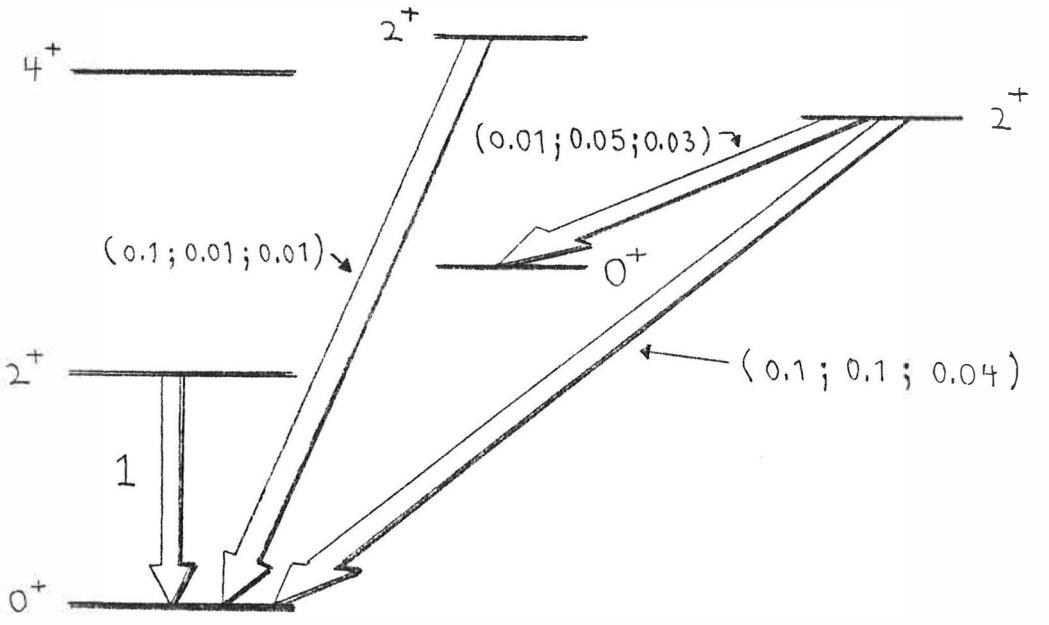

ground band β band γ band

Fig. III.1.
Spectrum of a symmetric rotor /Gn71/ with typical B(E2)'s from J=2 to J=0 indicated. The figures in parentheses are the yield of the BMM, IBA /Li83b/ and EPM (with H=$\hat{N}$). The normalization is chosen to be B(E2;2g-->0g)=1. It should be kept in mind that in the pure SU(3) limit of the IBA the β and γ bands belong to an SU(3) representation different from the ground band representation, and so the transitions from β and γ bands to the ground state band are strictly zero.

In fig.III.1 one can see that both the IBA and the EPM have a much weaker $2\beta \rightarrow 0g$ transition than the $2\gamma \rightarrow 0g$ transition, the value for the $2\gamma \rightarrow 0\beta$ transition being inbetween. This is quite the opposite to the description of the Bohr-Mottelson type models where the β and γ excitations are equally strong and the transitions from the γ to the β band are weak. Because the experimental results are in favour of the IBA description a great deal of argumentation is pursued about the validity of the geometrical quasi-band concept especially in the case of the β band /Li83b; Wa81a; Wa82a,b; Bo82; Ca80a,b; Ca83b/. The above behaviour is nicely shown by the asymptotic B(E2) expressions at the end of section II.6.

In figs 15-17 are shown some branching ratios which are the best known experimentally. The same branching ratios are also calculated for the earlier PM as a function of d in figs. 14 and 15 of ref. /Li76/. As is easy to see from fig. 17, the branching ratios behave quite violently as a function of d which , of cource, is a consequence of the complex behaviour of the B(E2)´s discussed above. When these EPM results are compared with those of /Li76/ one notices that the overall bahaviour of the branching ratios is more or less the the same in both models, but in the EPM most of the branchings have huge peaks (note the logarithmic scale) in the middle region d=1.0-3.5. This is due to the fact that the B(E2)´s go to zero at some specific values of the deformation parameter. These peaks indicate that in certain regions of the fitting parameters (even when the anharmonic terms are taken into account) the branching ratios range on a short parameter interval from $\sim 10^{5}$ to $\sim 10^{1}$ or from ~ 1 to 10^{-4} thus serving as a very sensitive indicator of the quality of the energy fit (much more sensitive than in the earlier PM).

The behaviour of the quadrupole moments in the EPM (for $\hat{H} = \hat{N}$) is more or less the same as in the earlier PM and in the BMM. The behaviour of the quadrupole moment of the J=2 triplet is shown in fig. 18. There one can see that the behaviour of the quadrupole moments is quite smooth (the same is true also for the other states of the bands). As pointed out in section II.6, the BM relation (B.17) holds true for asymptotic deformation parameters. By assuming the BM relation to hold exactly for large d, it is easy to get values for the intrinsic quadrupole moment of the BMM, eQ_0, by demanding the formula to agree with the EPM results for the J=2 states. After that one can check the deviation of the rest of the EPM values, as a function of d, from the values given by formula (B.17). The resulting intrinsic quadrupole moments are different for each band and thus one obtains a measure of the quadrupole shape of the nucleus in a consistent manner (it turned out that the intrinsic quadrupole moment of the β band is only a little greater than that of ground band, but for the γ band the difference is about 30%. This is in agreement with the intuitive pictorial representation of these vibration modes /Co71b,p.151/). The

study of the asymptotic limit of the EPM indicates that the γ band quadrupole moments behave exactly according to the BM formula, but the ground and β quadrupole moments seem to converge very slowly to the BM values. This is evidently due to the slow 1/d-convergence of the overlap $\langle g_0 | \beta_0 \rangle$ which causes here the adiabaticity to set in very slowly. One thing to be noticed is that for all these geometry-based models the quadrupole moment of the 3γ state is always zero and that $Q(2\gamma) \approx -Q(2\beta)$. In BMM this follows from the fact that

$$Q \propto 3K^2 - J(J+1) \quad .$$

It is to be noted that the $Q(3\gamma)=0$ property is not due to the vanishing of a 3j symbol, but is a more general feature of collective models, because it is true also for the IBA model (at least in the SU(3) limit).

III.4.Collective Potential Energy Surfaces in the EPM

Collective potential energy surfaces (=CPES) have been used by many authors (for example /Gn69,70a,71; Ku74/) to visualize the nuclear intrinsic shape and to get hold of the systematics of different nuclear spectra, i.e. the harmonic and anharmonic vibrators, symmetric and triaxial rotors /Da58,60 ; Ei75/ , γ-soft (or γ-unstable) nuclei /Gn70b, He77/ and nuclei with shape coexitence. It is remarkable that these special limits can also be realized as analytically solvable dynamical symmetries in the IBA model. In the CPES approach the potential energy of the nucleus (in intrinsic coordinates) is expressed as a function of the collective coordinates, which are here chosen to be the amplitudes of small vibrations, a_μ ,defined in eqs.(B.1) and (A2.12) (these were also chosen by the above authors). Moving over to first-quantized coordinates $\hat{\alpha}_m$ and performing second quantization (B.4) one has an effective means of classifying the states and calculating the matrix elements /Gn71/.

In the EPM one must transform from the oriented system to the intrinsic system. The oriented system was used to generate basis states for the diagonalization of the laboratory Hamiltonian. This diagonalization in the deformed 3-state basis yielded, after fitting to experimental data, a number of parameters that defined the form of the effective boson expansion (III.2.3) (in the work of Gneuss et al. harmonic-oscillator basis states corresponding up to 33 phonons were used). Now, one can use the inverse transformation of eq. (B.4), i.e.

$$b_m^+ = \sqrt{\frac{\omega B_0}{2\hbar}}\left(\hat{\alpha}_m + \frac{1}{i\omega B_0}(-1)^m \hat{\pi}_{-m}\right)$$

(III.4.1)

$$b_m = \sqrt{\frac{\omega B_0}{2\hbar}}\left((-1)^m \hat{\alpha}_{-m} - \frac{1}{i\omega B_0}\hat{\pi}_m\right) \quad ,$$

where $\omega = \sqrt{C_0/B_0}$,and then transform the potential part to the intrinsic coordinates by (A2.12). A usual way of expressing to potential is the form

$$V = V(\beta,\gamma) \quad ,$$

where the Hill-Wheeler coordinates β and γ are defined by (B.5). Transforming, for example, the number operator $\hat{N}$ by the formulas (III.4.1) one obtains

(III.4.2) $$\hat{N} = \frac{1}{2\hbar\omega}\left[\frac{1}{B_0}\hat{\bar{\pi}}^2 + C_0\hat{\alpha}^2 - 5\hbar\omega\right], \quad \hat{\bar{\pi}}_m = (-1)^m \hat{\pi}_{-m}$$

which corresponds to the harmonic Hamiltonian (B.2) when taking into account the relation (B.3) and remembering that $\hat{\bar{\pi}}$ and $\hat{\alpha}$ are Hermitian tensor operators, eq. (A1.25), and that in first quantization $\alpha^* \to \hat{\alpha}^\dagger$. Also the classical relation

$$\pi_m = \partial L / \partial \dot{\alpha}_m$$

is used (L is the Lagrangian of the harmonic system). In the same way one obtains for the term B_{20} the expression

(III.4.3) $$B_{20} = \frac{1}{\hbar\omega}\left(-\frac{1}{B_0}\hat{\bar{\pi}}^2 + C_0\hat{\alpha}^2\right).$$

The third-order terms are a bit more involved, and for them one obtains

(III.4.4) $$B_{30} = B_{21} = (2\hbar^3\omega B_0)^{-\frac{1}{2}}\left\{-[\hat{\bar{\pi}}\hat{\bar{\pi}}]_2\cdot\hat{\alpha} + \right.$$
$$\left. + 2[\hat{\bar{\pi}}\hat{\alpha}]_2\cdot\hat{\bar{\pi}} + (B_0\omega)^2[\hat{\alpha}\hat{\alpha}]_2\cdot\hat{\alpha}\right\}$$

Performing this transformation on all the terms of the effe-

ctive Hamiltonian (III.2.3) and then dropping the terms which include the canonical momentum operator $\hat{\pi}$, one obtains

$$
\begin{aligned}
V(\hat{\alpha}) = {} & \tilde{d}^2(c_0+2c_1-c_2-2c_3+2c_4+c_5+6c_6)\hat{\alpha}^2 + \\
& + \sqrt{14}/d\cdot\tilde{d}^3(-\tfrac{1}{2}c_2-c_3+2c_4+c_5)[\hat{\alpha}\hat{\alpha}]_2\cdot\hat{\alpha} + \\
& + \tilde{d}^4(10c_4/d^2-6c_6)[\hat{\alpha}\hat{\alpha}]_0[\hat{\alpha}\hat{\alpha}]_0 + \\
& + \tilde{d}^4(7c_5/2d^2-3c_6)[\hat{\alpha}\hat{\alpha}]_2\cdot[\hat{\alpha}\hat{\alpha}]_2 + \\
& + 4\tilde{d}^4c_6[\hat{\alpha}\hat{\alpha}]_4\cdot[\hat{\alpha}\hat{\alpha}]_4 - \\
& - 5\hbar\tilde{d}^2/\omega B_0(c_0-c_1+c_5+6c_6) \quad ,
\end{aligned}
$$

where

$$
\tilde{d} = \sqrt{C_0/2\hbar\omega} = d/\beta_0 \tag{III.4.5}
$$

After performing the transformation on the intrinsic (principal axis) system and utilizing the relation (B.5) one obtains

$$
\begin{aligned}
\alpha^2 &= \beta^2 \\
[\alpha\alpha]_2\cdot\alpha &= -\sqrt{2/7}\beta^3\cos3\gamma \\
[\alpha\alpha]_0[\alpha\alpha]_0 &= \tfrac{1}{5}\beta^4 \\
[\alpha\alpha]_2\cdot[\alpha\alpha]_2 &= 2\beta^4/7 \\
[\alpha\alpha]_4\cdot[\alpha\alpha]_4 &= 18\beta^4/35
\end{aligned}
$$

and

$$
V(\tilde{\beta},\gamma) = d^2\tilde{\beta}^2\left[A_1 - 2\tilde{\beta}A_2\cos3\gamma + \tilde{\beta}^2A_3\right] - 5A_4/2 \quad , \tag{III.4.6}
$$

where

$$A_1 = c_0 + 2c_1 - c_2 - 2c_3 + 2c_4 + c_5 + 6c_6$$

(III.4.7) $$A_2 = -\tfrac{1}{2}c_2 - c_3 + 2c_4 + c_5$$

$$A_3 = 2c_4 + c_5$$

$$A_4 = c_0 - c_2 + c_5 + 6c_6$$

and

(III.4.8) $$\tilde{\beta} \equiv \beta/\beta_0 \quad ,$$

i.e. $\tilde{\beta}$ indicates the deformation β in units of the oriented deformation (which was defined in eq. (II.1.1)) β_0 of eq. (II.1.1). (Note that the potential of eq. (III.4.6) is the same as in /Gn71/, p. 455 , but there is a difference of $1/\sqrt{5}$ stemming from different scalar coupling conventions. Also now in (III.4.6) there is a constant term and all the parameters A_i have a definite value coming from the energy fits).

It is not surprising that one ends up with such a simple expression (III.4.6) for the potential. This is due to the fact that the most general rotationally invariant potential $V(\alpha_{2\mu})$ can always be written as a function of two invariants

$$\gamma_1 \equiv [\hat{\alpha}\hat{\alpha}]_0 \equiv [\alpha^2, v=0, L=0] = \beta^2/\sqrt{5}$$

$$\gamma_2 \equiv [[\hat{\alpha}\hat{\alpha}]_2\hat{\alpha}]_0 \equiv [\alpha^3, v=3, L=0] = -\sqrt{2/35}\,\beta^3\cos 3\gamma \quad ,$$

where v denotes the seniority quantum number. So

$$[[\hat{\alpha}\hat{\alpha}]_L[\alpha\alpha]_L]_0 = \zeta_L \cdot \gamma_1^2 \dashrightarrow \zeta'_L \beta^4 \quad .$$

In the general case of any tensor the seniority quantum number is also active /No68/.

In the work of Gneuss and Greiner only the harmonic kinetic energy was extensively used (higher-order kinetic terms proved to be unimportant), and the ansatz for the potential $V(\beta,\gamma)$ reached up to sixth order in $\hat{\alpha}$. Consequently a considerable asymmetry between the kinetic terms and the potential terms existed. In the EPM the effective Hamiltonian (III.2.3) is built up of $b^\dagger$'s and $\bar{b}$'s and therefore it includes many kinetic terms (pure $\hat{\pi}$'s and mixed terms) which may considerably affect the nuclear spectrum without it showing up in the expression (III.4.6). This makes comparison between the energy spectrum and the nuclear intrinsic potential landscape more difficult and thus excludes the possibility of a Gneuss- Greiner type of interpretation of the spectra.

In order to reproduce all physically relevant potential

energy surfaces one needs enough terms in the potential expansion (at least the sixth order must be included, /Gn71, He77/). In the case of the EPM, potential terms only up to fourth order are included, which makes the potential surfaces very unstable against negative divergences at infinity. These divergences cause the local minimum solutions to be quasi stationary, i.e. non-stationary continuum solutions with a long tunneling time. In this sense the potential energy expansion in the EPM may only be viewed as perturbative because one uses a vastly truncated effective boson Hamiltonian and because of the fact that in choosing only a three-state model space the diagonalization in this space corresponds to a perturbation calculation in that matrix elements connecting this three-state basis to the rest of the collective space are neglected (the same aspect is seen also in the work of G&G, but there the model space is larger and the convergence is tested /Gn71/).

Together the limited (although deformed and thus somehow optimized) basis and the truncated Hamiltonian yield potential surfaces (of fitted nuclei) that have a very rich structure, but mostly bending down to negative infinity in some part(s) of the β-γ plane unless there is an absolute minimum at zero deformation. So, one cannot make definite conclusions about the shape of the nucleus, nor can one establish a one-to-one correspondence with energy spectrum. The inclusion of higher-order terms in the boson expansion and/or the extension of the model space could make Gneuss & Greiner type investigations possible also in the EPM.

IV. APPLICATION OF THE EPM TO VARIOUS CHAINS OF ISOTOPES

IV.1. General

The earlier isotropic PM was tested extensively in /Sa77/ and had a surprisingly good success in describing nuclear low-spin spectra from vibrators to almost rigid rotors. The main reason for this was the chosen model space which had properties that were tailor made for describing nuclear deformations. The fitting to experimental data was easy because the model contained only two free parameters, the deformation/softness parameter d and the energy scale parameter c_1 (the anisotropic version of the model contained four parameters /Ho72/). The fitting procedure was easy because one usually fixed the levels 2g and 4g and thus obtained a very good description of the ground-state band (also the projection procedure is the most accurate for the ground band). A drawback of the model was the incapability to affect the β and γ band heads, which often were totally wrong, and the spectroscopic moment of inertia of a band.

The EPM has a cure for the above-mentioned shortcomings at the cost, of course, of introducing more fitting parameters, thus making the fitting process more complicated and reducing the transparency of the interpretation of the parameters involved in the fit. The process of searching for the absolute minimum of a many-parameter surface is always a complicated task, and the inaccuracy in the calculation of the functional to be minimized (i.e. numerical noise) causes additional difficulties in the areas of small directional derivatives. In the work /Sa77/ no systematic study was made of the behaviour of d and c_1 as functions of mass number in any isotopic chains. Such a systematic study, however, was performed in the case of the EPM by the author /Su84/ for the Sm, GD, Er and Yb chains. These results have been plotted and are discussed separately in the context of the discussion of each isotopic chain. Because the only free parameter of the transition probabilities and the static quadrupole moments is fixed by the 2g-->0g transition, The above energy-based systematics will also give as a byproduct the systematics for various quadrupole moments and transition probabilities. The parameter systematics (a byproduct of the

energy fits) is represented in figs. 19 and 23 and the (most interesting) E2 systematics in figs. 24 and 25.

Because the relative transition probabilities contain no further parameters and because their behaviour is very sensitive to the fitted parameters (see section III.3), they serve as an indicator of the goodness of the energy fit and often help to decide which one of the nearly equally deep minima is the more correct one. Sometimes the decision is still very hard to make and a subjective opinion is needed to decide which one of the bands is to be fitted well or which of them need not be so accurate.

In this work a comparison of three models is performed for many nuclei. These models are the EPM, the isotropic PM and IBA-1 model. The older IBA fits are done using the normal boson numbers, but some recent fits use the effective boson number discussed in /Sc83/. The IBA fits are done either with four parameters /Li82,Li83c/ or with six parameters /Kr84a, Kr84b, Li84a, Li84b,Kr84c/. As an indicator of the goodness of the energy fit the so-called RMS value

$$\text{(IV.1.1)} \qquad RMS \equiv \sqrt{\frac{1}{N}\sum_{i=1}^{N}\left(E_i^{th} - E_i^{exp}\right)^2}$$

(N is the number of the energy levels included) is used. In many other works, however, a dimensionless quantity

$$\text{(IV.1.2)} \qquad RMS\% \equiv \sqrt{\frac{1}{N}\sum_{i=1}^{N}\left(\frac{E_i^{th}}{E_i^{exp}} - 1\right)^2} \cdot 100\,\%$$

is used /Ha70, Ho72, Ha73/.

IV.2. Parameter Systematics and the Convergence of the Boson Expansion

One can make systematic fits to real nuclei using second-, third- and fourth-order effective Hamiltonians of eq. (III.2.2). When the deformation parameter d is taken into account, this means a three-, four- and five-parameter fit, and a test of the convergence of the phenomenological boson expansion is attained. In figs. 19 to 23 these three different types of fit are represented by displaying the values of the parameters d, C_0, C_1, C_2 and C_5 as a function of isotopic mass number. The fitting is performed in four isotopic chains, namely for the even-even Gd, Sm, Er and Yb isotopes of which only those are selected about which there are enough low-energy data (mostly obtained by Coulomb excitation) available. The fit was made to more than one or two levels of each band (if possible) as a least-squares fit using weighted terms in the summation. (see eq. (III.1.4)) In this way, in addition to a proper description of the band heads, a proper description of the spectroscopic moments of inertia could be achieved.

The parameter systematics of the above-mentioned figures show a very consistent overall scheme, and clear trends may be observed in the behaviour of the fitting parameters. The deformation parameter grows all the way from mass number 146 to mass number 174 (with few exceptions). This is consistent with the shell model picture that going farther from the closed shells towards the middle of the shell the nuclei develop from vibrators towards rigid rotors. The compressive effect on the energy spectrum of increasing d is counterbalanced by an increasing scale factor of the effective Hamiltonian, which means an increase in the absolute values of the rest of the Hamiltonian parameters. The spacial behaviour of the parameters in the beginning of the Sm chain is to be attributed to the lack of experimental data (causing the fit to be unreliable to a certain extent) and/or to real shell effects (shell closure at N=82)

The convergence of the boson expansion may be seen from two features of the systematics. One is the diminishing of the absolute values of the parameters when going from C_0 to C_5, which is clearly seen in the figures. The other feature is that the parameters do not change much in absolute value when going from a three-parameter to a five-parameter fit. It is seen, however, that there is a greater change in the parameter values when going from the third-order Hamiltonian to the fourth-order one than when going from second order to third order (in the case of convergence one would expect the behaviour to be the other way round). This can be explained by the absence of many terms from the fourth-order Hamiltonian, and so when comparing the complete 2^{nd}, 3^{rd} and 4^{th}

ordes, the situation would evidently be the other way around.

The most consistent fits seem to occur in the case of Sm and Gd isotopes, for which the convergence seems to be quite rapid. On the other hand, the convergence seems to be slower for the Yb isotopes, where the incompleteness of the fourth-order of the Hamiltonian seems to play a more important role. The most striking is the behaviour of the parameters in the Er chain, where the convergence seems to be the slowest but the relative importance of the incomplete fourth-order does not seem to be as great as in the Yb chain.

It may be noted that the parameters behave quite smoothly all the way and their values seem to be reasonable (i.e. the absolute minimum of the many-parameter surface is evidently found). In the case of the old PM the there was no real need for doing this kind of parameter systematics because there were only two parameters involved /Sa77/. However successful attempts have been made at establishing such systematics in the case of the IBA model /Ca82b/. On the other hand, Kracíková et al. /Kr84a,b/ discovered some surprising discontinuities in the IBA-1 parameter behaviour in the parts of the Sm chain where the EPM gives this smooth behaviour of parameters. This is a good example of the difficulties involved in fitting to experimental data. A possible cure for this lack of uniqueness in the IBA is the so-called consistent-Q framework discussed in /Wa82b,Wa83/.

IV.3. Application of the EPM to Different Isotopic Chains

Comparison with Experiment and Other Models

Comparison between the EPM and the earlier PM and IBA-1 models is given mainly in the tables of the following chapters. The main emphasis is put on comparison with the latest 6-parameter IBA-1 fits of Lipas et al.. For the EPM all the calculated energy level data are gathered into tables H.1 to H.4 of appendix H, where the 4- and 5-parameter results are shown. As a measure of the goodness of fit the RMS value of eq.(IV.1.1) is shown.

For the IBA model there are some difficulties in choosing the right number of valence bosons in the proton shell 50-82. This is because there have been ambiguities is choosing the correct proton number for the inert core stemming from the closed-shell features of proton number 64 /Ca81,Og78/. To solve this ambiguity, the so-called effective proton-boson number, Z_{eff}, is introduced and it is obtained from figure 1 of ref. /Sc83/. In recent work by Lipas et al. this Z_{eff} is used and it gives in many cases better results than the boson number based on the Z=50 core.

IV.3.A. The Samarium Isotopes

The Sm isotope chain in this work begins with the two-neutron hole isotope $^{142}_{62}Sm_{80}$. The chain extends to the well-deformed nucleus $^{156}_{62}Sm_{94}$. As pointed out in /St81/, an

BAND	J	^{146}Sm EXP.	^{146}Sm IBA	^{146}Sm EPM 4	^{146}Sm EPM 5	^{148}Sm EXP.	^{148}Sm IBA	^{148}Sm EPM 4	^{148}Sm EPM 5
γ	2	747	733*	700*	694*	550	559*	557*	547*
	4	1381	1353*	1383*	1360*	1180	1188*	1161*	1197*
	6	1812	1869*	2034*	2011*	1906	1823*	1773*	1884*
	8	2738	2287	2656*	2661*	2545	2453*	2384	2488
	10	(3723)	2615	3258	3316	(3235)	3343*	2995	2904
β	0	1452	1459*	1421*	1416*	1426	1428*	1372*	1432*
	2	(2156)	2173*	2030*	2162*	1664	1752*	1804*	1658*
	4	--	2790	2805	3039	(1895)	2123*	2423	1869
	6	--	--	3553	3920	--	3086	3132	2236
	8	--	--	4301	4813	--	--	3878	2723
	10	--	--	5053	5725	--	--	4642	3420
γ	2	1648	1610*	1708*	1659*	1454	1430*	1472*	1454*
	3	(2269)	2457*	2389	2438	(1904)	1861*	1923	1755
	4	(2439)	2256*	2297	2448	(1733)	1828*	2076	2042
	5	--	2800	3104	3254	(2147)	1986*	2582	2250
	6	--	--	2930	3183	--	2276	2667	2541
	7	--	--	3816	4052	--	2476	3260	2770
RMS		--	187	102	91	--	58	98	24
		--	(388)	(182)	(156)	--	(106)	(243)	(142)

BAND	J	^{150}Sm EXP.	^{150}Sm IBA	^{150}Sm EPM 4	^{150}Sm EPM 5	^{152}Sm EXP.	^{152}Sm IBA	^{152}Sm EPM 4	^{152}Sm EPM 5
γ	2	334	340*	342*	326*	122	110*	127*	120*
	4	773	771*	749*	798*	366	344*	377*	377*
	6	1279	1279*	1188*	1294*	707	679*	693*	725*
	8	1837	1821*	1657*	1814*	1125	1099*	1038*	1115*
	10	2432	2432*	2152*	2367*	1609	1579*	1399*	1522*
β	0	740	724*	773*	757*	685	665*	717*	720*
	2	1046	983*	1067*	999*	810	776*	812*	799*
	4	1449	1491*	1933*	1462*	1023	1030*	1017*	982*
	6	--	--	2131	2085	1310	1328*	1321*	1275*
	8	--	--	2745	2795	1666	1762*	1709*	1682*
	10	--	--	3388	3558	2080	2082*	2158*	2188*
γ	2	1194	1214*	1274*	1203*	1086	1052*	1131*	1134*
	3	1504	1504*	1486*	1430*	1234	1239*	1233*	1226*
	4	1643	1635*	1564*	1764*	1372	1365*	1365*	1348*
	5	2020	2028*	2066*	1994*	1559	1621*	1510*	1491*
	6	--	--	2660	2514	(1728)	--	1696	1670
	7	--	--	2687	2657	(1946)	--	1865	1850
RMS		--	24	176	49	--	36	66	46
		--	--	--	--	--	--	(66)	(51)

Table IV.3.1. Comparison of the EPM and the 6 parameter IBA fits for $^{146-152}$Sm . For the EPM four and five parameter fits are indicated. The RMS's in parentheses correspond to the energy data in parenthesis (the asignment of the Sakai quasi-band label to these levels is not unambiquous). The experimental and IBA data are taken from /Kr84a/ and /Li84c/ . The asterisk indicates a fitted level. All the data are in keV.

B(E2;J-->J')		^{146}Sm				^{148}Sm			
J	J'	EXP.	IBA	EPM		EXP.	IBA	EPM	
				4	5			4	5
2g	0g	0.048	0.016	0.028	0.048	0.146	0.146	0.146	0.146
4g	2g	≥0.061	0.029	0.094	0.098	0.25	0.21	0.26	0.24
6g	4g	0.04	0.04	0.14	0.15	--	0.23	0.38	0.31
8g	6g	--	--	0.20	0.19	--	0.21	0.50	0.27
0β	2g	--	--	0.083	0.10	--	0.050	0.17	0.058
2β	0g	--	--	$9\cdot10^{-5}$	$7\cdot10^{-6}$	--	0.0016	0.0002	$6\cdot10^{-4}$
2β	2g	--	--	0.013	0.004	--	0.002	0.002	0.003
2β	4g	--	--	0.033	0.043	--	0.012	0.11	0.054
2γ	0g	--	--	0.004	0.002	0.008	0.008	0.007	0.007
2γ	2g	--	--	0.039	0.065	0.089	0.209	0.13	0.076
2γ	4g	--	--	0.026	0.012	--	0.0104	0.0066	$2\cdot10^{-4}$
2γ	0β	--	--	0.044	0.019	--	0.010	0.023	0.008

B(E2;J-->J')		^{150}Sm				^{152}Sm			
J	J'	EXP.	IBA	EPM		EXP.	IBA	EPM	
				4	5			4	5
2g	0g	0.269	0.269	0.269	0.269	0.680	0.680	0.680	0.680
4g	2g	0.515	0.470	0.51	0.454	1.02	0.93	1.04	1.01
6g	4g	--	--	0.73	0.68	1.18	0.96	1.29	1.20
8g	6g	--	--	0.90	0.87	1.38	0.88	1.57	1.43
10g	8g	--	--	1.0	1.0	1.54	0.75	1.86	1.71
4γ	2γ	--	--	0.35	0.23	0.343	0.333	0.53	0.52
0β	2g	0.25	0.43	0.46	0.27	0.161	0.026	0.169	0.091
2β	0g	0.0043	0.036	0.0015	0.0053	0.0046	0.0067	0.0012	0.0014
2β	2g	0.362	0.020	0.026	0.036	0.029	0.006	0.023	0.013
2β	4g	0.639	0.161	0.140	0.240	0.095	0.021	0.19	0.12
4β	2g	--	--	$1\cdot10^{-5}$	0.017	0.0053	0.0071	0.0009	0.0005
4β	4g	--		0.014	0.065	0.034	0.0025	0.04	0.02
2γ	0g	0.0102	0.0102	0.015	0.0095	0.018	0.018	0.035	0.027
2γ	2g	0.0335	0.0171	0.140	0.0643	0.046	0.075	0.090	0.061
2γ	4g	0.043	0.038	0.090	0.038	0.0037	0.0047	0.013	0.0077
4γ	2g	--	--	0.006	$1\cdot10^{-4}$	0.0036	0.0009	0.0095	0.0083
4γ	4g	--	--	0.11	0.032	0.034	0.071	0.10	0.074
2γ	0β	0.036	0.061	0.17	0.046	--	--	0.016	0.010
4γ	2β	--	--	0.017	0.052	0.0011	0.0050	0.0219	0.0112
2β	0β	0.723	0.255	0.212	0.395	1.85	0.40	1.09	1.08

TABLE IV.3.2. The same as table IV.3.1, now for transition probabilities. The asterisk indicates a fitted transition. All the figures are given in units of e^2b^2 .

abrupt shape change may be noticed between neutron numbers 88 and 90, i.e. ^{150}Sm may be considered spherical and ^{152}Sm deformed (this is seen in the EPM from the discontinuous behaviour of the fitting parameters in A=150,152 region). It may be noted that the use of the shell model is simple only up to ^{150}Sm because of the onset of deformation at ^{152}Sm /St81, Zo80/.

The EPM results can be compared with the results given by the IBA model. There have been numerous IBA calculations (fits to individual nuclei, to a whole chain and fits by the schematic monopole and quadrupole pairing model) in Sm region /Ca80a,Ca80b,Sc78,Sc79a,Sa79,Su77,Su79,Ca79,Ca82b, Ar82/. The purpose now is to compare the EPM results with 6-parameter IBA-1 results of Lipas et al. for ^{146,148,150,152}Sm (I have performed the fit with the EPM also to ^{142,144,154,156}Sm, and the results are tabulated in appendix H). In the IBA calculations the effective proton number Z_{eff} is used for $^{148-152}$Sm, but the usual Z is used for ^{146}Sm because the use of Z_{eff} gives bad results. Z_{eff} and the other IBA-1 parameters are tabulated in appendix G.

The comparison for the isotopes is presented in table IV.3.1, where the ^{146}Sm IBA data are taken from /Kr84a/ and the IBA data of ^{148,150,152}Sm from /Li84c/ (the corresponding normal boson-number IBA data can be found in refs. /Li84a,b; Kr84a,b,c/). The IBA and EPM fits are strikingly good, The EPM fits being a bit better in the case of ^{146,148}Sm and the IBA fits being a little better for ^{150,152}Sm. As one can see from the tables of appendix H, also the EPM fits for ^{154}Sm and ^{156}Sm are excellent (especially for ^{154}Sm for which 4- and 5-parameter fits give RMS=12keV including all the 11 known states). Appendix G tells that the IBA parameters behave very strangely for ^{148}Sm and ^{150}Sm. The fits are excellent, but the initial parameter values obtained from perturbation theory /To83,Li84d/ lead to strange values for the final parameters (this is especially noticeable in the case of the single-boson energy parameter EPS, see also /Kr84b/). Such strange behaviour is attributed to the effective nature of the parameters by Van Isacker et al. /Is82/. Instead of using this effective boson number, one could use the normal boson number /Kr84b/, or one can count proton bosons from Z=64 /Gi82,Wo83/; yet another choise is to use only four bosons /Ha78, Ha79/. (in the above refs. this was done for ^{148}Sm). However, it seems that the results are more or less of the same caliber, independently of the boson number used in the calculations.

The transition probabilities for the four isotopes are indicated in table IV.3.2 including experimental, IBA and EPM values in units of e^2b^2. In the case of ^{146,148}Sm, the EPM gives the following results for the branching ratios whose experimental and IBA values are tabulated in table 7 of ref. /Kr84a/ and in the footnote of table 6 of ref. /Kr84b/.

B(E2;J-->J') / B(E2;J-->J")			^{146}Sm				^{148}Sm		
J	J'	J"	EXP.	IBA	EPM[b]		EXP.	EPM[b]	
					4	5		4	5
2γ	2g	0g	50	50*	11	27	--	19	11
3γ	4g	2g	4.8	9.7	2.6	3.1	--	9.5	6.5
3γ	2γ	4g	1.2	3.0	1.2	1.1	--	4.8	7.5
5γ	6g	4g	6.3	8.3	3.0	3.8	--	15.6	12.6
2β	2g	0g	11	65	146	634	11[a]	10	5

TABLE IV.3.3.
Experimentally known branching ratios for ^{146}Sm and ^{148}Sm. The experimental and IBA figures are from /Kr84a,b/.
a) 1.25 in /Kr84b/ for the IBA
b) four and five parameter fits
* means a fitted branching.

The EPM results are very good compared with the IBA results especially when taking into account that the transition operator in EPM has only one free parameter which is always fixed by the 2g-->0g transition. In the IBA one has two phenomenological parameters in the transition operator and one can fit either two transition probabilities or branching ratios or their combinations. For the isotopes ^{150}Sm and ^{152}Sm quite an extensive comparison between the IBA and the EPM can be made because there are extensive experimental data available (as can be seen in table IV.3.2). Comparing the corresponding figures, one easily sees that for ^{150}Sm the EPM does better than the IBA but for ^{152}Sm the models apply roughly equally well. Again the EPM has the advantage of

using fewer parameters both in the energy fit and in the transition probability fit. As can be seen in table 1 of ref. /Li76/, already the old PM does very well with the branching ratios in the case of ^{152}Sm using only two energy-fit parameters; in this case the EPM gives no significant improvement.

The parameter systematics of figs. 19 to 23 give an indication of discontinuities in parameter behaviour at $^{144}_{62}$Sm and at $^{152}_{62}$Sm. The first cusp at ^{144}Sm can be explained by the closure of the 50-82 neutron shell. The second one is of the same kind as the discontinuity in the Gd chain at ^{158}Gd (though not so distinctive, see section IV.3.B). The fits for ^{142,144}Sm are uncertain because of the lack of experimental data. The same features are also clearly seen in the quadrupole moment and transition probability systematics of figs. 24 and 25, where, for example, the shell closure at ^{144}Sm is realized by local extremum values of the curves at A=144.

IV.3.B. The Gadolinium Isotopes

In this chapter the chain $^{150-160}$Gd of gadolinium isotopes is discussed in the light of the EPM, the IBA and the earlier PM. There are several publications about IBA fits to Gd isotopes /Ca80a,b; Go81c; Ca82b; Li82; Li84a; Gi83/, but there are two publications that are used in this work for comparison purposes; these are /Li82, Li83c/ and /Li84a/. (/Li83/ and /Li83c/ have the same content).

First one can compare the earlier PM and 4-parameter IBA results of refs. /Li82, Li83c/ with the 4-parameter EPM calculation for the whole chain $^{150-160}$Gd. As can be seen from the parameter systematics, figs. 19 to 23, the behaviour of the four EPM fitting parameters agrees with the behaviour of the PM and IBA fitting parameters of figs.7 and 8 of ref. /Li83c/. This behaviour reveals a shape/phase transition at N=88-90 (A=150-152), which has been discused in a qualitative microscopic way by Casten et al. /Ca83/. Another common feature of the earlier PM (isotropic and anisotropic) and the EPM is the discontinuous behaviour of the parameters at N=94-96 (A=158-160), which seems to be of the same origin as the discontinuity in the Sm chain at ^{152}Sm (see chapter IV.3.A). No good explanation for this behaviour is thus far

known. As in the case of the Sm isotopes, the quadrupole moment and transition probability systematics of figs. 24 and 25 support the above speculations of a shape transition and also give indications of the discontinuity at ^{158}Gd.

A quantitative comparison of the three models is performed in table IV.3.4, which gives the RMS values corresponding to the known experimental levels (taken from /Li82/) for the three models. The PM and IBA data are taken from /Li83c/ and the EPM data from the tables of appendix H. One can clearly see from the table below that the EPM does not work very well in the case of ^{150}Gd and ^{152}Gd.

NUCLEUS	NUMB. OF LEVELS	PM[a]	four. param. IBA-1[a]	four param. EPM
150 Gd	9 (11)	355 (324)	188 (178)	195 (237)
152 Gd	16 (17)	288 (291)	52 (51)	167 (164)
154 Gd	16 (17)	225 (231)	126 (123)	64 (62)
156 Gd	16 (17)	250 (257)	117 (113)	23 (26)
158 Gd	12 ---	186 ---	22 ---	18 ---
160 Gd	8 (9)	105 (104)	11 (13)	29 (27)

TABLE IV.3.4 :
Comparison of the isotropic PM, the 4-parameter IBA and the EPM using the RMS deviation of eq.(IV.1.1). The figures in parenthesis correspond to each other.
a) Calculated from the data of refs./Li82, Li83c/.

In addition to the complex level structures of these isotopes, a reason for this is the band recognition difficulties and (possibly) the inaccuracy in calculating the functional to be minimized. Also the earlier PM and the IBA have difficulties in this region although the IBA can predict the Gd levels surprisingly well. It must be remembered that the earlier projection model gives very good fits to ground

B(E2;J--›J´)/B(E2;J--›J*)			^{150}Gd				^{152}Gd			
J	J´	J*	EXP.	PM	IBA	EPM	EXP.	PM	IBA	EPM
2β	0g	2g	0.051	0.29	0.05	0.006	0.020	0.41	0.06	0.22
2β	2g	4g	--	0.15	0.17	0.11	--	0.22	0.45	0.28
2β	0β	2g	--	17.6	4.54	14	2.14	13.8	2.14	4.96
4β	2g	4g	0.0017	0.30	0.13	0.072	--	0.43	0.11	0.22
4β	2β	4g	--	60.7	0.46	0.72	7.3	35.8	6.0	6.4
2γ	0g	2g	0.032	0.09	0.12	0.039	0.14	0.19	0.06	0.06
2γ	2g	4g	--	20	0.77	4.4	--	333	0.41	1.8
3γ	2g	4g	0.12	0.68	0.82	0.077	0.45	0.98	0.39	0.32
4γ	2g	4g	>0.009	0.0067	0.34	0.0061	0.071	0.021	0.11	0.029

B(E2;J--›J´)/B(E2;J--›J*)			^{154}Gd				^{156}Gd				^{158}Gd			
J	J´	J*	EXP.	PM	IBA	EPM	EXP.	PM	IBA	EPM	EXP.	PM	IBA	EPM
2β	0g	2g	0.12	0.58	0.61	0.04	0.17	0.63	0.82	0.20	0.49	0.65	0.55	0.59
2β	2g	4g	0.36	0.37	0.39	0.15	0.92	0.43	0.35	0.27	1.22	0.46	0.51	0.22
2β	0β	2g	--	19.3	103	31	--	28.3	310	61	--	37.2	688	81
4β	2g	4g	0.10	0.73	0.84	0.02	0.20	0.85	2.6	0.04	1.05	0.91	0.50	1.15
4β	2β	4g	33.9	34.6	177	23.2	--	46.8	956	53	--	60	881	236
2γ	0g	2g	0.49	0.47	0.60	0.38	0.67	0.56	0.61	0.53	0.61	0.60	0.64	0.45
2γ	2g	4g	5.95	33	14	4.88	11.5	25	17	5.9	17	20	14	14
3γ	2g	4g	1.00	1.7	1.75	0.72	1.5	1.9	1.8	1.1	0.37	2.1	1.96	1.16
4γ	2g	4g	--	0.12	0.24	0.08	0.16	0.19	0.24	0.18	--	0.22	0.28	0.09

TABLE IV.3.5. Comparison of experimental branching ratios with the theoretical ones given by the PM, IBA and the EPM. The PM is the isotropic projection model of /Li76/ and IBA means the four parameter IBA-1. The figures for both these models and the experimental ones are taken from /Li82,Li83c/.

state levels (fitting parameters are fixed by ground band levels) but the β and γ bands are predicted badly because there are not enough parameters to fit the β and γ band heads. The isotopes $^{154-160}$Gd are fitted quite well by both the IBA and the EPM. The EPM is much better than the IBA for Gd; and both are about equally good for ^{158,160}Gd.

In the table IV.3.5 the three models are compared with experiment in the case of known branching ratios (^{160}Gd is missing from the table because there are no experimental data available). Comparing the figures of the table, one sees that none of the models is very superior to the others. The EPM always seems to give the best or second best branchings. The PM and the IBA seem equally good on the average. Because there are not many experimental data available the comparison is not on a very firm basis. However, it is worthwhile noting that the old PM gives in many cases very good results despite the fact that in the energy fit it describes the β and γ band heads quite inaccurately.

In ref. /Li83c/ the internal structure of the quasi-bands was studied by drawing pictures of certain spectroscopic moments of inertia as a function of the angular momentum (figs. 4,5 and 6 in /li83c/; actually first and second energy differences were drawn). The so-called kinematic moment of inertia is a purely kinematic quantity and is defined as /St83/

$$\text{(IV.3.1)} \qquad \mathcal{J}/\hbar^2 \equiv I/\hbar\omega = I(\partial E/\partial I)^{-1} \quad .$$

The dynamic moment of inertia $\tilde{\mathcal{J}}$ describes how the nucleus responds to to a force and is defined as /St83, Go81a,b/

$$\text{(IV.3.2)} \qquad \tilde{\mathcal{J}}/\hbar^2 = (\partial^2 E/\partial I^2)^{-1} = 1/\hbar\, \partial I/\partial\omega$$

One gets the corresponding spectroscopic quantities by remembering the discreteness of I and thus writing (with an obvious notation and J = ħI)

$$\text{(IV.3.3)} \qquad \mathcal{J}^{\gamma|\beta\ -1}_{SPEC}(J) \equiv \frac{1}{2J}\Delta E^{\gamma|\beta}_J = \frac{1}{2J}(E_{J+2} - E_J) \quad ,$$

$$\mathcal{J}^{\gamma\ -1}_{SPEC}(J) \equiv \Delta E^{\gamma}_J / J = \frac{1}{J}(E_{J+1} - E_J) \quad ;$$

1) ^{154,156}Gd

$$\tilde{\mathcal{J}}^{-1}_{SPEC}(J) \equiv \frac{1}{4}\Delta^2 E_J^{\gamma/\beta} = \frac{1}{4}\left[\Delta E_{J+2} - \Delta E_J\right]$$

(IV.3.4)

$$\tilde{\mathcal{J}}^{-1}_{SPEC}(J) \equiv \Delta^2 E_J^{\gamma} = \Delta E_{J+1} - \Delta E_J$$

The latter reduces to

$$\tilde{\mathcal{J}}^{-1}_{SPEC}(J) = \frac{1}{4}\left[E_{J+4} - 2E_{J+2} + E_J\right] \quad ,$$

(IV.3.5)

$$\tilde{\mathcal{J}}^{-1}_{SPEC}(J) = E_{J+2} - 2E_{J+1} + E_J \quad .$$

Plotting the first and second energy differences involved in expressions (IV.3.3,4) as functions of J tells much about the spectroscopic structure of the band. For a rigid rotor the behaviour of ΔE_J is linear and $\Delta^2 E_J$ is constant. For a harmonic vibrator $\Delta E_J = \hbar\omega$ = constant and $\Delta^2 E_J = 0$. For a symmetric and triaxial rotor all the bands behave as indicated above, but for a γ-unstable nucleus the γ-band energy differences behave in a non-smooth way yielding a saw-tooth line in the difference plot. This γ-band behaviour is called the even-odd staggering effect /He77/ and can be explained by a repulsion of the states with the same angular momentum in the β and γ bands /OI77/. In addition, for triaxial and γ-unstable nuclei the γ band head is mostly quite low.

Judging by the appearance of the difference plots for the γ bands of the gadolinium isotopes in ref./Li83c/, the rotor gadoliniums $^{154-160}$Gd seem to be γ-unstable nuclei (Here the criterion is the odd-even staggering which resembles the one encountered in the O(6) limit of the IBA). In /Li83c/ it was observed that the IBA model nould not produce as good difference plots as the isotropic PM (so in this respect a larger pairing term would have been needed in the IBA fits). However, both models gave indications of the γ-unstable features of the isotopes In the PM the reason for this is the under rotational behaviour of the even J-levels in the bands as seen in fig. 7 of the ref./Li76/ for the ground band. This results in the right even-odd staggering for the γ band. The EPM produces good difference plots for the ground and β bands, but fails for γ bands in the case of the Gd isotopes. In the EPM the lower-lying J levels of the β band tend to push the higher- lying J levels of the γ band even higher, resulting in an opposite even-odd staggering compared to the γ-unstable case. This produces saw-tooth plots having a 'phase difference' with the experimental plots. However, because for ^{158,160}Gd the β levels are higher than the corresponding γ levels, the repulsion is downward and the experimental results are re-

gained (this is, however, hard to see because there are not enough experimental data available for these isotopes).

Finally I wont to compare the 6-parameter IBA-1 calculation of Lipas et al. /Li84a/ with the EPM calculations. The parameters that were used in the calculations by Lipas et al. are tabulated in appendix G. The main purpose in /Li84a/ was to describe the E2/M1 mixing ratios in ^{154}Gd by the IBA model, but they also mention the RMS value of the energy fit, which was RMS=31keV. In this RMS the following levels were included /Li84c/: 2g - 10g , 0ß - 10ß , 2γ - 7γ . The corresponding RMS value for the 4-parameter EPM is 62keV, and for the 5-parameter EPM it is 51keV (as seen in appendix H). So both models give very good energy fits (Girit et al. /Gi83/ report an RMS of 80 keV). However, one must take into account that in the EPM four fewer levels are fitted, and when considering only the EPM-fitted levels, the EPM gives a better RMS value both for 4 and 5 parameters.

IV.3.C. The Erbium Isotopes

The erbium isotopes fitted in this work range from $^{156}_{68}$Er to $^{170}_{68}$Er . The Er isotopes have been studied much for their high-spin properties and γ-band structure. The isotope ^{156}Er is studied in refs. /By81, Zo80/ for its high-spin properties. As mentioned in chapter III.1, the EPM contains no real internal degrees of freedom to describe back-bending phenomena, so the levels above the band crossing are, in principle, not describable by the EPM. So, for example, in the case of ^{156}Er one must stop the EPM fitting and comparison with experimental data at the first backbend of the bands, which in this case is for the ground band at J = 10g --> 14s (s denotes here the so-called s-band which crosses the ground band and then becomes the yrast band. S can be interpreted as super band or side band. Fig. 2 of ref./By81/ shows also a second back bend at 24s --> 28s´). These backbending phenomena are better described by special high-spin models, like the Coriolis antipairing model /Mo60/, the rotational alignment model /St75,St72/ the shape transition model /Th73/ and the HFBC theory /Be79/. It seems that, at least for the Er isotopes, the alignment model is the most suitable for describing the back-bending

phenomena /Ya80/.

In the region of rare-earth nuclei the back-bending occurs at angular momenta $12_g \rightarrow 16_s$, and especially for $^{158-164}$Er it occurs at $14_g \rightarrow 16_s$ /Ry73, Ja77, Ya80/. In addition to a back bending in the ground state band, one may observe backbending also for other bands. For example, one can observe a back bend in the γ band at $12_\gamma \rightarrow 14_s$ in ^{164}Er, where the odd-J side band becomes the yrast odd-J band and the even-J side band becomes the yrare even-J band /Jo78, Ya80/. In table IV.3.6 and in appendix H all the levels are interpreted as not belonging to any side bands, so that the low-energy boson nature of the excitations is preserved.

Another point worth mentioning in connection with the Er isotopes is the odd-even staggering phenomenon already encountered in the Gd isotopes. In the Er isotopes the staggering is the same way as in the Gd isotopes, ie. because of the higher-lying β band the inter-band interaction tends to lower the even-J levels in the γ band with respect to the odd ones, as is clearly seen in fig. 4 of ref./Ja77/ and in fig.12 of ref. /Ya80/. Because β levels are quite high compared to the γ levels for the erbiums, the repulsion of the same-J levels in the EPM seems to be insufficient to produce this effect. As a result an almost rigid rotor spacing is produced in the EPM (of course the fitting was made harder by the fact that only one or two β levels were, with some certainly, assigned in experiments).

The main purpose here, however, is to compare the EPM calculations with the 6-parameter IBA-1 calculations of /Li84b,c/. Here the comparison is performed only for the energies because there are not many experimental data on the transition probabilities or branching ratios. (Except for ^{162}Er in table 4 of ref./Ja77/ where the experimental figures were compared with those given by the Alaga rules and by the RVM (=Rotation Vibration Model, see ref./Ei75/). The EPM results for these branchings are very much the same as the RVM($g\beta\gamma$) results of the above reference. Several experimental branchings are also known for ^{168}Er which were compared with those given by IBA-1 in ref./Wa81a/. Again the EPM gives quite nice results, especially for the γ branching). The only Er isotope fitted by the IBA so far is ^{168}Er /Ca80a,b; Wa80a; Wa81a; Ca83b/. It has been one of the most glorious successes of the IBA model and of modern experimental techniques. In table IV.3.6 the isotopes ^{162,164,166,168}Er are represented in the light of experiment, IBA-1 and the EPM. The effective proton- boson number is used in the IBA fits (except for ^{166}Er) and /Sc83/ yields for the erbium isotopes $Z_{eff}=3$.

As can be seen in the table, both models give very good RMS's the 5-parameter EPM being the best (the EPM is especially good for ^{168}Er for which an RMS of 2.4 can be achieved). In the case of the EPM fever levels are fitted because the predicting ability of the model is being tested.

From the parameter systematics of appendix H one can see that the convergence of the boson expansion is slower for the erbiums than for the other isotopic chains. Especially

BAND	J	^{162}Er				^{164}Er			
		EXP.	IBA	EPM		EXP.	IBA	EPM	
				4	5			4	5
γ	2	102	94 *	105 *	102 *	91	88 *	94 *	91 *
	4	330	311 *	333 *	331 *	299	289 *	303 *	299 *
	6	667	641 *	655 *	668 *	614	602 *	604 *	615 *
	8	1097	1081 *	1041 *	1092 *	1025	1020 *	975 *	1026 *
	10	1603	1614 *	1477	1581	1518	1540 *	1396	1513
	12	2165	2241	1953	2127	2083	2150	1856	2065
	14	2746	2922	2464	2724	2703	2851	2352	2671
β	0	1087	1096 *	1086 *	1084 *	1246	1226 *	1233 *	1233 *
	2	1171	1167 *	1185 *	1174 *	1315	1318 *	1314 *	1309 *
	4	--	--	--	--	1470	1500 *	1502 *	1486 *
γ	2	901	891 *	903 *	908 *	860	850 *	862 *	867 *
	3	1002	983 *	1000 *	1001 *	946	947 *	947 *	948 *
	4	1128	1120 *	1129 *	1124 *	1058	1049 *	1060 *	1056 *
	5	1286	1286 *	1282 *	1274 *	1198	1189 *	1194 *	1189 *
	6	1460	1446 *	1465 *	1457 *	1359	1365 *	1364 *	1352 *
	7	1669	1668 *	1668 *	1661 *	1545	1559 *	1536 *	1532 *
	8	1873	1900 *	1891 *	1896 *	1745	1754 *	1761 *	1752 *
	9	2134	2180 *	2139	2151	(1977)	2002	1961	1974
	10	2347	2363 *	2388	2426	(2184)	2279	2233	2251
	11	2657	2714	2682	2735	--	--	--	--
	12	2911	3029	2943	3040	--	--	--	--
RMS		--	54	86	40	--	43	107	11
		--	--	--	--	--	(45)	(101)	(18)

BAND	J	^{166}Er				^{168}Er			
		EXP.	IBA	EPM		EXP.	IBA	EPM	
				4	5			4	5
γ	2	81	72 *	82 *	81 *	80	79 *	83 *	80 *
	4	265	239 *	267 *	265 *	264	261 *	268 *	264 *
	6	545	500 *	540 *	546 *	549	546 *	538 *	544
	8	911	853 *	884 *	911 *	928	931 *	874 *	909
	10	1349	1295 *	1282	1345	1397	1415 *	1258	1345
β	0	1460	1374 *	1462 *	1462 *	1217	1162 *	1197 *	1211 *
	2	1528	1447 *	1530 *	1527 *	1276	1241 *	1266 *	1274 *
	4	(1679)	1615 *	1688	1679	1411	1416 *	1425 *	1423 *
	6	--	--	--	--	1617	1693 *	1673	1658
	8	--	--	--	--	(1890)	2058	2007	1982
γ	2	786	825 *	784 *	789 *	821	790 *	828 *	829 *
	3	859	897 *	857 *	860 *	896	870 *	901 *	899 *
	4	956	992 *	955 *	955 *	995	968 *	999 *	992 *
	5	1075	1111 *	1072 *	1071 *	1118	1095 *	1116 *	1107 *
	6	1216	1252 *	1223 *	1216 *	1264	1249 *	1264 *	1248
	7	1376	1417 *	1373 *	1371 *	1433	1425 *	1415 *	1403
	8	(1556)	1602 *	1583 *	1570 *	(1625)	1620 *	1613	1594
RMS		--	49	20	2.4	--	30	42	20
		--	(50)	(20)	(2.5)	--	(50)	(50)	(30)

TABLE IV.3.6. Comparison of experiment and theory for some Er isotopes. The experimental figures are from NDS, appendix I, and from /Li84c/. The IBA figures are from /Li84c/. The levels marked with an asterisk are fitted. All energies are in keV, and the RMS's in parentheses correspond to the energy data in parentheses.

in the region of $^{164-168}$Er, going from second order to third in the boson Hamiltonian seems to alter the values of the fitted parameters a great deal. On the grounds of these parameter systematics one might suggest that some kind of shape transition should occur in the region of $^{164-166}$Er. However, one must be cautious about drawing such a conclusion just on the grounds of the behaviour of the fitting parameters of a slowly converging Hamiltonian because the quadrupole moment and transition probability systematics do not show any abrupt behaviour in this region.

IV.3.D. The Ytterbium Isotopes

The ytterbium chain dealt with here contains the isotopes $^{164}_{70}Yb_{94}$ - $^{174}_{70}Yb_{104}$. Recently the most interesting object of study in Yb nuclei has been the high-spin phenomena. The degree of backbending in the Yb chain is not a smooth function of neutron number as seen in fig. 18 of ref./Wa76/. This has been explained in ref./Fa74/ to stem from pairing effects and in refs./Be78, Be79/ to stem from the fact that the mixing between the ground state band and the s band is an oscillating function of neutron number. This oscillation is very clear in going from ^{166}Yb to ^{168}Yb and further to ^{170}Yb (between two backbending nuclei ^{168}Yb only slightly upbends). This behaviour is also clearly seen in the parameter systematics of figs. 19 to 23 and in the quadrupole moment and B(E2) systematics of figs. 24 and 25, where some discontinuous behaviour may clearly be observed at ^{168}Yb - ^{170}Yb (one may also notice that the convergence of the boson expansion is quite slow especially for the heavier Yb isotopes).

The backbending in the deformed rare-earth region is strongly influenced by the i(13/2) neutrons /St75/. The Coriolis interaction causes the i(13/2) orbitals to align, resulting in the emergence of a i(13/2) superband. The backbending starts for ^{164}Yb at 12g /Hu77/, for ^{166}Yb at 14g /Wa76/, for ^{170}Yb al 14g /Wa81a,Ha73/ and for ^{172}Yb at 18g /La78,Wa80b/; ^{174}Yb does not seem to backbend /Wa76/. There are not many electromagnetic data available (only in table 4 of ref./Hu77/, in tables 3,4 and 6 of ref./Ca73/ and in tables 7 and 8 of ref. /Kr84c/), so the comparison of the

BAND	J	EXP.[b]	IBA[a]	IBA[b]	EPM[c]	
					4	5
g	2	79	79*	75*	82*	79*
	4	260	262*	248*	266*	260*
	6	540	544*	516*	540*	541*
	8	911	919*	875*	886*	913*
	10	1370	1381*	1320*	1284*	1368*
	12	1907	1925	1845	1722	1891
	14	2518	2543	2446	2192	2472
	16	3198	3231	3117	2688	3103
β	0	1043	966*	1023*	1059*	1058*
	2	1118	1046*	1099*	1125*	1122*
	4	1286	1231*	1272*	1278*	1271*
	6	1537	1514*	1540*	1519*	1508*
	8	1854	1887*	1894*	1846*	1836*
	10	2212	2344*	2333*	2255*	2260*
	12	2607	2877	2843	2739	2785
	14	3044	3479	3430	3285	3416
γ	2	1466	1406*	1454*	1475*	1472*
	3	1549	1497*	1537*	1547*	1541*
	4	1658	1612*	1644*	1642	1634
	5	1779	1760*	1780*	1758	1749
	6	--	1921	1934	1900	1888
	7	--	2125	2123	2055	2048
RMS		--	148	110	156	97

TABLE IV.3.7. Comparison of EPM- and IBA-calculated energy levels of ^{172}Yb with experiment. Levels with an asterisk are fitted. All energies are in keV.
a) Data from /Li84c/ .
b) Data from /Kr84c/ .
c) Four and five parameter fits .

B(E2;J-->J´)		EXP.[b]	[a] IBA	[b] IBA	EPM	
J	J´				4	5
2g	0g	1.087	*1.087	*1.087	*1.087	*1.087
4g	2g	1.80	1.54	1.54	1.58	1.56
6g	4g	1.76	1.66	1.67	1.81	1.74
8g	6g	1.95	1.69	1.71	1.99	1.86
10g	8g	2.24	1.67	1,71	2.19	1.97
12g	10g	1.78	1.61	1.67	2.39	2.08
0β	2g	0.0162	0.0180	0.0685	0.0949	0.0381
2β	0g	0.0013	0.0033	0.0121	0.0072	0.0035
2γ	0g	0.0079	*0.0079	*0.0079	0.0332	0.0147
B(E2;J-->J´)/B(E2;J-->J")						
J	J´	J"				
2β	4g	0g	7.55	3.05	3.12	11.2	8.61
2β	4g	2g	2.54	2.19	2.09	4.30	3.89
4β	6g	4g	4.6	2.8	2.3	5.2	5.3
6β	8g	6g	3.4	3.8	2.5	5.2	6.7
8β	10g	8g	≈45	5.4	2.8	4.3	7.7
2γ	2g	0g	1.69	2.51	2.28	1.86	1.71
2γ	4g	0g	0.165	0.251	0.228	0.170	0.128
2γ	4g	2g	0.098	0.100	0.100	0.092	0.075
3γ	4g	2g	0.486	1,.12	1.00	0.729	0.603
4γ	4g	2g	3.24	17.0	10.7	5.42	4.52
5γ	6g	4g	≤0.88	2.95	2.46	1.43	1.09
6β	4β	8g	84	115	35	17	36

TABLE IV.3.8. Comparison of EPM- and IBA-calculated B(E2)´s and branching ratios with experiment for ^{172}Yb. All B(E2)´s are in units of e^2b^2. Transitions marked with an asterisk are fixed.
a) Data from /Li85c/ .
b) Data from /Kr84c/, tables 7 and 8 .
c) Four and five parameter fits .

EPM with experiment is not easy. However, /Kr84c/ contains appreciable electromagnetic data for ^{172}Yb and a useful comparison can be made. The comparison is performed for the energies in table IV.3.7 and for the B(E2)'s and branching ratios in table IV.3.8. In addition, the tables contain the results of two 6-parameter IBA-1 calculations. One is performed with the ordinary boson number (figures from /Kr84c/) and the other with the effective boson number (figures from /Li84c/). The parameter values used in the calculations are tabulated in appendix G.

As can be seen from appendix G, the two IBA fits are performed with quite different fitting parameters. The calculation with an effective boson number is done between the dynamic symmetries U(5) and SU(3) (no pairing term included), and the other between SU(3) and O(6) (the d-boson number term is excluded). The effective IBA calculation gives better results for the ground state band but fails for the β and γ bands, which are, on the other hand, treated quite well by the second IBA calculation. As can be seen, also the total RMS deviation is smaller for the ordinary boson-number calculation, but the 5-parameter EPM calculation gives a still better RMS. The EPM figures are superior to both the IBA figures in the case of ground and β bands and about the same quality as the fit /Kr84c/ for the γ band (the other IBA fit is worse). Because the IBA fits are done with different parameter combinations, extraction of the effect of the effective proton-boson number in the calculations is not possible.

From table IV.3.8 one can see that the two IBA fits give about the same results, but the 5-parameter EPM fit is a bit better. However, both models give a good qualitative (and even quantitative) description of the electromagnetic properties of ^{172}Yb.

By making the first and second energy difference plots as in fig.5 of ref./Kr84c/ (discussed in section IV.3.B of this work), one sees the fact that the EPM gives quite a good description of the internal structure of the ground and γ bands of ^{172}Yb. However, the dynamic moment of inertia of the β band is not very well described by the EPM for which the 4-parameter fit gives roughly the IBA result and the 5-parameter fit even a slightly opposite trend. A 5-parameter fit stressing the β band could improve the situation.

V. DISCUSSION AND COMPARISON WITH THE COHERENT STATE MODEL (CSM) OF RĂDUŢĂ ET AL.

In /Ra76a,b,c/ Răduţă, Badea and Dreizler introduced a model called the coherent state model (CSM). This model is very much like the earlier PM and the EPM. In the CSM one projects laboratory states from intrinsic states obtained by acting with deformed-phonon operators on a deformed coherent vacuum for intrinsic axially symmetric excitations. The intrinsic ground state is the same as in the PM and the EPM and can be written as (This form is identical to the form $\exp(-\frac{1}{2}d^2)|\tilde{0}\rangle \equiv |0^{\beta}\rangle$ used in the EPM. Here $|\tilde{0}\rangle$ is defined in (II.1.7) or (A2.6). This equivalence is easy to prove using the relation /Me70/ $\exp(A)\exp(B) = \exp(A+B+\frac{1}{2}[A,B])$).

$$\Psi_g \equiv \exp\left[d(b_0^{\dagger}-b_0)\right]|0\rangle \quad , \tag{V.1}$$

i.e. it is the deformed intrinsic vacuum state. The calculations in these references are performed in a two-state basis for every J. The other basis states are projected from the intrinsic β state

$$\Psi_{\beta} \equiv (b_0^{\dagger}-d)\Psi_g \tag{V.2}$$

just as in the PM and EPM. The laboratory Hamiltonian is a boson expansion like (II.2.10) (up to fourth or sixth order) with the specific form suggested in /Da72/. (The coefficients are free parameters as in the EPM. In principle these coefficients could be calculated microscopically by using the boson expansion techniques or phenomenologically by using the potential energy surface approach.) The energies are calculated either as expectation values (as in the PM, but only with a 2-state basis and with a Hamiltonian including also anharmonic terms) or diagonalizing in the projected state basis (as in the EPM, but first orthogonalizing by the Schmidt scheme and then performing the usual diagonalization).

From the very beginning the purpose of the CSM was to attack also the high-spin region of nuclear spectra. In order to do this, a method for describing a crossing of ground and β bands was proposed in /Ra76a/. There the β band became the yrast band at some critical J, J_{cr}, and the fitting was extended to the high-spin levels beyond the bac-

kbending region. The fits performed in /Ra76b/ indicate, however that this kind of boson description does not have very much capacity for describing the band crossing in the backbending region. The CSM description smooths out the drastic behaviour of the dynamic moment of inertia (i.e. $\mathcal{I}^2$)in the back bending region and thus gives only an average description of the effects of the Coriolis interaction in the rotating nucleus. So, contrary to Raduta et al., I do not believe in the capability of this kind of model to describe high-spin phenomena, and so I have assumed the ground state band to be always the yrast band (see section III.1.). However, also the EPM could be used, like the CSM, for a high-spin description by using in the fits a non-weighted chi-squared function.

In /Ra76d, Ra78a/ the above model was extended to odd-A nuclei by coupling the odd nucleon (moving in a shell model orbital) to the collectively excited core (the first attempt in this direction was in /Ik73/ where the PM states of Lipas et al./Li76/ were used as core states). In /Ra77/ it was proved that, for the ground state band, the models dealing with completely aligned states (=highest-seniority states in an N-phonon multiplet) and the quasi-rotational models (the level energies are an expansion in J(J+1)) are just extreme cases of the CSM (this is true also for the EPM). Also closed forms for the matrix elements of the quadrupole collective operators were derived /Ra78b, Gd78/. A new step in the development of the CSM was the inclusion of the γ degree of freedom in the system /Ra81; Ra82; Ra83a,b,c;Ra84/.

There, instead of using the Sheline-Sakai (SS) scheme (which is used in the PM and EPM), the results obtained by Roulet et al. /Ro78/ for the Pt isotopes suggest the use of a modified SS scheme. This modified SS scheme seems to be a basic feature of models using γ-soft potential energy surfaces /Sh60,Li75/, and is in accordance with the experimental facts that for many isotopes $B(E2; 0^+_\beta \rightarrow 2^+_\gamma)/B(E2; 0^+_\beta \rightarrow 2^+_g) >> 1$ and that states of the γ band exhibit a doublet structure as seen also in fig 2. In the modified SS scheme the state 0^+_β is assumed to have a three-phonon structure instead of a two-phonon content as in the EPM. By demanding the realization of specific experimental features and orthogonality before and after projection for the model states, one ends up with a specific form of the intrinsic states Ψ_g, Ψ_β and Ψ_γ. A carefully chosen boson Hamiltonian is then diagonalized in the three-state projected basis and for the harmonic part $\hat{N}$ of the Hamiltonian one gets an excitation spectrum that resembles that produced by the earlier PM and EPM.

The excitation spectra of the three models could be compared with each other by looking at fig.8 of ref./Li76/, fig.2 of this work and figs. 1,2 and 3 of ref. /Ra82/. From these figures one can conclude that the ground state band has exatly the same structure in every one of the models The β and γ bands have a similar internal structure (for example the bunching of the states J = odd, J+1 = even together has same features in each of the models), but the band head energies behave quite diffrently (this behaviour being

very different in the EPM from the other two models).

The bunching of the odd- and even-J γ states is a consequence of the γ-unstable structure built into the CSM. This has been exploited for example in the fit to the platinum isotopes ^{190,192}Pt in ref./Ra81/. For the platinum isotopes the deformation parameter d was smaller than unity and the level bunching was correct in order to produce a right kind of even-odd staggering (see fig. 3 of /Ra82/) for the γ-unstable platinums. Another kind of situation is encountered when one looks at the CSM fits to the γ-unstable osmium isotopes $^{182-186}$Os in ref./Ra84/. Because the deformation parameter is in these fits quite large (d≈2,5), the nice γ-unstable bunching encountered at small d in the platinum fits becomes an opposite bunching yielding also an opposite odd-even staggering (compared to experimental data) in the osmium isotopes. This is the same phenomenon that is encountered in the EPM fits to the gadolinium isotopes in section IV.3.B, and it is due to the specific behaviour of the γ-band energies as a function of the deformation parameter. This behaviour is similar in the CSM and the EPM, but in the earlier PM the γ-unstable features tended to last to slightly greater d values. This tendency in the PM also explains the fact that it could reproduce quite nicely the even-odd staggering (i.e. Δ and Δ^2) encountered in the Gd isotopes while EPM failed in most cases. So, in order to reproduce better results in the case of γ unstable nuclei, the two models (CSM and EPM) should stick to a bit smaller deformation parameters in the fits. This in turn seems to contradict the tendency of the fitting procedures to find large-d minima on the parameter surfaces, especially in the case of the EPM for which d could be up to 4 in the Gd chain and even larger for the Er and Yb chains.

In the three-state CSM the projected wave functions become the three highest-seniority U(5) states (for each n) in the zero-d limit, and in the large-d limit they become the g, β and γ states of the BMM for the case of weak coupling of the β and γ vibrations to the rotational motion /Ra82/. This introduces specific selection rules in the small-d limit and the Alaga rules at large d, which is the case also for the EPM with a Harmonic $\hat{H}$ (this is true when both models use the harmonic approximation (II.6.4) of the transition operator). Also the absolute value of the quadrupole moments of the β-band states are greater than those of the ground-band states in both models. It is worth noting, however, that in the EPM the B(E2)'s are calculated between eigenstates of the harmonic Hamiltonian in the projected state basis, but in the CSM the B(E2)'s are calculated directly between the projected states (they are orthogonal in the CSM) which are the eigenstates of the harmonic Hamiltonian only in the limit d-->0. Instead, in the CSM the model Hamiltonian is chosen so as to yield approximately the projected states as eigenstates.

Figs. 1,2 and 3 of ref. /Ra83c/ show some transition probabilities $B(E2;J_i \text{-->} (J-2)_i)$ i=g,β,γ, as a function of the deformation parameter d obtained by using the harmonic transition operator between the projected states. These figures

resemble very much the corresponding EPM figures 8,9 and 10. The behaviour of the transition probability $J_g \dashrightarrow (J-2)_g$ is the same in both models, but some differences can be observed in the transition probabilities $J_\beta \dashrightarrow (J-2)_\beta$ and $J_\gamma \dashrightarrow (J-2)_\gamma$. For the latter two B(E2)'s the CSM yields a monotonically decreasing function of d, while the EPM curves have a maximum at some d value. For the B(E2)'s this is around $d \approx 1.5$ and for B(E2)'s around $d \approx 1.0$. These differences in energy spectra and transition probabilities are very likely to stem from the fact that in the EPM one performs a complete diagonalization, while in the CSM one assumes for the energies that the β band is totally decoupled from the g and γ bands and that the projected states serve as the basis for the B(E2) calculations.

From the energy fits of appendix H it is easy to see that in the EPM the ground state band has underrotational features (the theoretical level energies lag behind the experimental ones), while the γ-band energies tend to grow too fast. This is a very general feature in many collective theories and in the case of the EPM it follows from the omission of the J^2 term from the boson expansion Hamiltonian(III.2.3) (the exclusion of J^2 means, according to (II.2.9), a partial exclusion of the term $B_{22}^{(4)}$, which is 'overrotational' according to /Li76/). In the CSM the term J is included in the model Hamiltonian and so the theoretical spectra seem to lack the above-mentioned features.

In the case of ^{150}Sm and ^{152}Sm the 4-parameter fit gives better RMS's than the 5-parameter one (see appendix H). This is due to an inaccurate minimization in the 5-parameter case (an increase in the number of fitting parameters also increases the difficulties in the search for a minimum) following from the less accurate behaviour (at small d) of the functional to be minimized. It is wortwhile to note, however, that the 5-parameter fit is in this case still better at low energies because of the weighting of the chi-squared function.

VI. SOME CONCLUDING REMARKS

The concluding remarks of this chapter concern the possible future applications and extensions of the EPM.

The most obvious future application of the present EPM framework is the calculation of the magnetic dipole transition probabilities B(M1) and consequently the multipole mixing ratios defined by /Ha75/

$$\delta \equiv (f \| T^{(E2)} \| i)/(f \| T^{(E2)} \| i) \quad , \tag{VI.1}$$

which has been recently studied to some extent in the IBA model /Li84a,e; Gi83; Sa84, Is80, Di84/. In the IBA the M1 operator has three adjustable phenomenological parameters while in the EPM there is just one adjustable M1 parameter (note, that the lowest order possible operator $[b^\dagger \tilde{b}]_1$ will not do, because it is proportional to $\vec{J}$ and hence would not give any contribution to M1 transitions between states of good angular momentum). The lowest order non-trivial M1 operator would read in the EPM

$$T^{(M1)} = m^* \cdot \mathcal{M}_{31} \quad , \quad \mathcal{M}_{31} \equiv \left[\left[b^\dagger b^\dagger \right]_2 \tilde{b} \right]_1 + H.c. \quad , \tag{VI.2}$$

where m^* is an effective magnetic coupling constant (the g factor). Of course, to get some more flexibility to the ratio (VI.1) one could include in the calculations the lowest order anharmonic part of $T^{(E2)}$ (brings in two more parameters)

$$T^{(E2)}_{anh.} = q_1 E_{11} + q_2 E_{20} \quad , \tag{VI.3}$$

where

$$E_{11} = [b^\dagger \tilde{b}]_2 \quad ; \quad E_{20} = [b^\dagger b^\dagger]_2 + H.c. \tag{VI.4}$$

or the fourth-order part of $T^{(M1)}$ (brings in four more parameters)

$$T'^{(M1)} = \sum_{k=2,3} \alpha_k \mathcal{M}_{31}^{(k)} + \sum_{k=2,4} \beta_k \mathcal{M}_{22}^{(k)} \quad , \tag{VI.5}$$

where

$$\mathcal{M}_{31}^{(k)} \equiv \left[\left[b^\dagger b^\dagger b^\dagger\right]_k \bar{b}\right]_1 \quad ; \quad \mathcal{M}_{22}^{(k)} \equiv \left[\left[b^\dagger b^\dagger\right]_k \left[\bar{b}\bar{b}\right]_k\right]_1 \tag{VI.6}$$

It is worth noting that the four parameter δ-ratio calculations performed with the above anharmonic $T^{(E2)}$ and the $T^{(M1)}$ of eq. (VI.2) would be quite compatible with the 5-parameter δ calculations of the IBA (here the energy parameters are not counted).

A possible future extension of the model is the addition of the oriented two-phonon excitations to the system. (Not much literature existets on this subject because this matter is not well established experimentally). According to the Bohr-Mottelson picture these would be the following excitations

	$(b_0^\dagger - d)^2 \lvert\tilde{0}\rangle$	ββ	K=0
(VI.7)	$(b_2^\dagger)^2 \lvert\tilde{0}\rangle$	γ+γ	K=4
	$b_2^\dagger b_{-2}^\dagger \lvert\tilde{0}\rangle$	γ-γ	K=0
	$(b_0^\dagger - d) b_2^\dagger \lvert 0\rangle$	βγ	K=2

After projection this would introduce four new bands into the present description and thus increase the dimension of the model space up to seven. So one would have four K=0 bands, two K=2 bands and one K=4 band. One possible extension, of course, is the inclusion of the negative-parity octupole bands as was done in the CSM in ref./Ra84/ (the K =0 and K=1 bands were included).

Figures

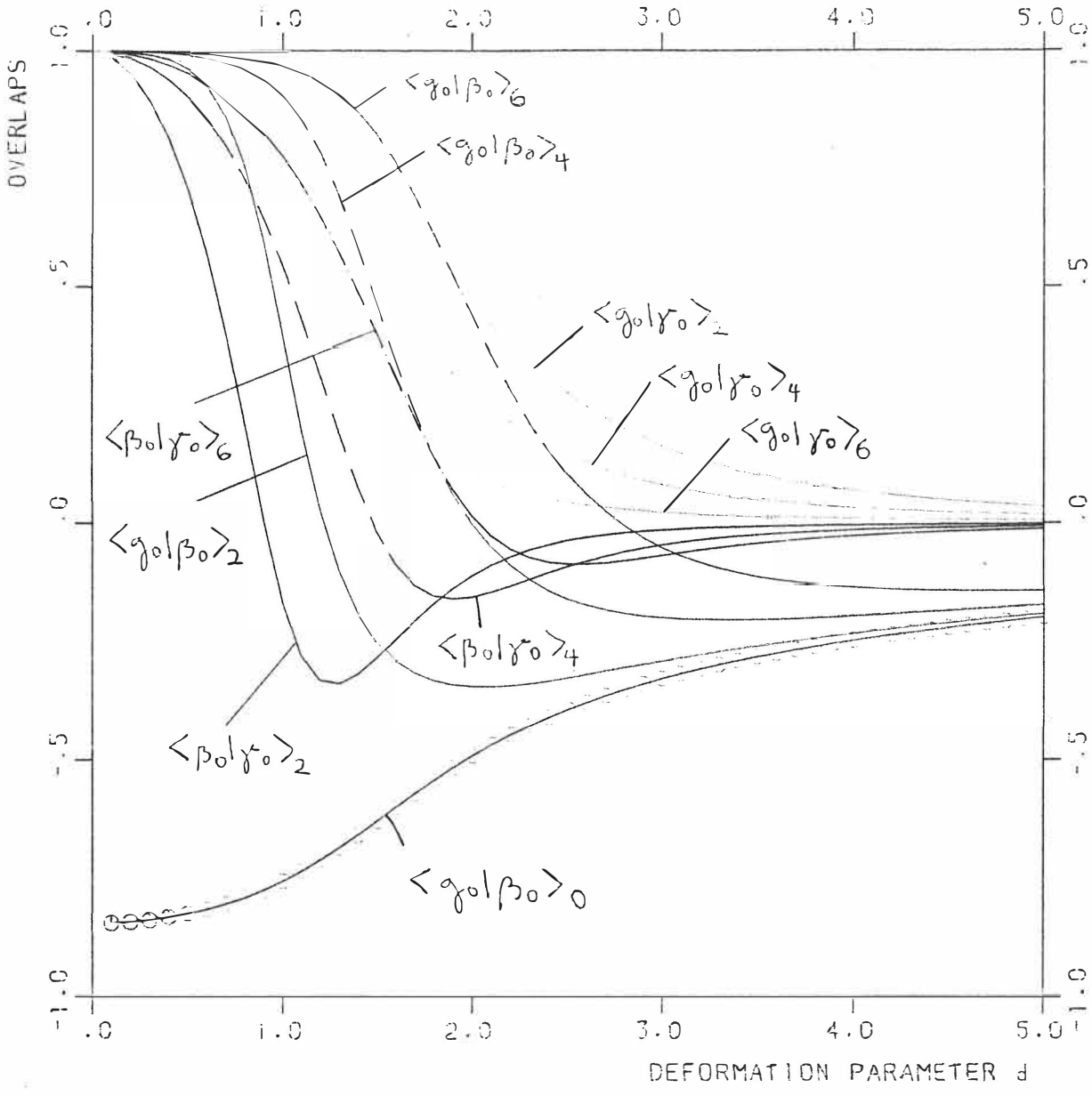

FIGURE 1 : Values of the overlaps of appendix D.2 as functions of the deformation parameter d .

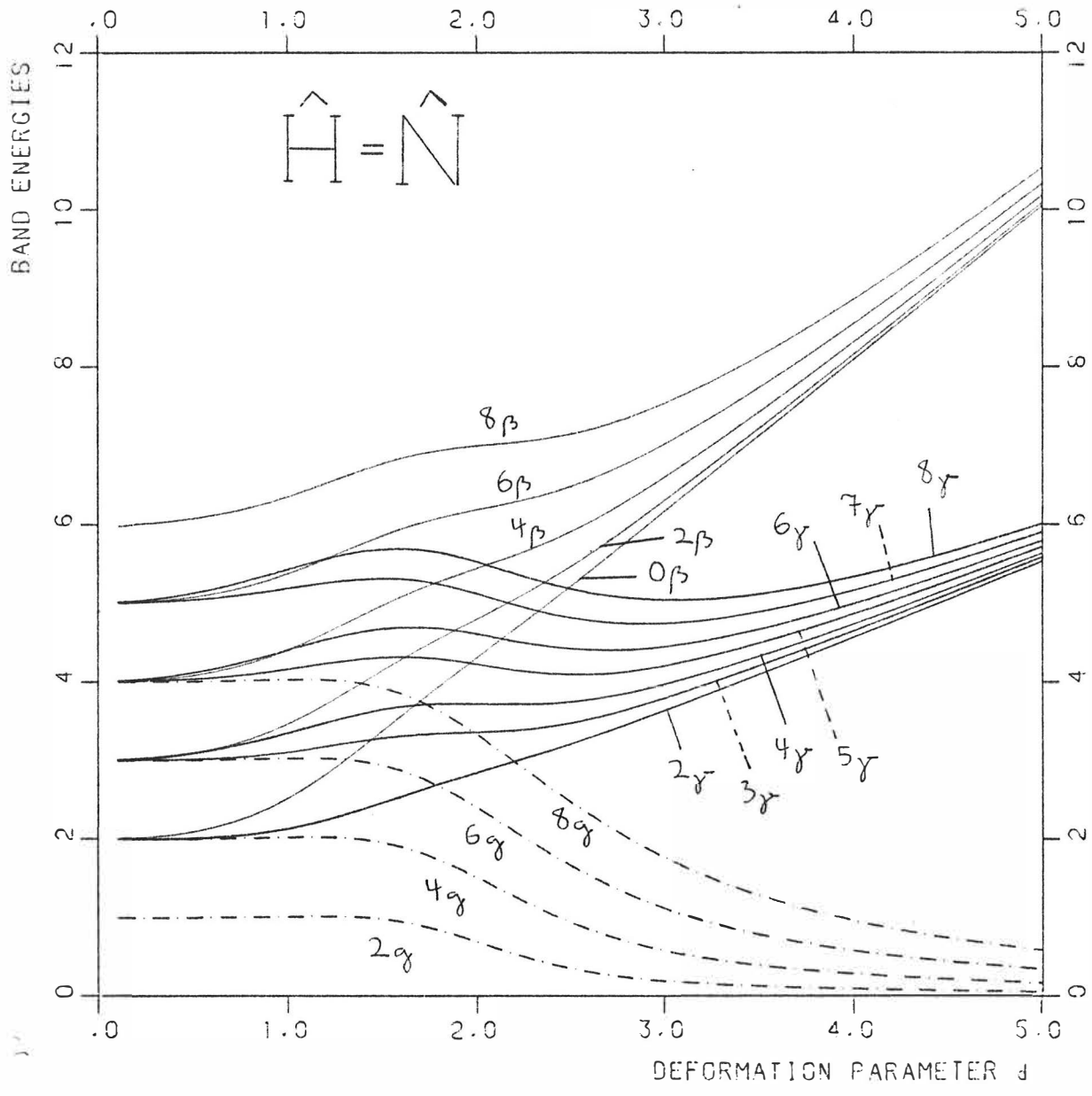

FIGURE 2 : Eigenspectrum of the number operator N as a function of the deformation parameter d .

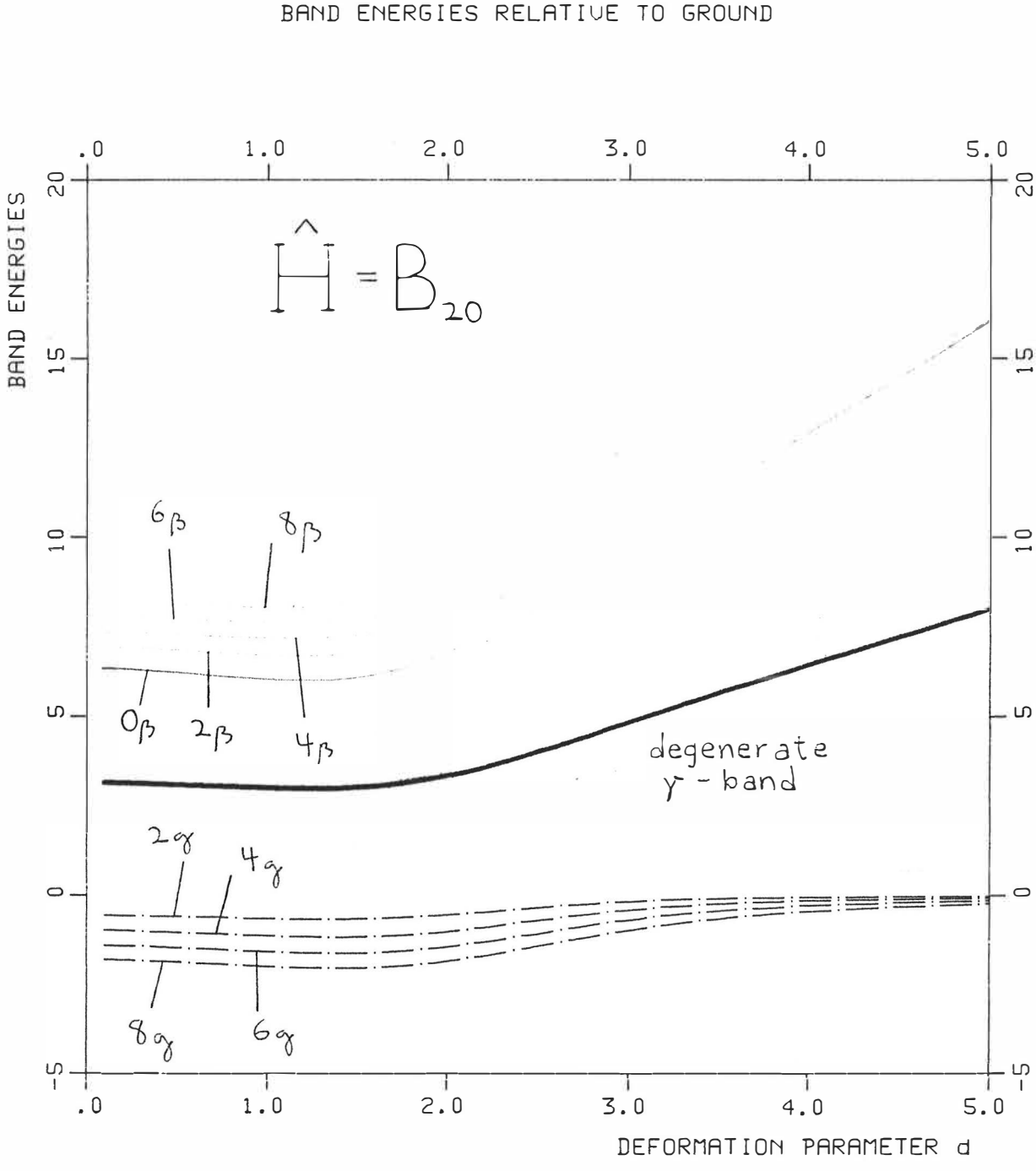

FIGURE 3 : Eigenspectrum of the operator B_{20} as a function of the deformation parameter d .

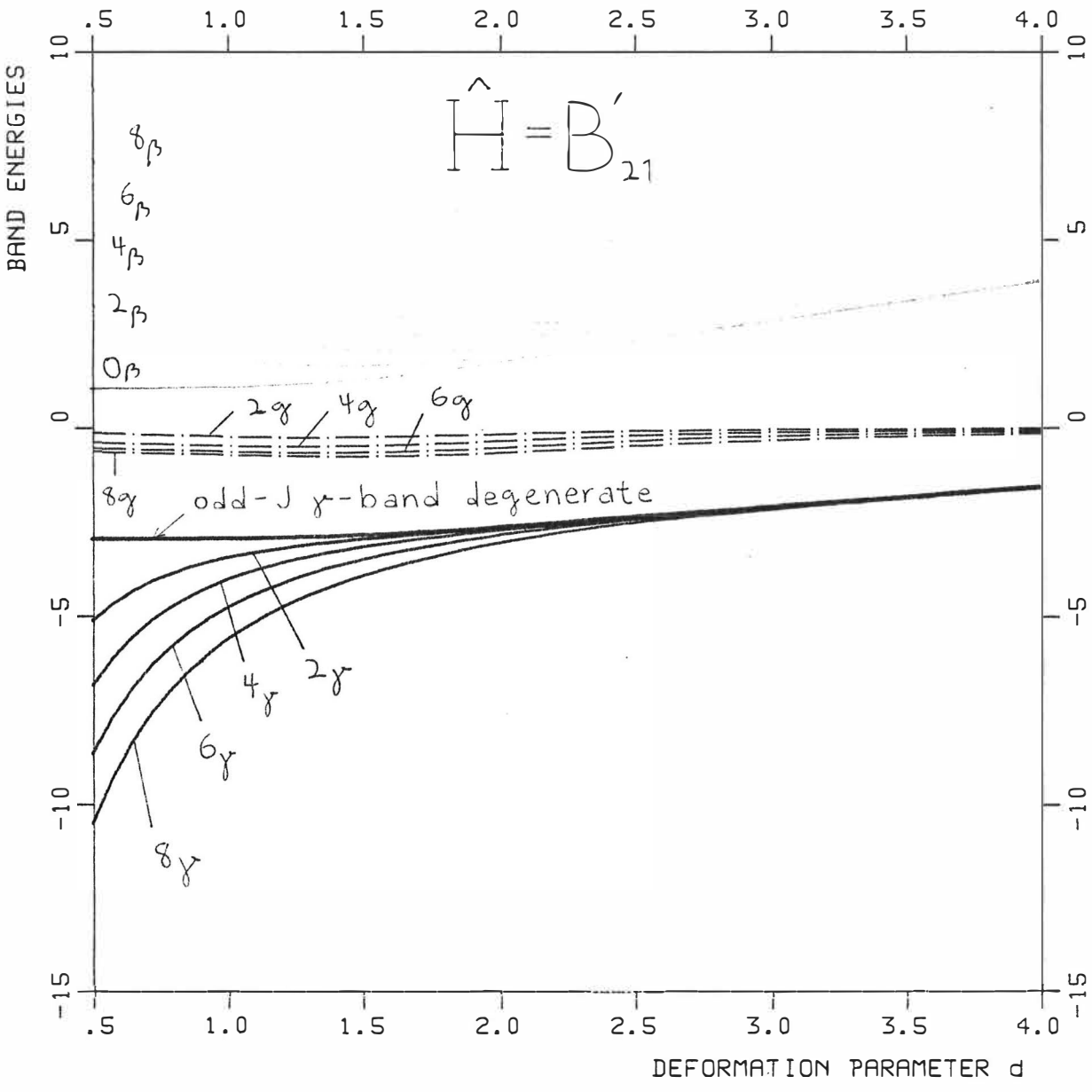

FIGURE 4 : Eigenspectrum of the operator B'_{21} as a function of the deformation parameter d .

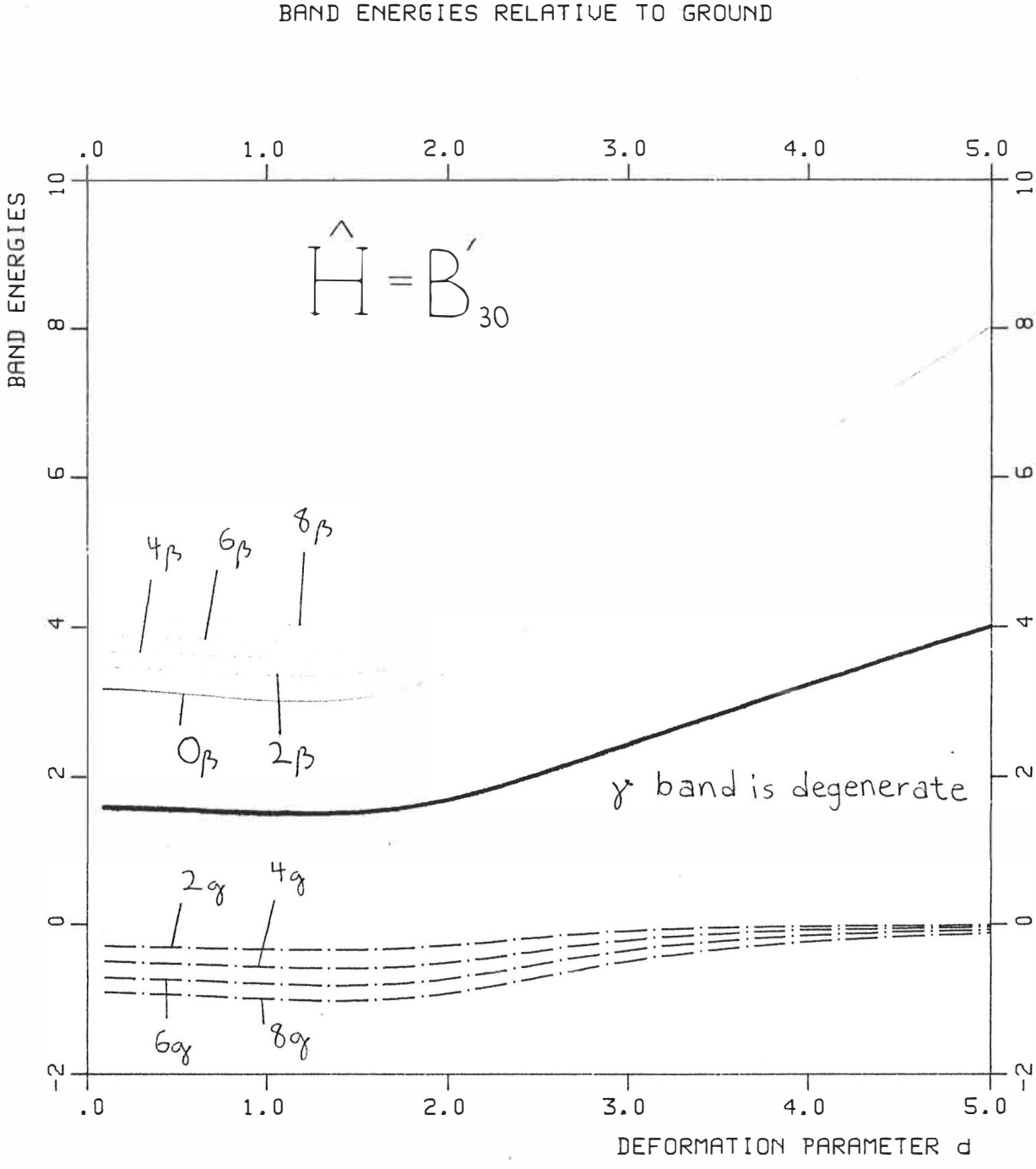

FIGURE 5 : Eigenspectrum of the operator B'_{30} as a function of the deformation parameter d .

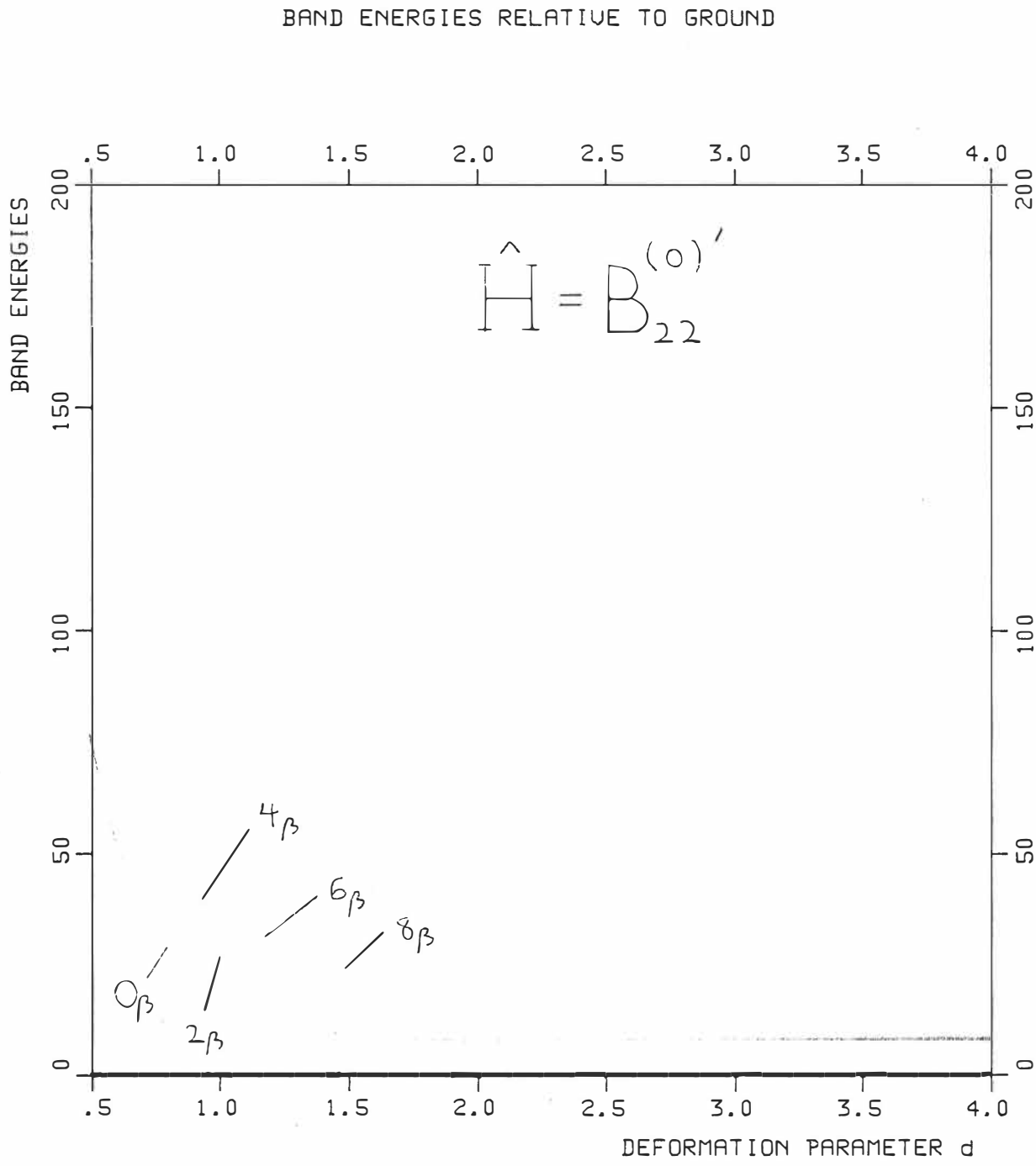

FIGURE 6 : Eigenspectrum of the operator $B_{22}^{(0)'}$ as a function of the deformation parameter d .

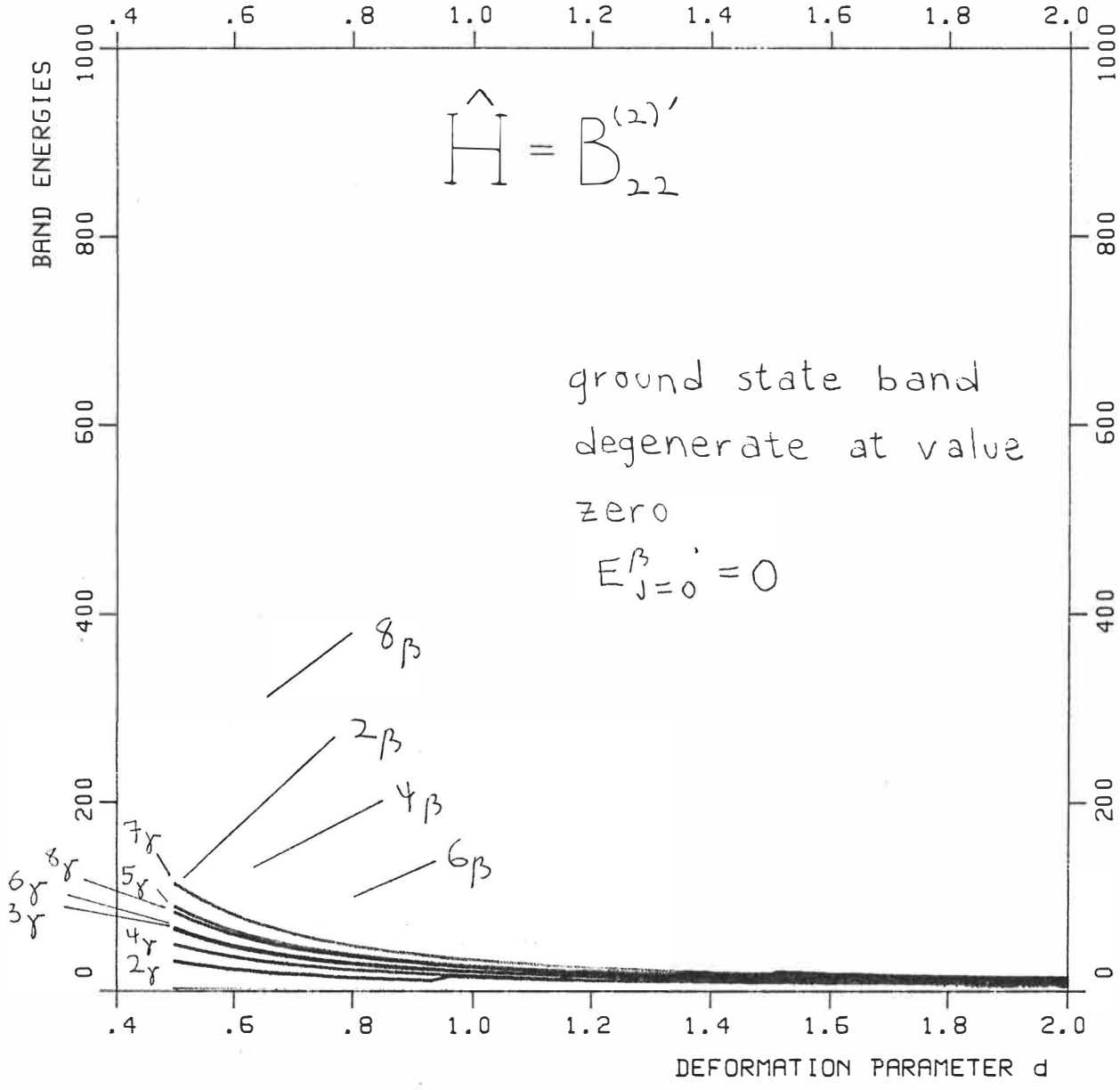

FIGURE 7 : Eigenspectrum of the operator $B^{(2)'}_{22}$ as a function of the deformation parameter d .

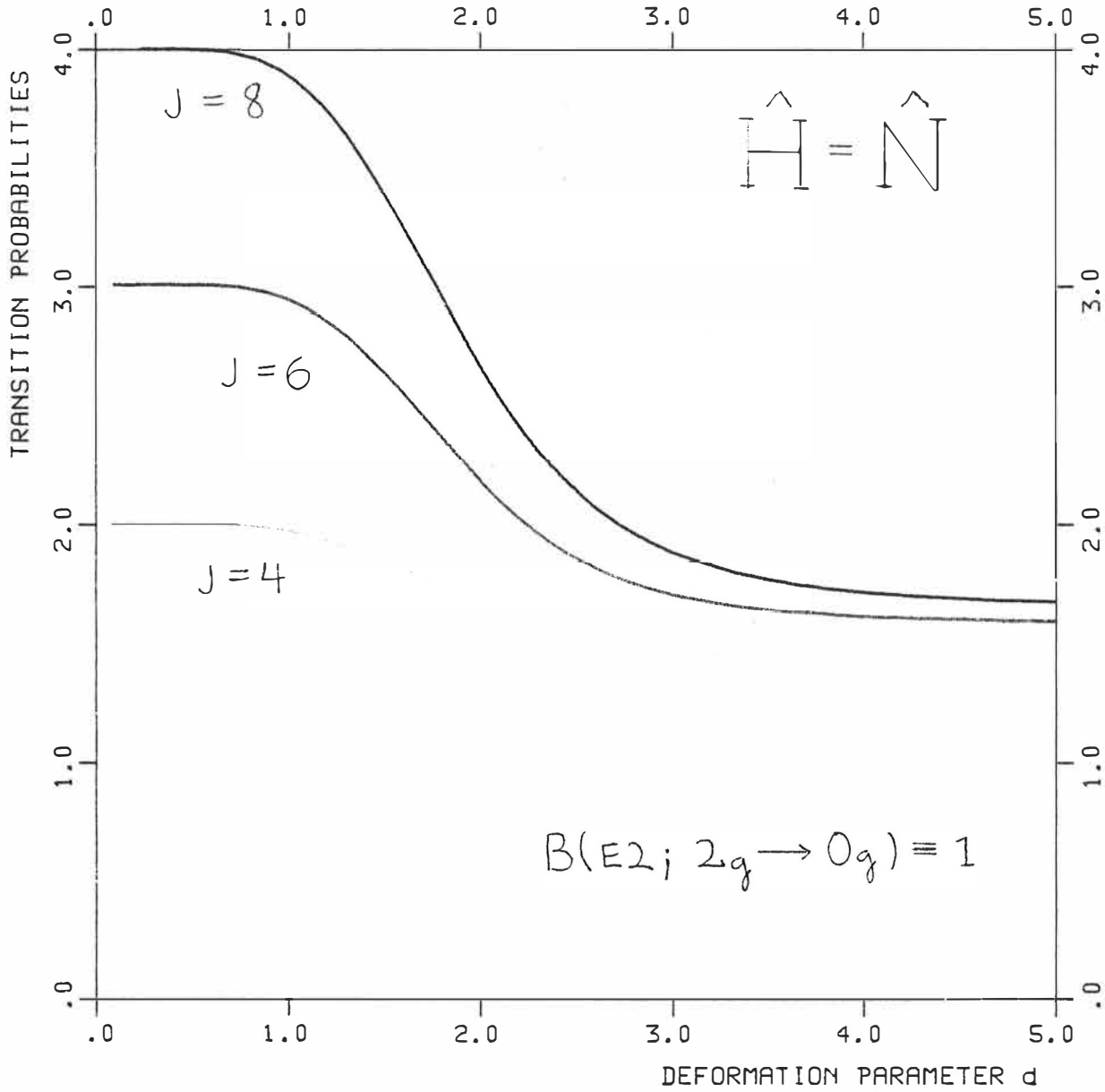

FIGURE 8 : Intraband E2 transition probabilities B(E2; ground ; J→ J-2) as functions of the deformation parameter d for the harmonic system $\hat{H} = \hat{N}$.

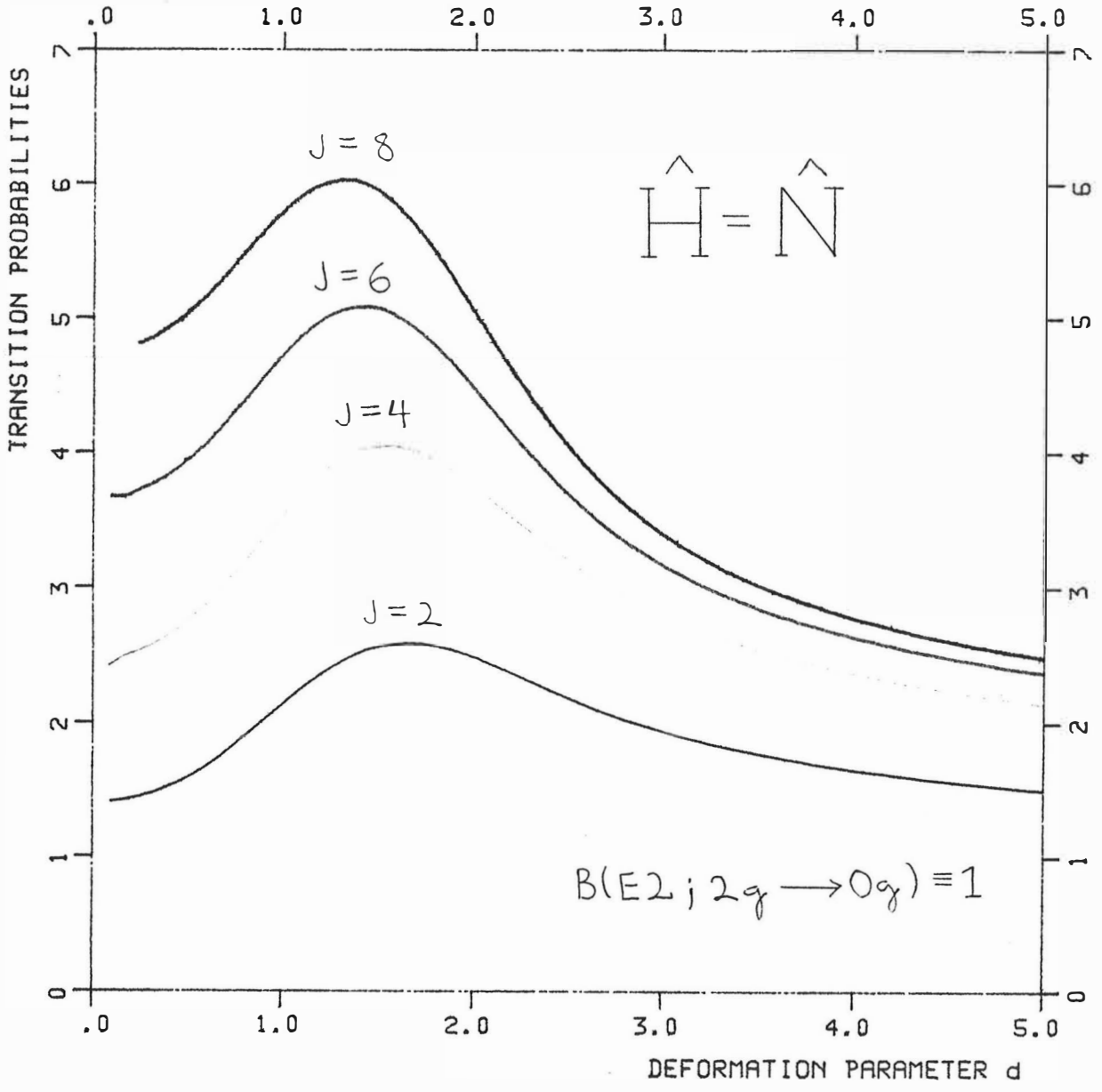

FIGURE 9 : Intraband E2 transition probabilities B(E2; beta ; J⟶J-2) as functions of the deformation parameter d for the harmonic system $\hat{H} = \hat{N}$.

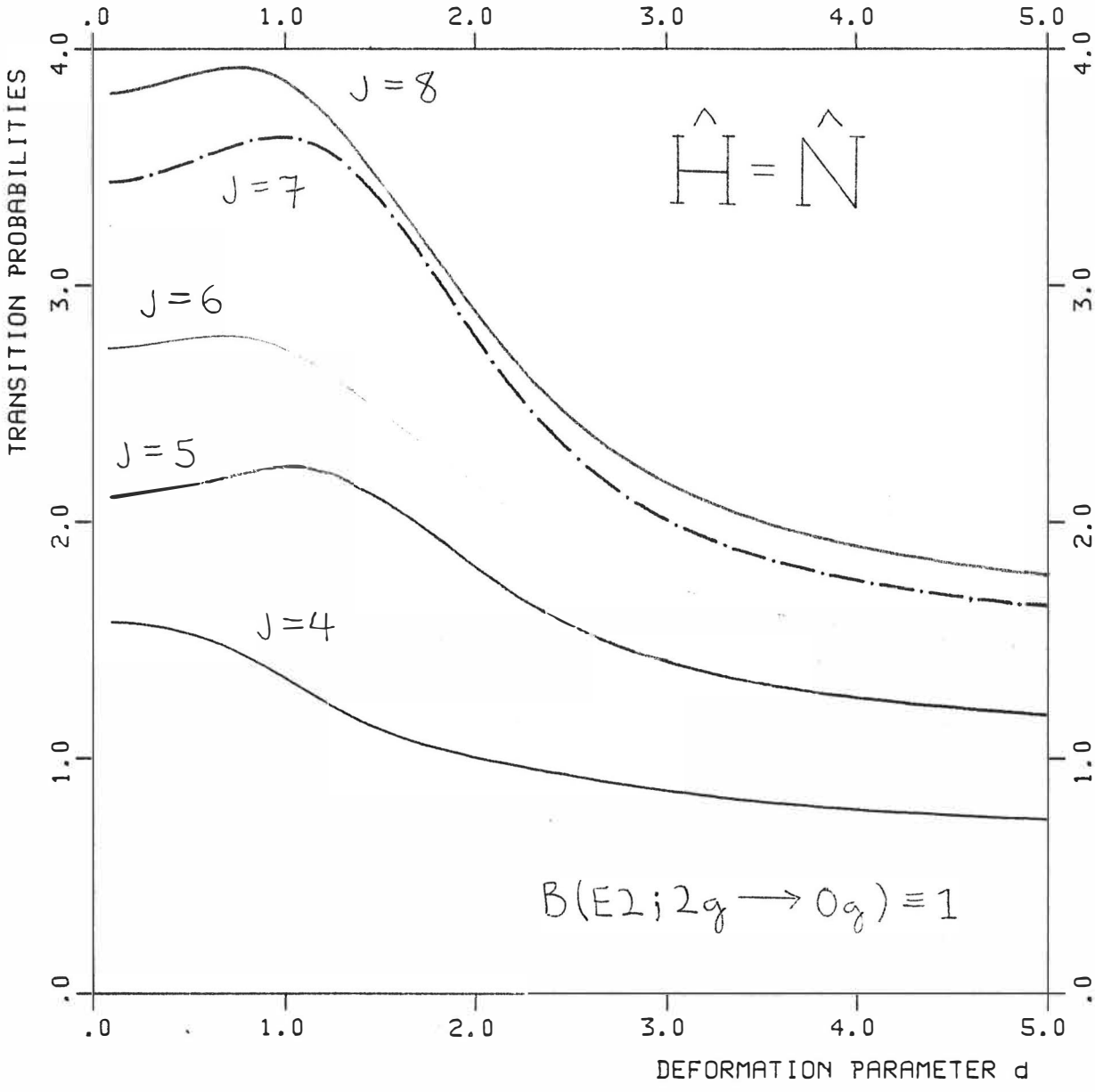

FIGURE 10 : Intraband E2 transition probabilities B(E2; gamma ; J⟶J-2) as a function of the deformation parameter d for the harmonic system $\hat{H} = \hat{N}$.

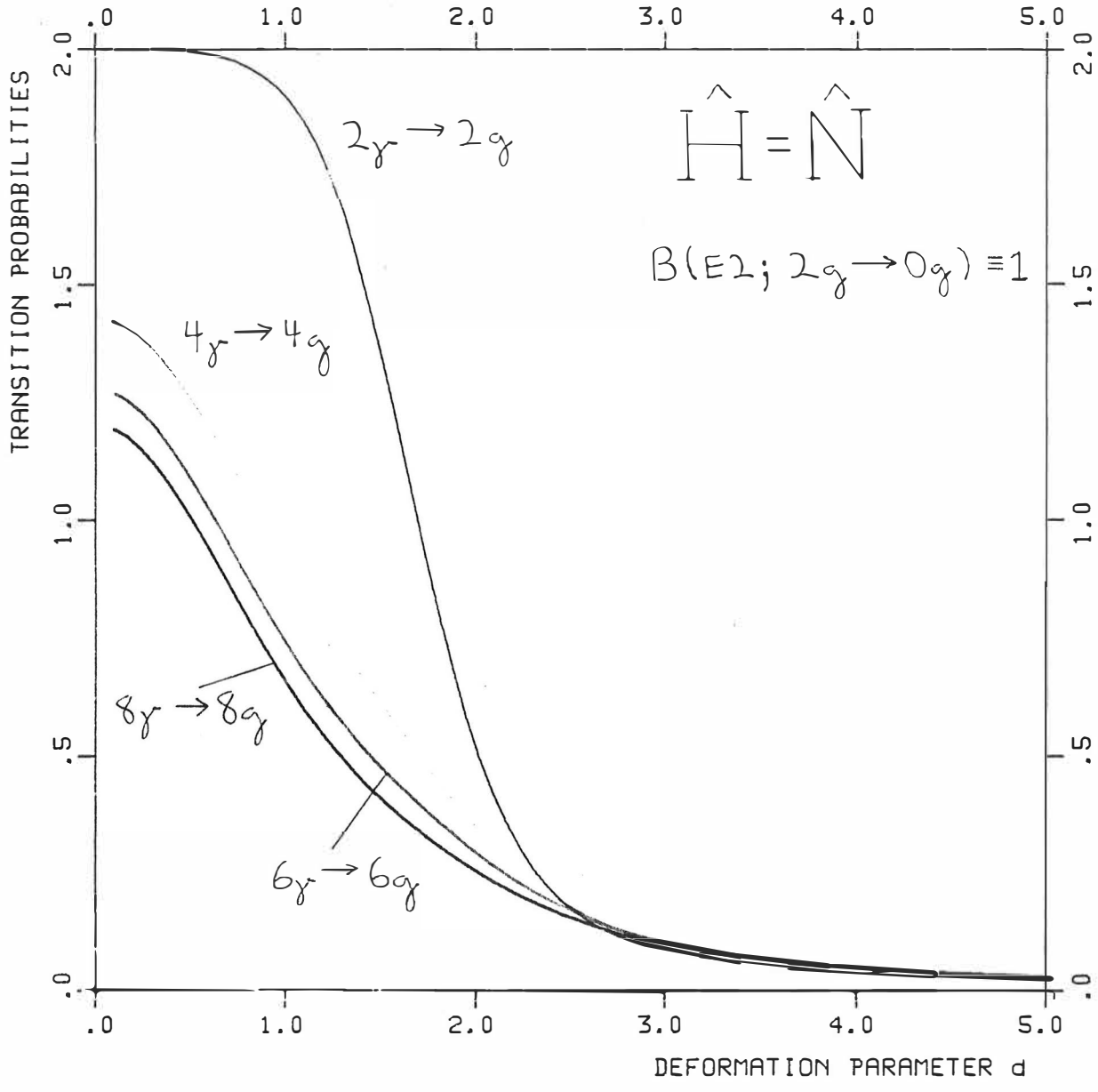

FIGURE 11 : Interband E2 transition probabilities B(E2; gamma J ⟶ground J) as functions of the deformation parameter d for the harmonic system $\hat{H}=\hat{N}$.

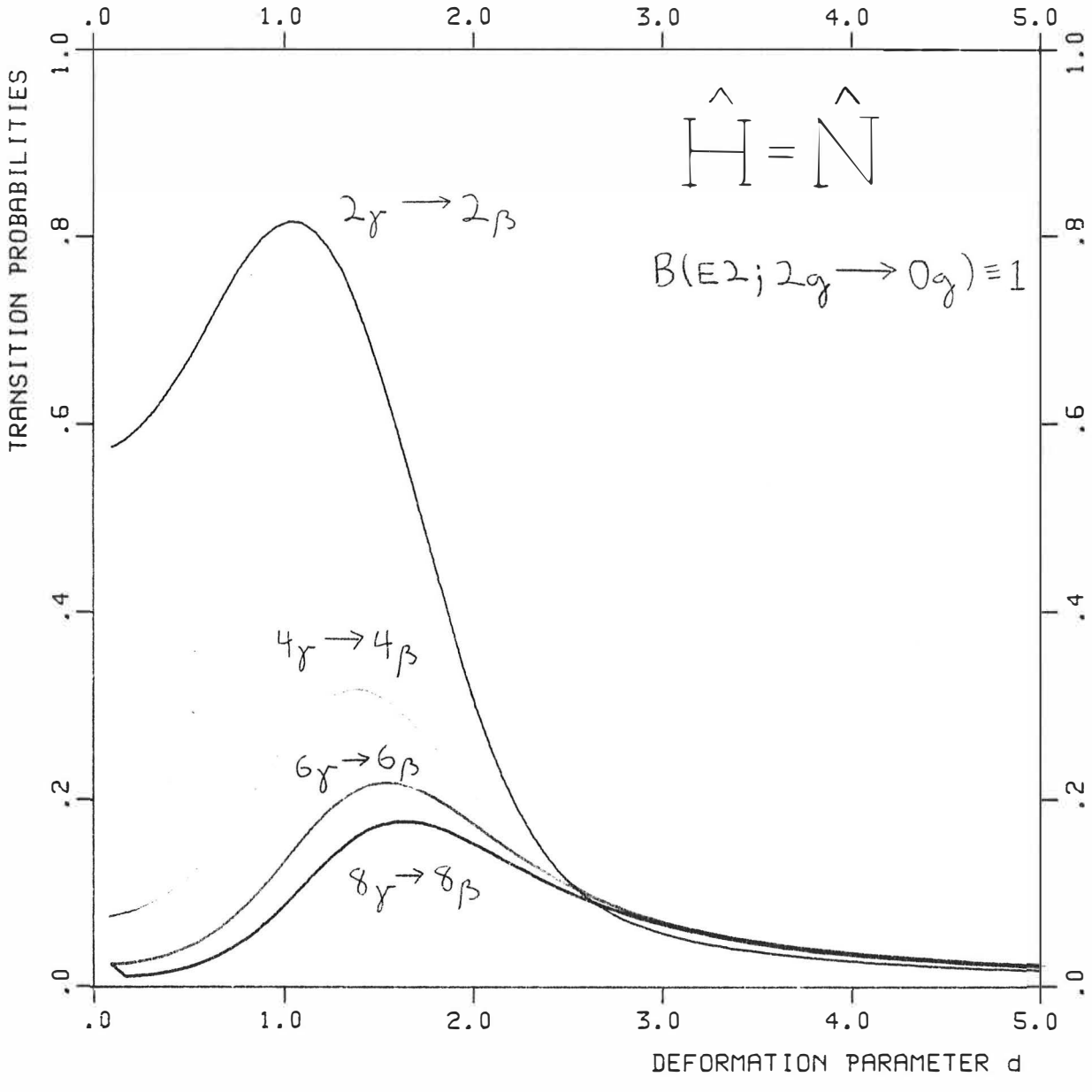

FIGURE 12 : Interband E2 transition probabilities B(E2; gamma J ⟶ beta J) as functions of the deformation parameter d for the harmonic system $\hat{H} = \hat{N}$.

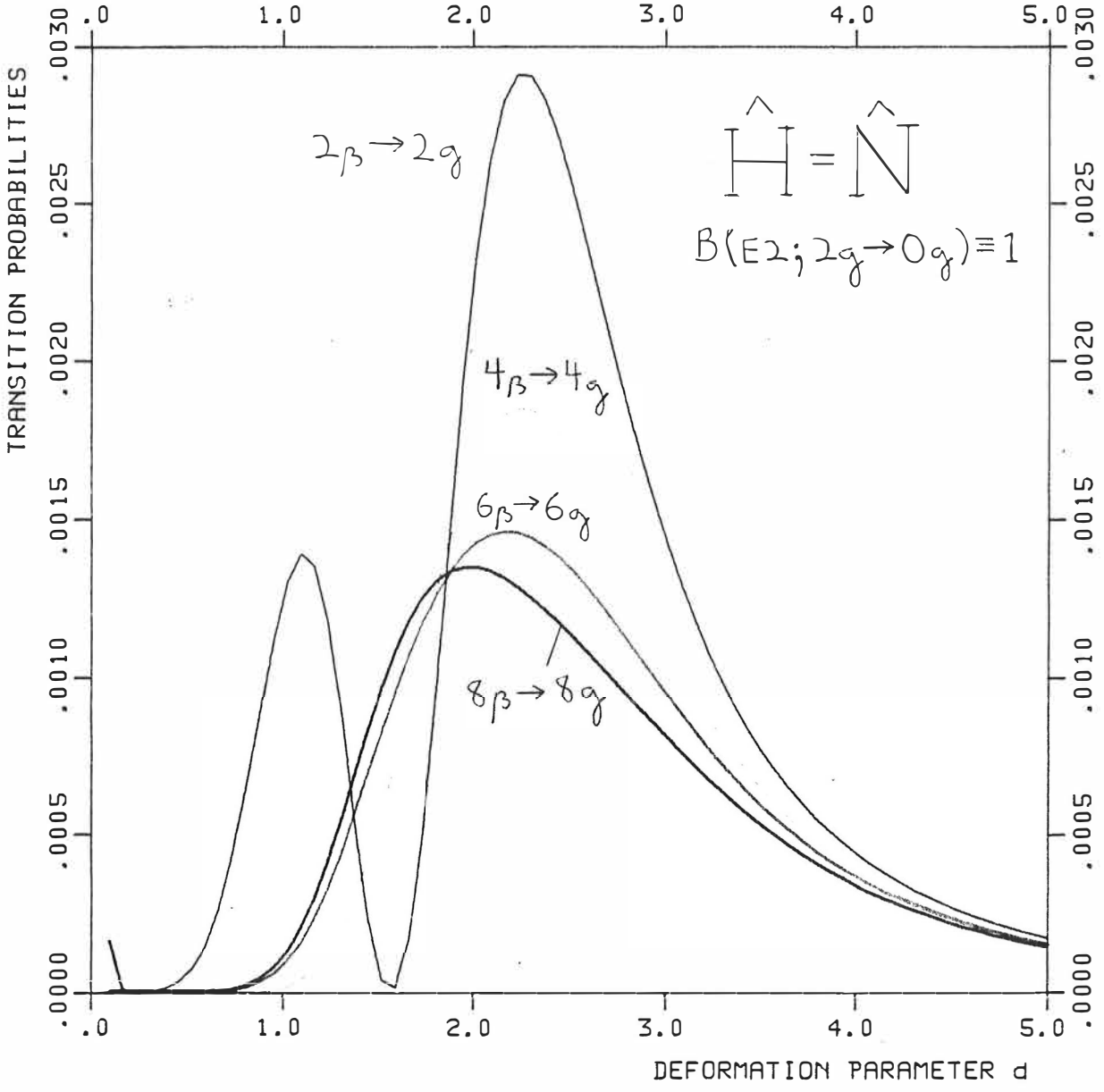

FIGURE 13 : Interband E2 transition probabilities B(E2; beta J $\rightarrow$ ground J) as functions of the deformation parameter d for the harmonic system $\hat{H}=\hat{N}$.

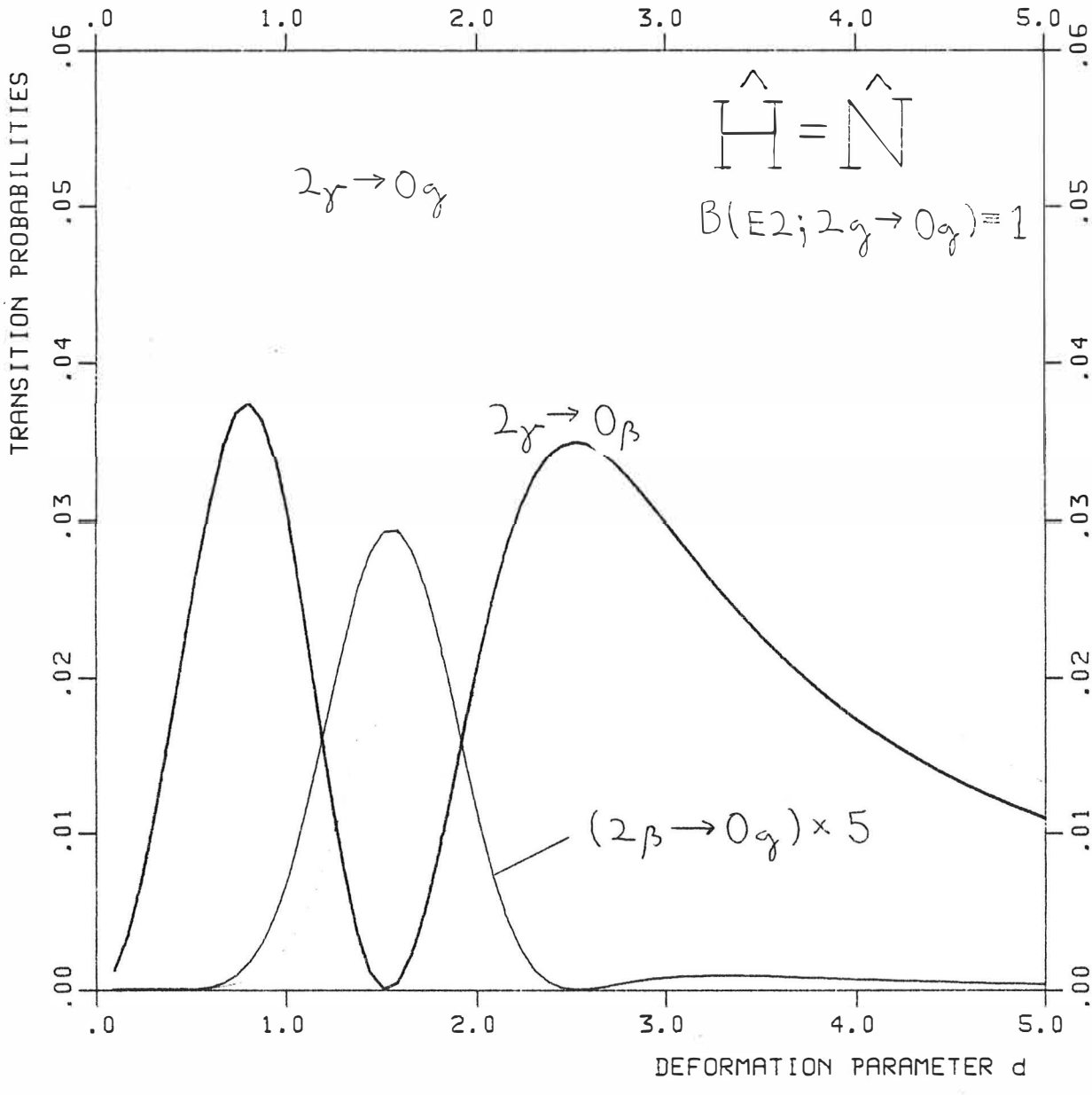

FIGURE 14 : The three interband probabilities B(E2; J=2 $\longrightarrow$ J=0) as functions of the deformation parameter d for the harmonic system $\hat{H}=\hat{N}$.

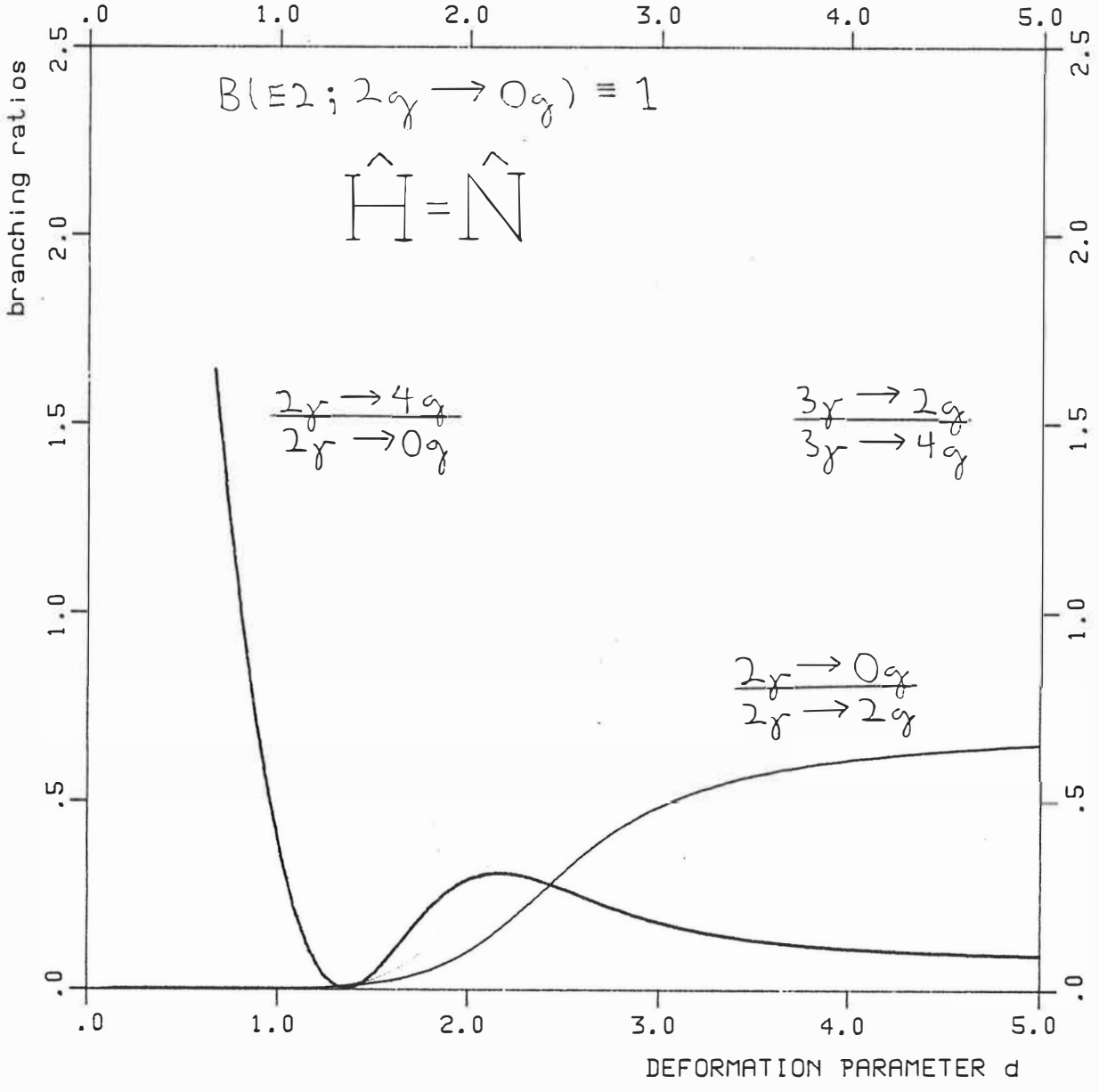

FIGURE 15 : Some specific branching ratios as functions of the deformation parameter d for the harmonic system $\hat{H} = \hat{N}$.

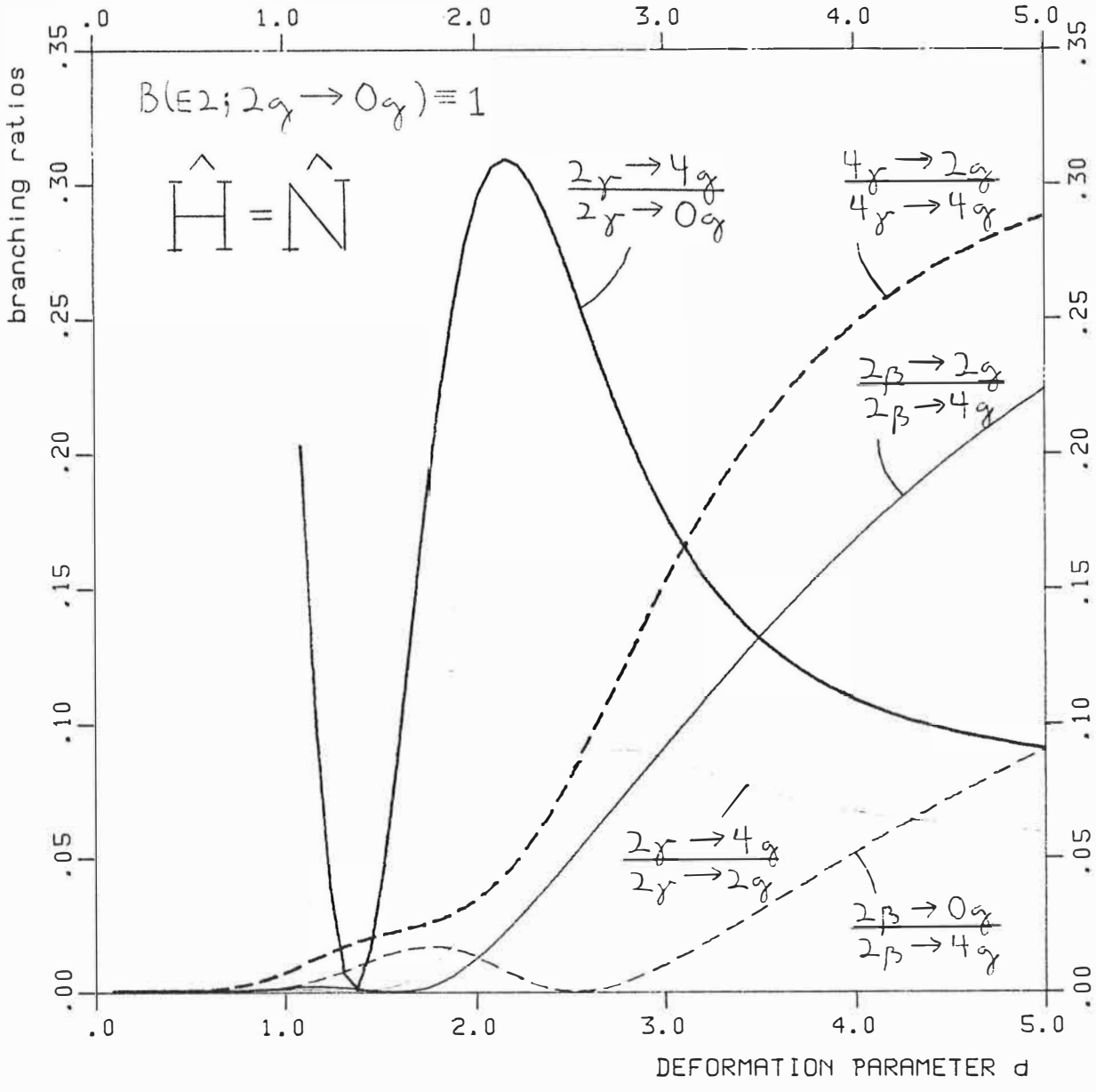

FIGURE 16 : Some specific branching ratios as functions of the deformation parameter d for the harmonic system $\hat{H} = \hat{N}$.

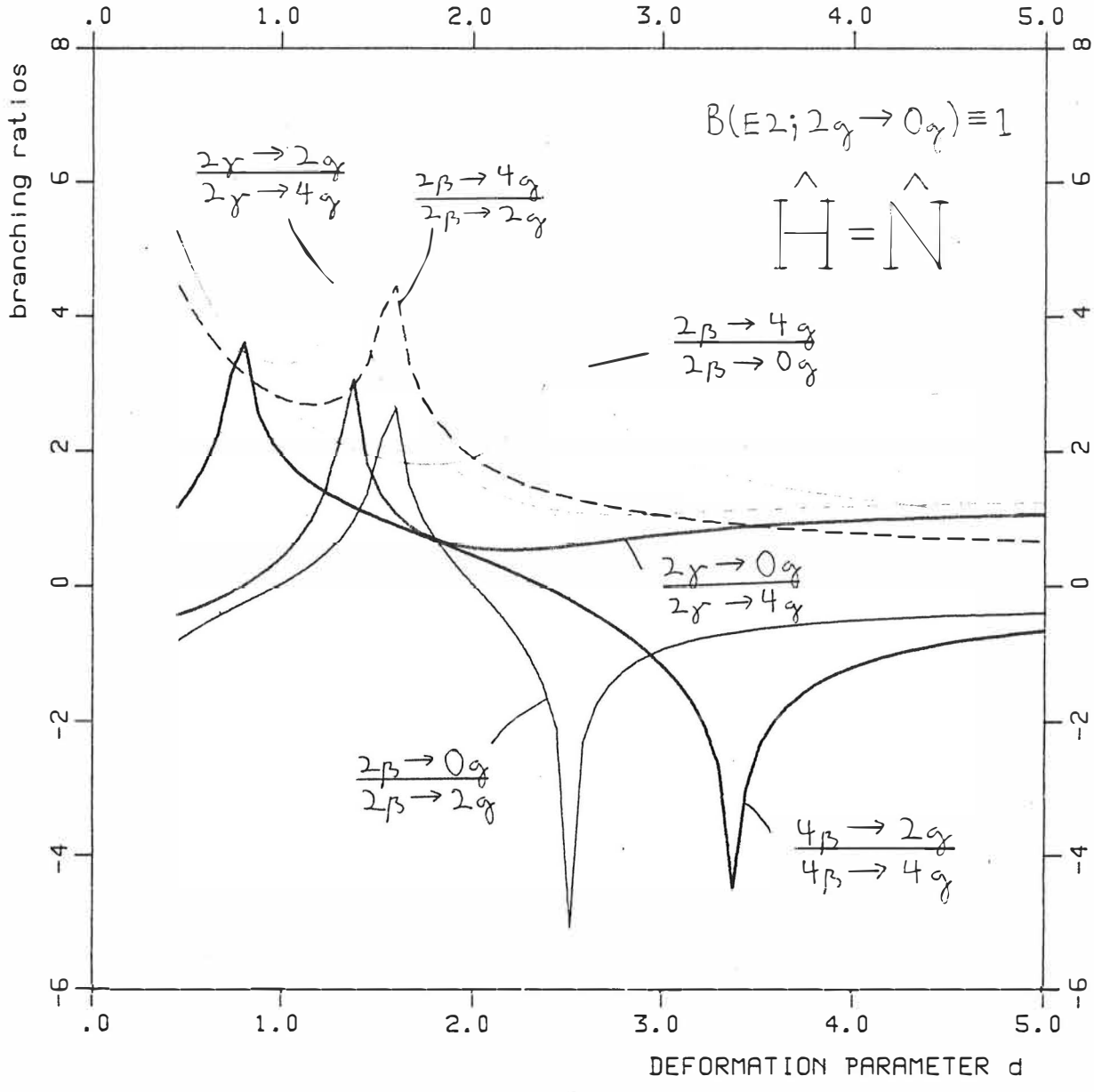

FIGURE 17 : Logarithms of some specific branching ratios as functions of the deformation parameter d for the harmonic system $\hat{H} = \hat{N}$.

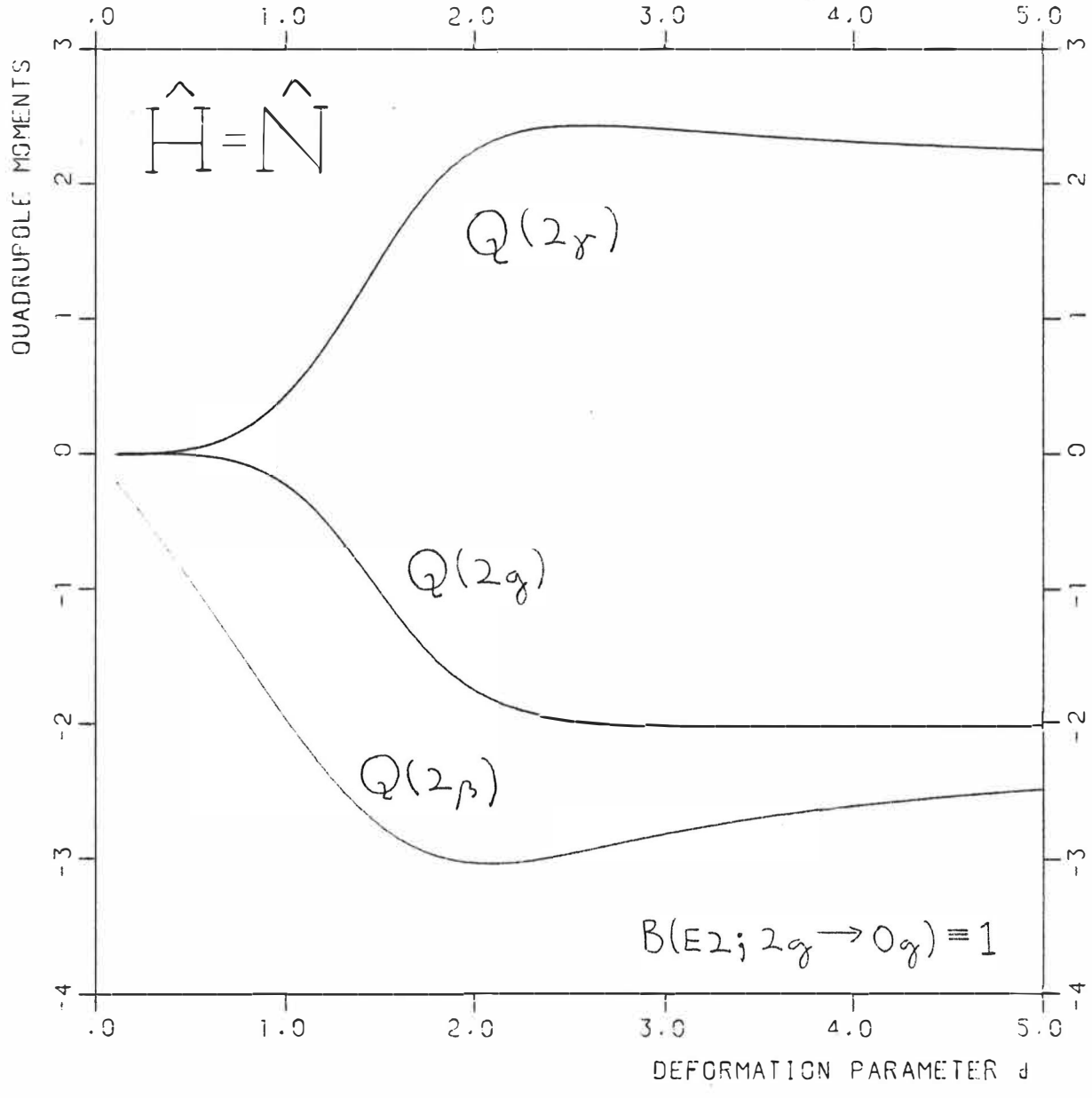

FIGURE 18 : Static quadrupole moments Q(J) of J=2 states as functions of the deformation parameter d for the harmonic system $\hat{H} = \hat{N}$.

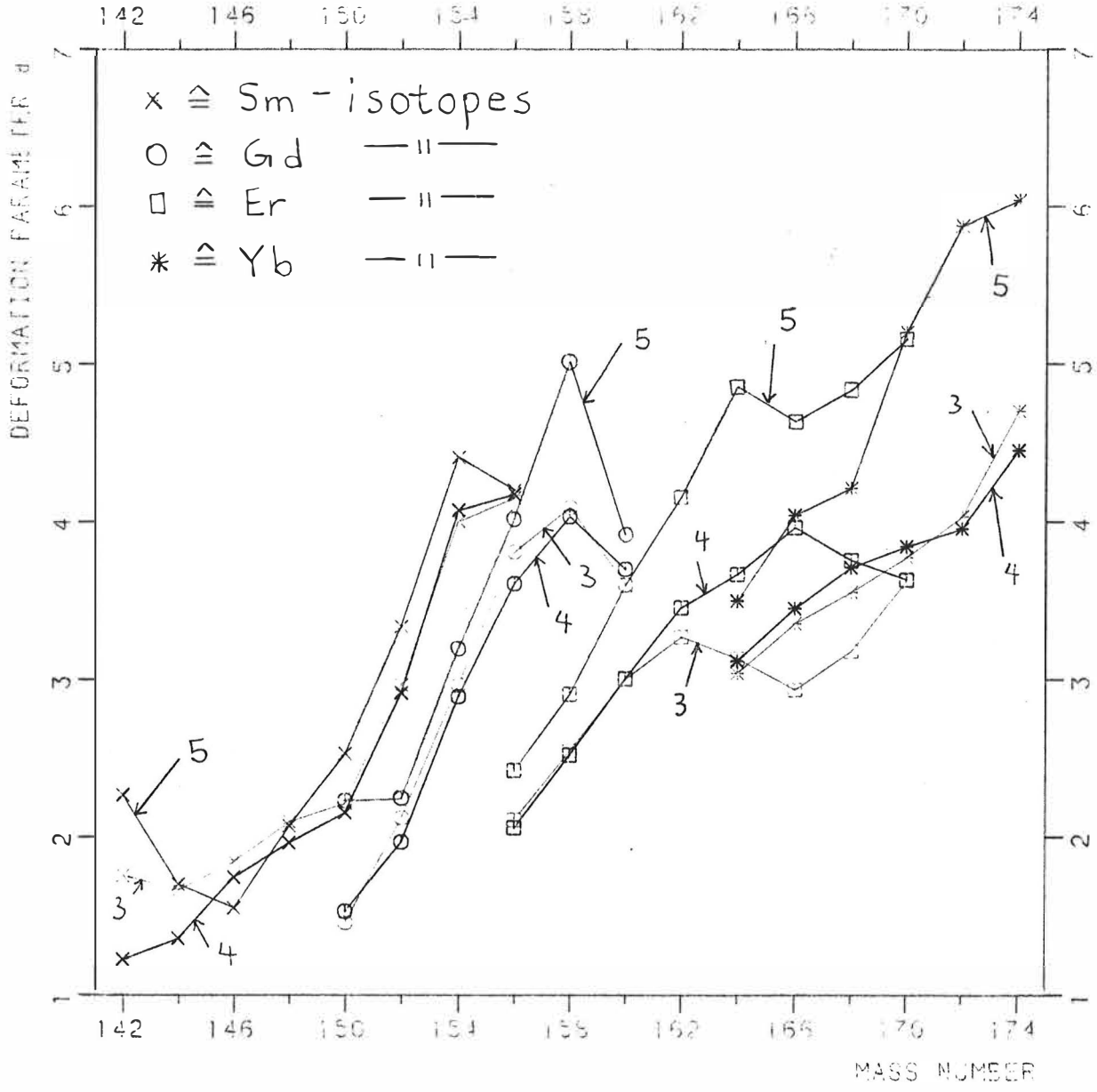

FIGURE 19 : The deformation parameter d as a function of the mass number in the Sm, Gd, Er and Yb chains. The parameter values are results of 3-,4- and 5-parameter fits to the experimental energy spectra.

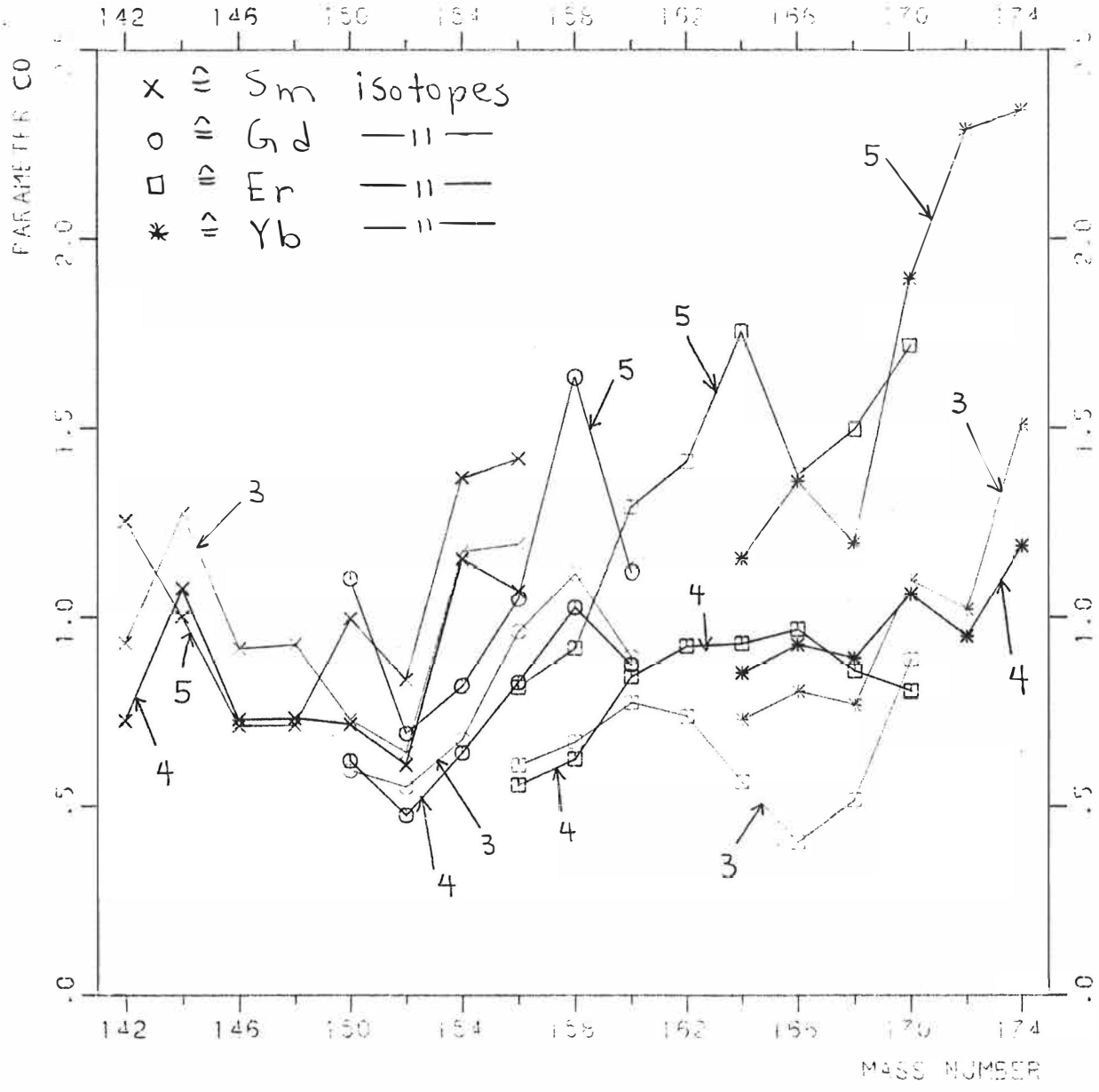

FIGURE 20 : The parameter c_0 of the effective Hamiltonian of eq. (III.2.2) as a function of the mass number in the Sm, Gd, Er and Yb chains. The parameter values are a result of 3-,4- and 5-parameter fits to the experimental energy spectra.

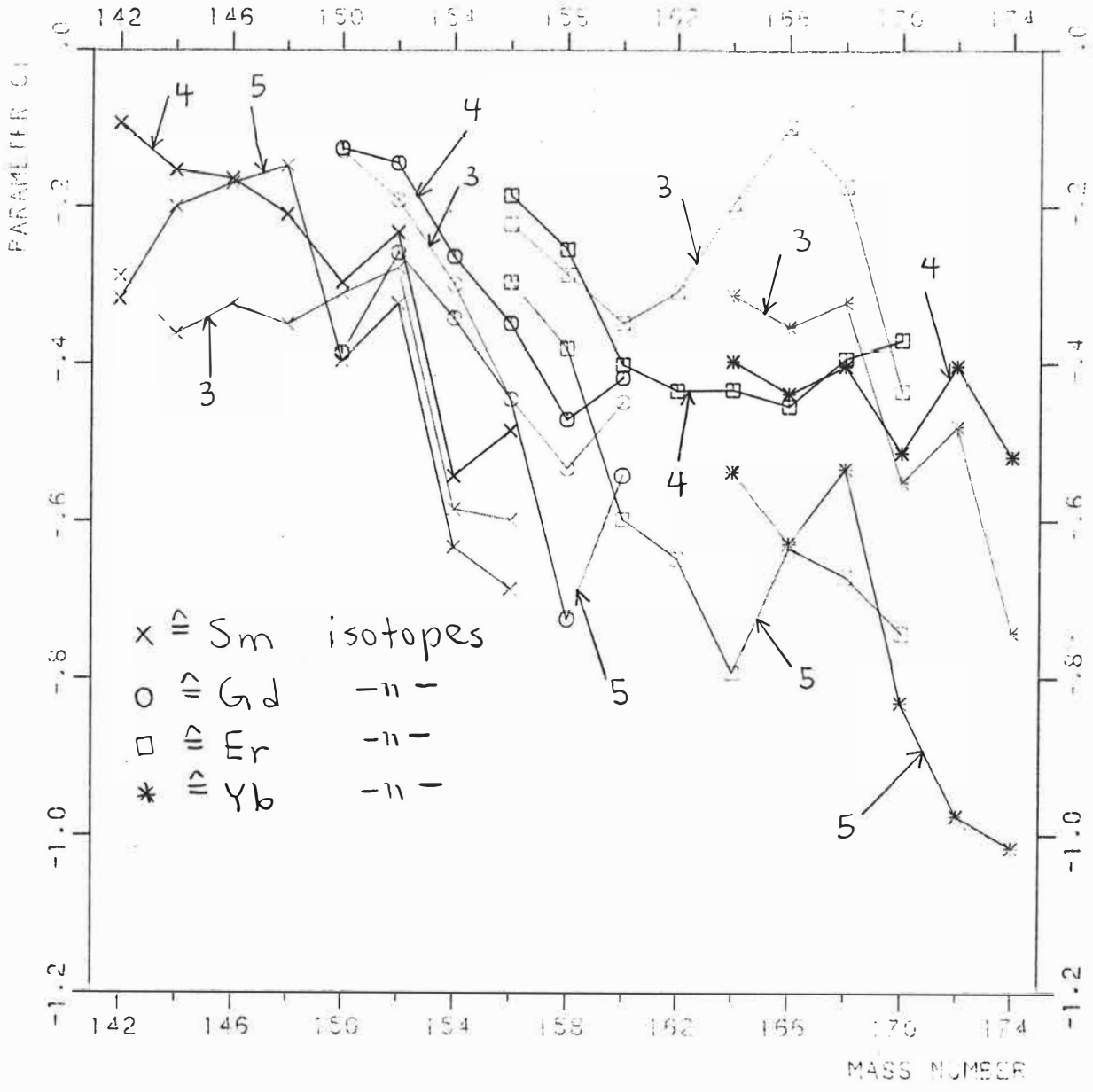

FIGURE 21 : The parameter c_1 of the effective Hamiltonian of eq. (III.2.2) as a function of the mass number in the Sm,Gd,Er and Yb chains. The parameter values are a result of 3-,4- and 5-parameter fits to the experimental energy spectra.

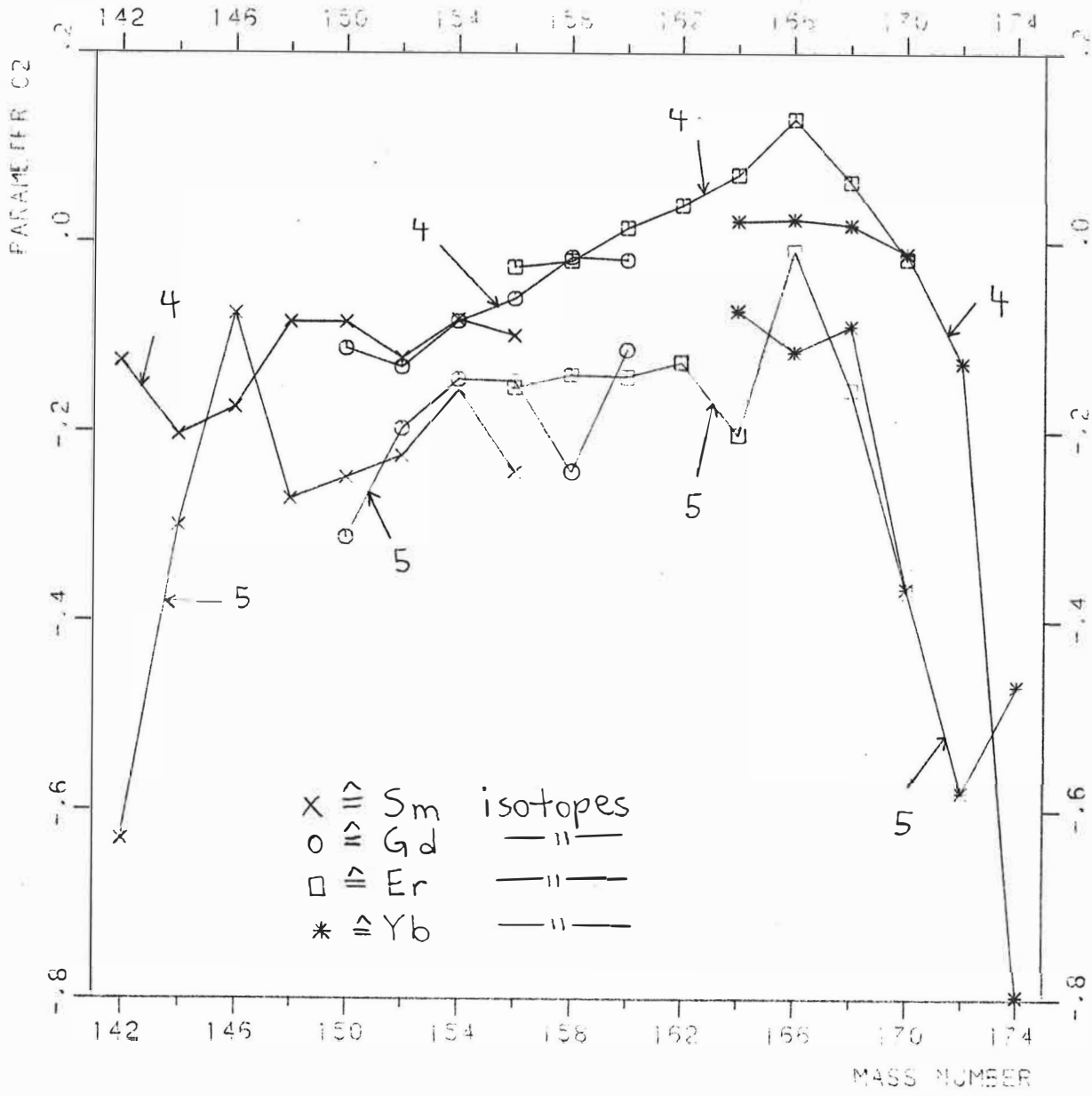

FIGURE 22 : The parameter c_2 of the effective Hamiltonian of eq. (III.2.2) as a function of the mass number in the Sm,Gd,Er and Yb chains. The parameter values are a result of 3-,4- and 5-parameter fits to the experimental energy spectra.

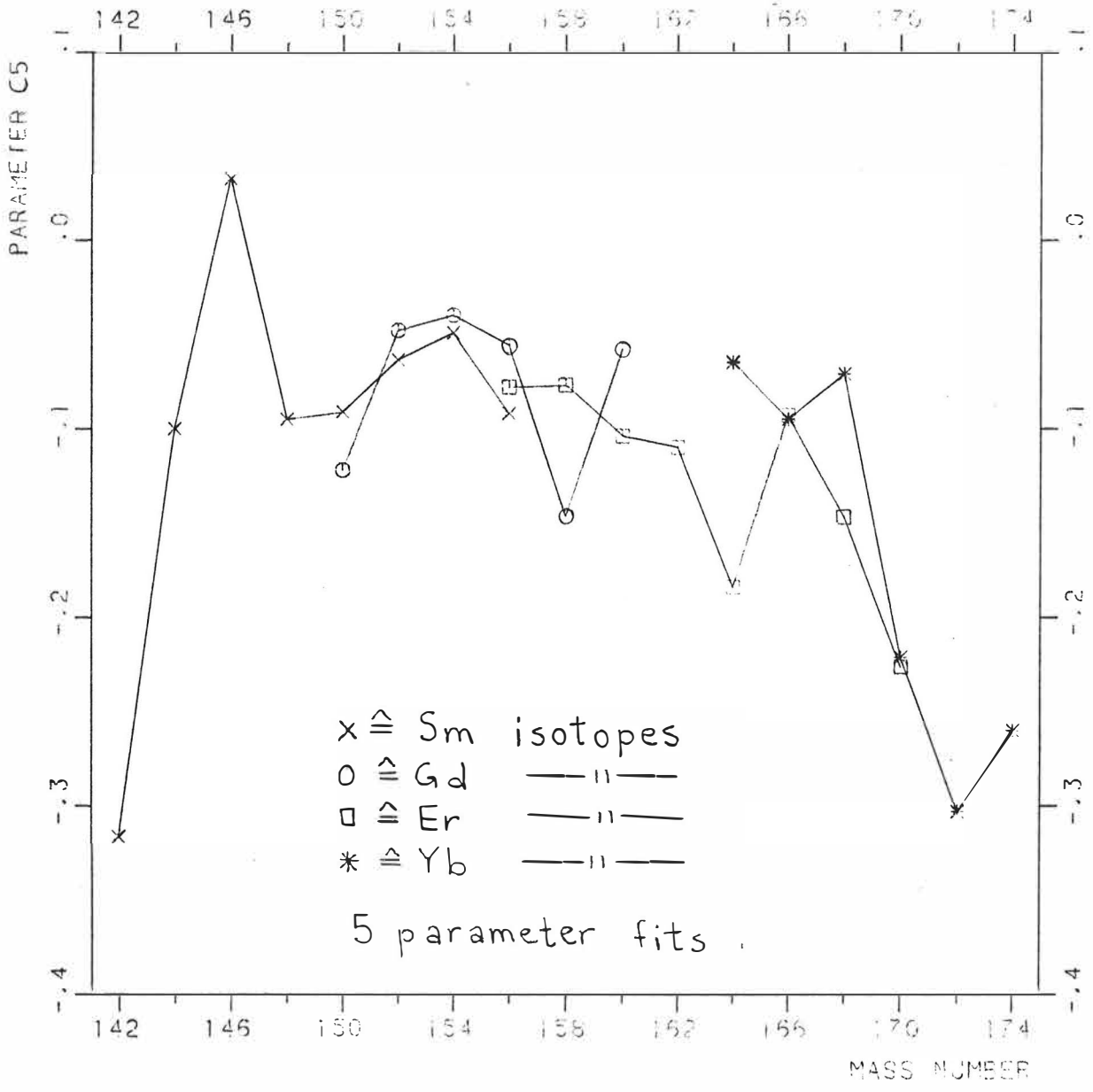

FIGURE 23 : The parameter c_5 of the effective Hamiltonian of eq. (III.2.2) as a function of the mass number in the Sm,Gd,Er and Yb chains. The parameter values are a result of 3-,4- and 5-parameter fits to the experimental energy spectra.

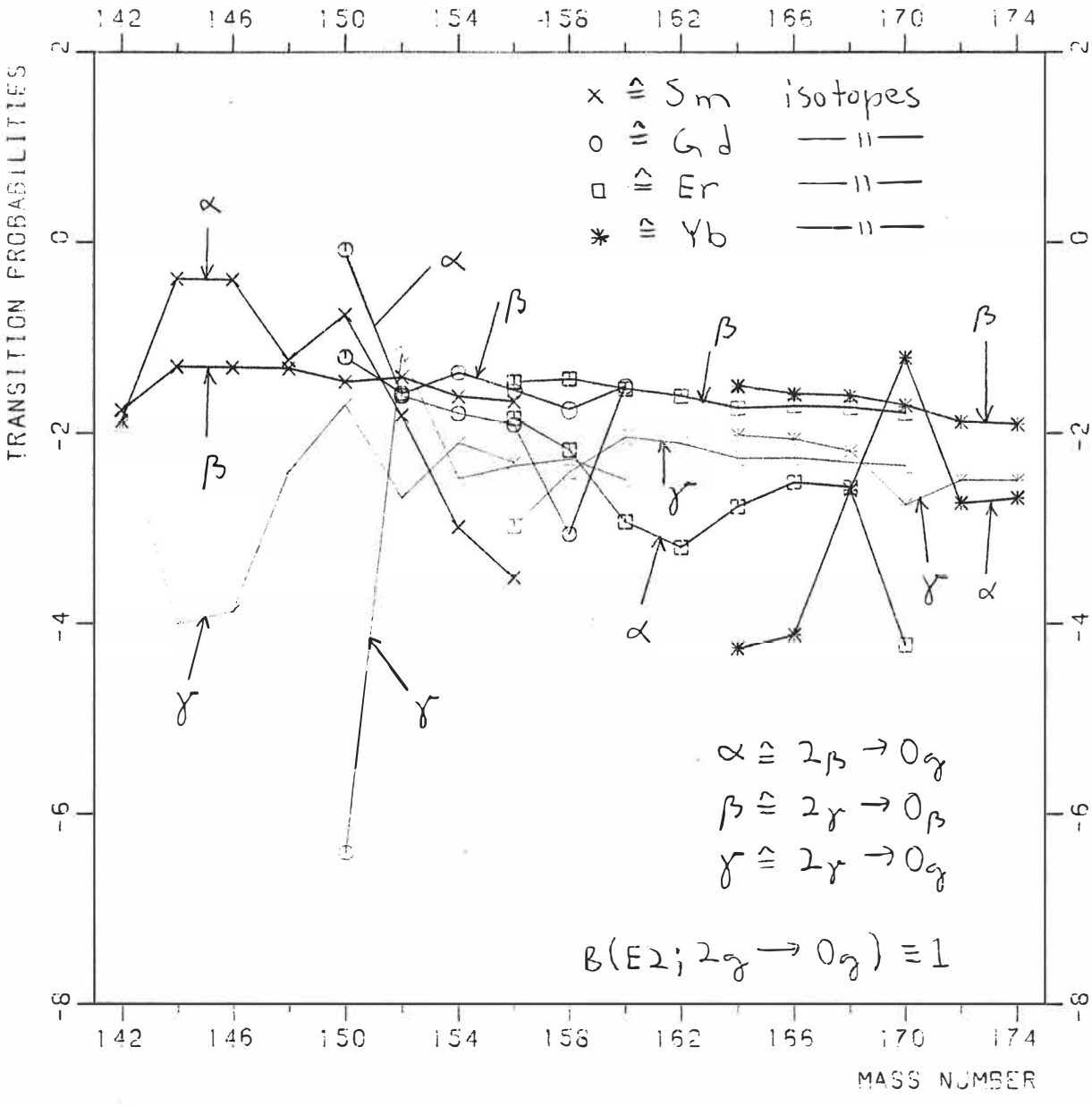

FIGURE 24 : Logarithms of all E2 transition probabilities B(E2; J=2 $\longrightarrow$ J=0) as functions of mass number in the Sm, Gd, Er and Yb chains. The normalization is B(E2; $2_g \longrightarrow 0_g$) = 1 . The wave functions used in the calculations result from a fit to the experimental energy spectrum.

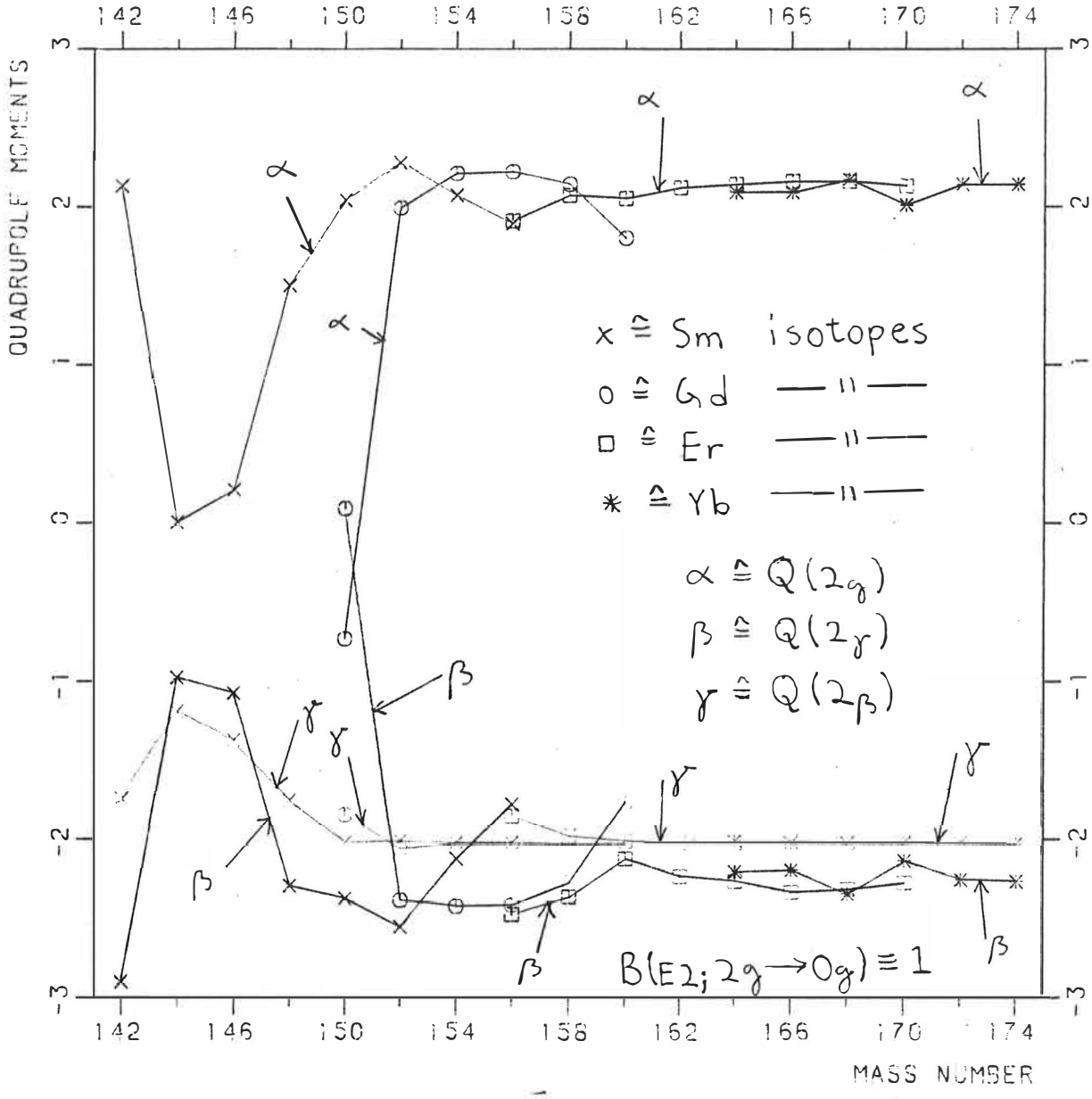

FIGURE 25 : Quadrupole moments of the J=2 states as functions of the mass number in the Sm, Gd, Er and Yb chains. The normalization is

$$B(E2; 2_g \longrightarrow 0_g) \equiv 1 \quad .$$

The wave functions used in the calculations are from a fit to the experimental energy spectrum.

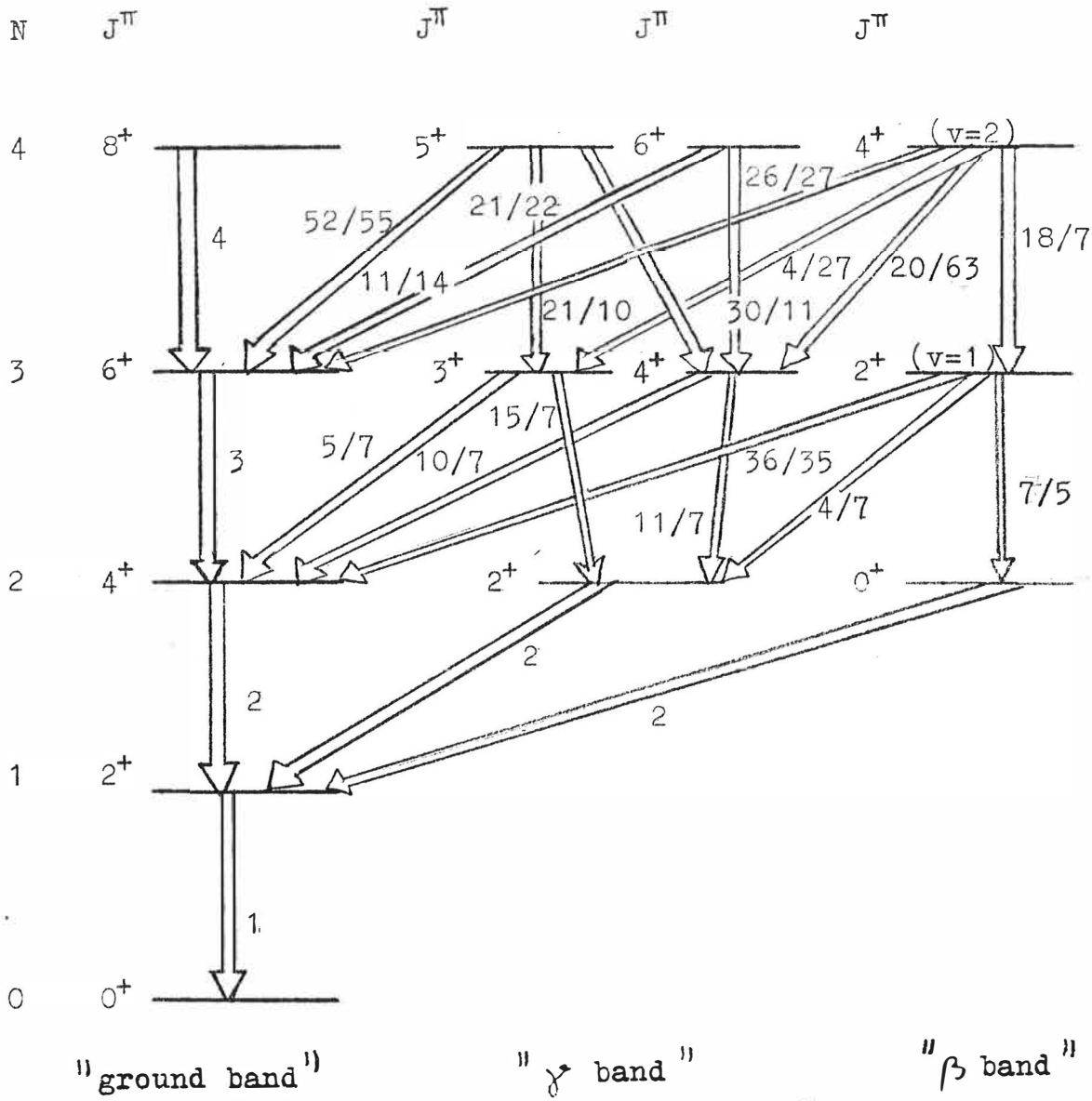

FIGURE 26:
U(5) multiphonon excitations up to four phonons. The E2 transition probabilities between the multiplet levels are also shown. (Only those levels are shown which constitute the zero-d limit of the EPM levels in the g, β and γ bands). The transition probability B(E2;2g-->0g) is normalized to unity. The states are labelled according to the irreducible representation labels of the chain U(5)⊃O(5)⊃O(3)⊃O(2), i.e.

$$|N\ v\ J\ M\rangle \quad ,$$

where N is the number of quadrupole phonons and v is the boson seniority. This set of quantum numbers is complete for N<5.

FIGURES 27-31:
Spectra of some typical EPM-calculated nuclei with distinct spectroscopic character. ^{172}Yb (in fig. 27) is a typical symmetric rotor nucleus with a J(J+1) structure within the bands. A stiff prolate rotor is characterized by a rather high-lying γ band. In the case of triaxial deformations the γ band begins at low excitation energies, even lower than the β band, as one can see in fig. 28 for ^{166}Er, which is considered to be a triaxial nucleus /Bo75/.

Fig.29 shows the spectrum of the nucleus ^{158}Gd, which possesses features of a γ-unstable rotor. It is characterized by even-odd staggering in the γ band. Also characteristic is the fact that the β- and γ-band energies are more or less the same or the γ band lies lower (as in the triaxial case).

Fig. 30 shows a typical vibrator nucleus, ^{150}Gd, with an almost even energy level spacing and the characteristic bunching of the levels to (almost) degenerate groups. Note especially the bunching of the J=even and J-1=odd levels in the γ band. This is in accordance with the γ band behaviour encountered in fig.2.

In fig. 31 I have shown the very peculiar spectrum of ^{148}Sm calculated by the EPM (a fit to experiment with 5 parameters). It shows rather nicely the flexibility of the EPM to describe also shape co-existence phenomena in nuclei (potential energy surfaces with two minima). In this case the β band shows a rotational-like low-energy behaviour, the high energy levels being evenly spaced. The γ band levels are more or less evenly spaced (with no tendency to bunch into the J=even, J-1=odd groups, however) and the ground-state band shows a typical shell-model single-particle pairing spectrum.

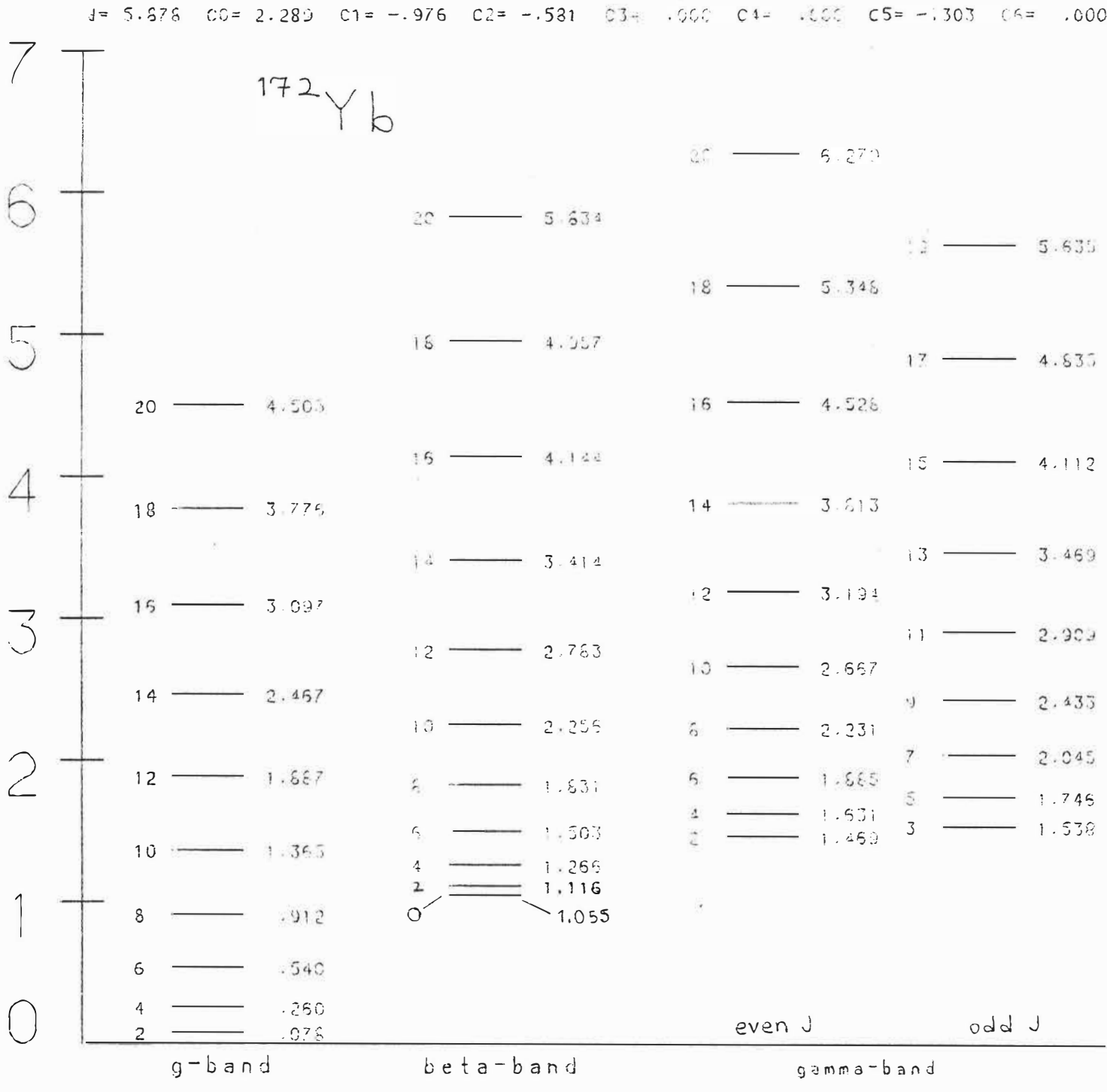

FIGURE 27 : The EPM fitted spectrum of ^{172}Yb.

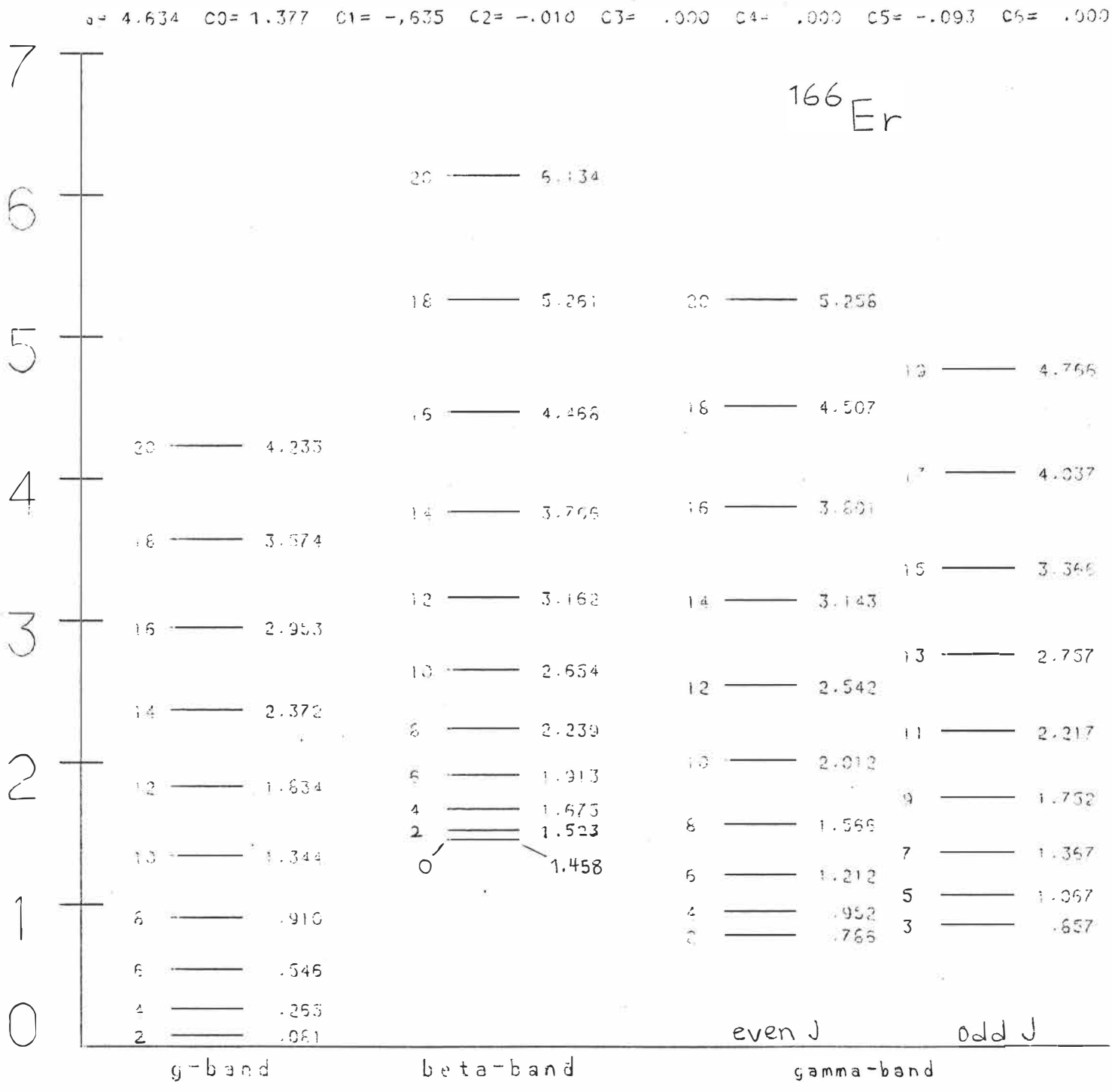

FIGURE 28 : The EPM fitted spectrum of ^{166}Er.

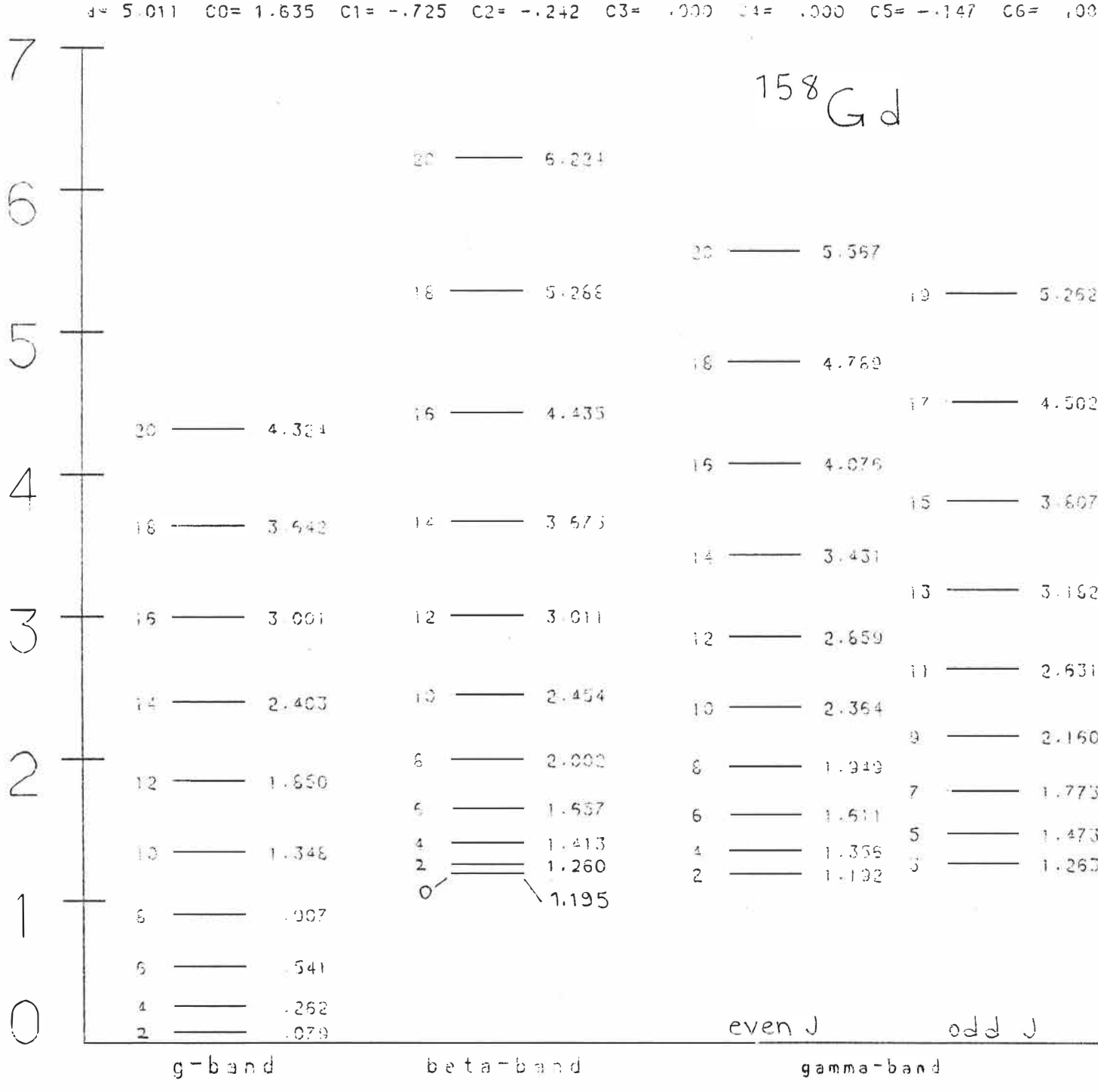

FIGURE 29 : The EPM fitted spectrum of ^{158}Gd.

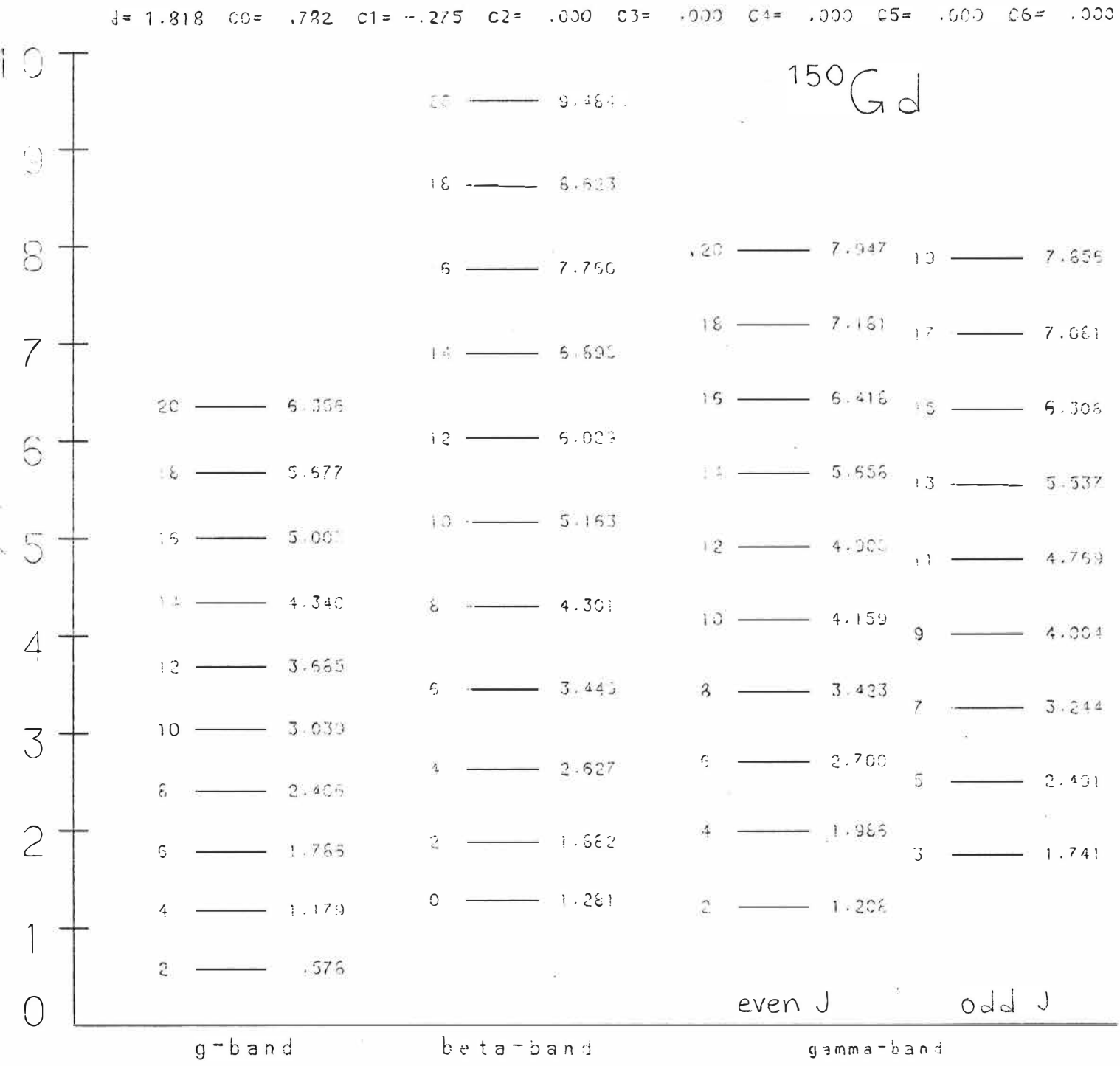

FIGURE 30 : The EPM fitted spectrum of ^{150}Gd.

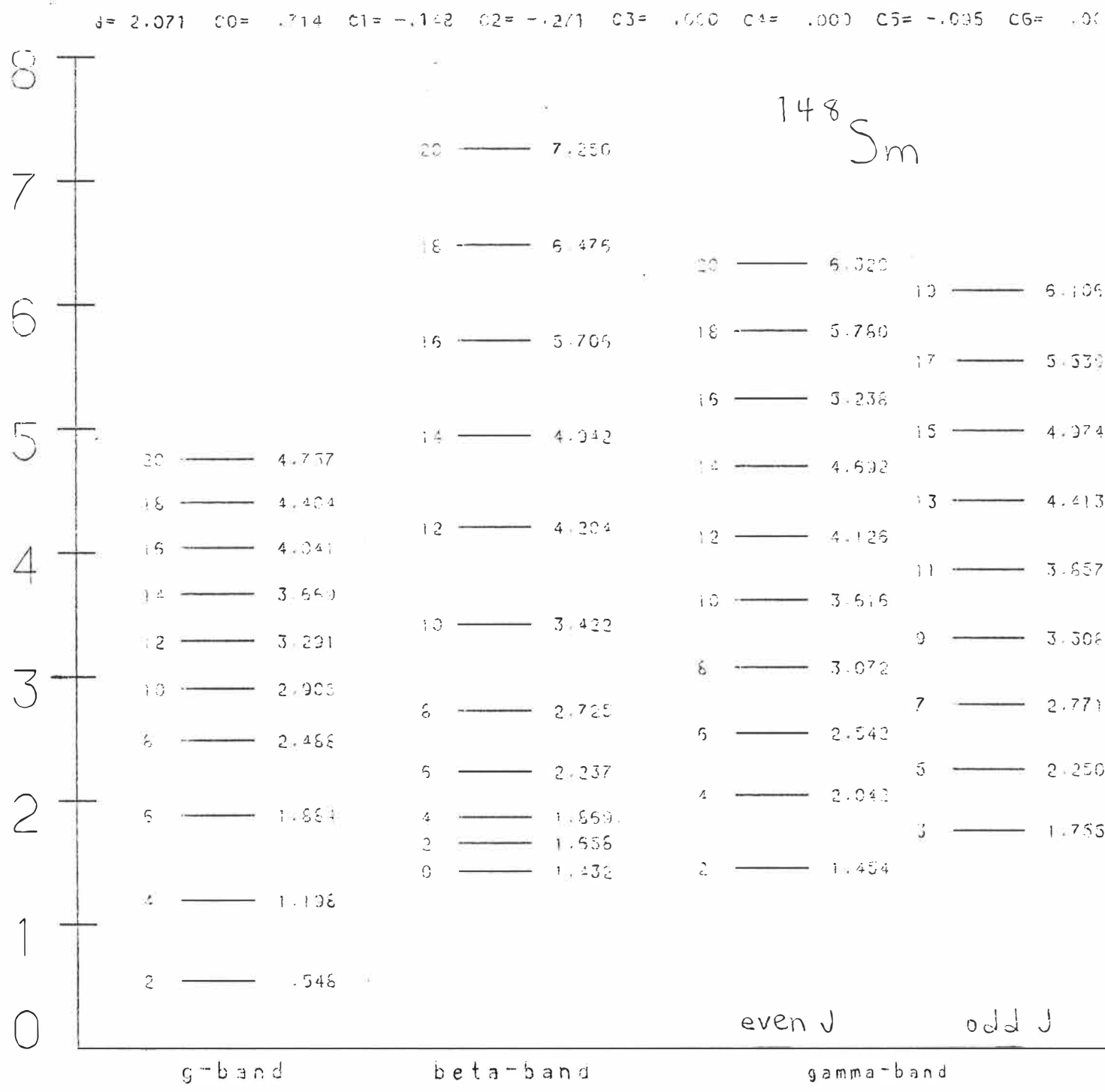

FIGURE 31 : The EPM fitted spectrum of ^{148}Sm.

APPENDICES

A. USEFUL FORMULAS

A1. Wigner D-functions and Tensor Operators

In this appendix the conventions of /Ro57/ and /Sh63/ are used.

$$D^{j}_{m'm}(\alpha,\beta,\gamma) = \langle j\,m'|\, e^{-i\alpha J_z}\, e^{-i\beta J_y}\, e^{-i\gamma J_z}\,|\, j\,m\rangle = \tag{A1.1}$$

$$= e^{-im'\alpha - im\gamma}\langle j\,m'|\, e^{-i\beta J_y}\,|\, j\,m\rangle \equiv e^{-im'\alpha - im\gamma}\, d^{j}_{m'm}(\beta)$$

$$d^{j}_{m'm}(\beta) = d^{j\,*}_{m'm}(\beta) \tag{A1.2}$$

$$d^{j}_{m'm}(-\beta) = d^{j}_{mm'}(\beta) \tag{A1.3}$$

$$d^{j}_{m'm}(\beta) = (-1)^{m'-m}\, d^{j}_{mm'}(\beta) \tag{A1.4}$$

$$D^{j}_{m'm}(\Omega) = (-1)^{m'-m}\, D^{j\,*}_{-m'-m}(\Omega) \tag{A1.5}$$

$$D^{j\,*}_{m'm}(\Omega) = (-1)^{m'-m}\, D^{j}_{-m'-m}(\Omega) \tag{A1.6}$$

$$D^{j}_{m0}(\Omega) = \sqrt{\frac{4\pi}{2j+1}}\, Y^{*}_{jm}(\beta,\alpha) \tag{A1.7}$$

(A1.8) $$Y_{\ell m}(\beta,\alpha) = \sqrt{\frac{2\ell+1}{4\pi}}\, d^{\ell}_{m0}(\beta) e^{-im\alpha}$$

(A1.9) $$D^{j}_{m'm}(-\gamma,-\beta,-\alpha) = D^{j\,*}_{mm'}(\alpha,\beta,\gamma)$$

(A1.10) $$\sum_{m''} D^{j}_{mm''} D^{j\,*}_{m'm''} = \delta_{mm'}$$

(A1.11) $$\int_{-1}^{1} d(\cos\beta)\, d^{j}_{m_1m_2}(\beta)\, d^{j'}_{m_1'm_2'}(\beta) = \frac{2}{2j+1}\,\delta_{jj'}\,\delta_{m_1m_1'}\,\delta_{m_2m_2'}$$

(A1.12) $$\int_{\text{all space}} \ldots\, d\Omega = \int_0^{2\pi}\int_0^{\pi}\int_0^{2\pi} \ldots\, d\alpha \sin\beta\, d\beta\, d\gamma$$

(A1.13) $$\int_{\text{all space}} D^{j\,*}_{m_1m_2}(\Omega)\, D^{j'}_{m_1'm_2'}(\Omega)\, d\Omega = \frac{8\pi^2}{2j+1}\,\delta_{jj'}\,\delta_{m_1m_1'}\,\delta_{m_2m_2'}$$

(A1.14) $$\int_{\text{all space}} D^{j}_{m'm}(\Omega)\, d\Omega = 8\pi^2\,\delta_{j0}\,\delta_{m'0}\,\delta_{m0}$$

Clebsch-Gordan series :

(A1.15) $$D^{j_1}_{m_1'm_1}(\Omega)\, D^{j_2}_{m_2'm_2}(\Omega) = \sum_{jmm'} (j_1\, m_1'\; j_2\, m_2' \mid j\, m')(j_1\, m_1\; j_2\, m_2 \mid j\, m)\, D^{j}_{m'm}(\Omega$$

(A1.16) $$D^{j}_{m'm}(\Omega) = \sum_{\substack{m_1 m_1' \\ m_2 m_2'}} (j_1\, m_1'\; j_2\, m_2' \mid j\, m') \times$$

$$\times (j_1\, m_1\; j_2\, m_2 \mid j\, m)\, D^{j_1}_{m_1'm_1}(\Omega)\, D^{j_2}_{m_2'm_2}(\Omega)$$

(notice: this is true for <u>any</u> j_1, j_2 for which $j_1 \otimes j_2 \ni j$)

(A1.17)
$$\frac{2j+1}{8\pi^2}\int d\Omega\, D^{j*}_{MM'}(\Omega) D^{j_1}_{m_1 m_1'}(\Omega) D^{j_2}_{m_2 m_2'}(\Omega) =$$
$$= (j_1\, m_1\, j_2\, m_2 \mid J\, M)(j_1\, m_1'\, j_2\, m_2' \mid J\, M')$$

(A1.18)
$$d^j_{mn}(\beta) = \sum_{\varkappa} \frac{(-1)^{\varkappa}\sqrt{(j+n)!(j-n)!(j+m)!(j-m)!}}{\varkappa!(j+n-\varkappa)!(j-m-\varkappa)!(\varkappa+m-n)!} \times$$
$$\times \left(\cos\tfrac{\beta}{2}\right)^{2j-2\varkappa-m-n}\left(-\sin\tfrac{\beta}{2}\right)^{2\varkappa+m-n}$$

(A1.19)
$$d^j_{mn}(\beta) = \sqrt{\frac{(j+n)!(j-n)!}{(j+m)!(j-m)!}}\left(\cos\tfrac{\beta}{2}\right)^{n+m}\left(\sin\tfrac{\beta}{2}\right)^{n-m} \times$$
$$\times P^{(n-m,n+m)}_{j-m}(\cos\beta)$$

For the Jacobi polynomial $P^{(a,b)}_j(x)$ one has the recursion relation

(A1.20)
$$2j(a+b+j)(a+b+2j-2)P^{(a,b)}_j(x) =$$
$$= (a+b+2j-1)\{(a+b+2j-2)(a+b+2j)x +$$
$$+ (a+b)(a-b)\}P^{(a,b)}_{j-1}(x) - 2(a+j-1)\times$$
$$\times (b+j-1)(a+b+2j)P^{(a,b)}_{j-2}(x)$$

For tensor operators $T_q^{(k)}$ of rank k and components q one has the relations

$$T_q^{(k)'} = U(\Omega) T_q^{(k)} U^{\dagger}(\Omega) = \sum_{q'=-k}^{k} T_{q'}^{(k)} D^{k}_{q'q}(\Omega) \quad , \tag{A1.21}$$

$$U(\Omega) = e^{-i\omega \hat{n}\cdot\vec{J}}$$

For Hermitian tensors

$$T_m^{(k)\dagger} = (-1)^m T_{-m}^{(k)} \tag{A1.22}$$

For the spherical components of the angular momentum one has

$$J_0 \equiv J_z \quad ; \quad J_{\pm 1} \equiv \mp \frac{1}{\sqrt{2}} \left(J_x \pm i J_y \right) \tag{A1.23}$$

$$J_{\pm 1} | j\ m \rangle = \mp \sqrt{\tfrac{1}{2}\left[j(j+1) - m(m\pm 1) \right]}\ | j\ m\pm 1 \rangle \tag{A1.24}$$

(Condon-Shortley phase convention)

$$\left[J_0 , T_q^{(k)} \right] = q\, T_q^{(k)} \quad , \tag{A1.25}$$

where $T_q^{(k)}$ is a spherical tensor.

A2. Relations for Projectors and Collective Coordinates

$$P^J_{MK} = \frac{2J+1}{8\pi^2}\int d\Omega\, D^{J\,*}_{MK}(\Omega)\,U(\Omega) =$$

(A2.1)
$$= \sum_{\alpha} |\alpha\, J\, M\rangle\langle \alpha\, J\, K|$$

σ = all additional quantum numbers

(A2.2) $$U(\Omega) = e^{-i\alpha J_z}\, e^{-i\beta J_y}\, e^{-i\gamma J_z} \equiv e^{-i\omega \hat{n}\cdot\vec{J}}$$

(A2.3) $$P^{J\dagger}_{MK} = P^J_{KM} \quad ; \quad P^{J\dagger}_{MK}\, P^{J'}_{M'K'} = \delta_{JJ'}\,\delta_{MM'}\,P^J_{KK'}$$

(A2.4) $$|J\, M\, K\rangle = N_{JK}\, P^J_{MK}\,|K\rangle$$

(A2.5)
$$b'^{\dagger}_m \equiv U(\Omega)\, b^{\dagger}_m\, U^{\dagger}(\Omega) = \sum_{m'} b^{\dagger}_{m'}\, D^2_{m'm}(\Omega)$$
$$b'_m \equiv U(\Omega)\, b_m\, U^{\dagger}(\Omega) = \sum_{m'} b_{m'}\, D^{2\,*}_{m'm}(\Omega)$$

The b 's are quadrupole phonon operators and transform as second-order spherical tensors.

(A2.6) $$|\tilde{0}\rangle = e^{d b^{\dagger}_0}\,|0\rangle \quad ; \quad |0^{\beta}\rangle \equiv e^{-\frac{1}{2}d^2}\,|\tilde{0}\rangle$$

(A2.7) $$b_m|\tilde{0}\rangle = d\,\delta_{m0}|\tilde{0}\rangle \; ; \; b_m|0^{\beta}\rangle = d\,\delta_{m0}|0^{\beta}\rangle$$

(A2.8) $$b_m\, U(\Omega)|\tilde{0}\rangle \equiv b_m|R\rangle = d\, D^2_{m0}(\Omega)|R\rangle$$

(A2.9) $$\langle \tilde{0} | U(\Omega) | \tilde{0} \rangle = e^{d^2 D^2_{00}(\Omega)}$$

(A2.10) $$P^J_{MK} T^{(k)}_q = (-1)^{M-K} (2J+1) \times$$
$$\times \sum_{\lambda\mu\nu q'} (J-M\, k\, q' | \lambda\, \mu)(J-K\, k\, q | \lambda\, \nu) \frac{T^{(k)}_{q'}}{2\lambda+1} P^{\lambda}_{\mu\nu}$$

(A2.11) $$U(\Omega) P^J_{MK} U^{\dagger}(\Omega) = \sum_{mm'} D^J_{mM}(\Omega) D^{J*}_{m'K}(\Omega) P^J_{mm'}$$

Transformation of the first quantized collective coordinates α_m to the intrinsic system (principal axis coordinates) :

(A2.12) $$a_m = U(\Omega) \alpha_m U^{\dagger}(\Omega) = \sum_{m'} \alpha_{m'} D^2_{m'm}(\Omega)$$
$$a_1 = a_{-1} = 0 \quad ; \quad a_2 = a_{-2}$$

Here the a_m are the collective coordinates in the principal axis system, the α_m are the collective coordinates in the laboratory system. The last relations specify the intrinsic system. More relations for α's can be found in /Ei75/ and /Ho72/ .

(A2.13) $$\alpha_m = \sum_{m'} a_{m'} D^{2*}_{mm'}(\Omega)$$

$$P^J_{MK}|0\rangle = \delta_{J0}\,\delta_{K0}\,|0\rangle$$

$$P^J_{MK}\,b^\dagger_m|0\rangle = \delta_{J2}\,\delta_{Km}\,b^\dagger_M|0\rangle$$

(A2.14)

$$P^J_{MK}(b^\dagger_m b^\dagger_{m'})|0\rangle = (-1)^K\sqrt{2J+1}\times$$

$$\times \begin{pmatrix} 2 & 2 & J \\ m & m' & -K \end{pmatrix}[b^\dagger b^\dagger]_{JM}|0\rangle$$

$$P^J_{MK}\left[b^\dagger_m (b^\dagger_{m'})^2\right]|0\rangle = (-1)^K\sqrt{2J+1}\times$$

$$\times \sum_{L=0,2,4}\sqrt{2L+1}\begin{pmatrix} 2 & 2 & L \\ m' & m' & -2m' \end{pmatrix}\begin{pmatrix} 2 & L & J \\ m & 2m' & -K \end{pmatrix}\times$$

$$\times\left[b^\dagger[b^\dagger b^\dagger]_L\right]_{JM}|0\rangle$$

A3. Clebsch-Gordan Coefficients and 3j-symbols

(A3.1) $$\begin{pmatrix} j_1 & j_2 & j_3 \\ m_1 & m_2 & m_3 \end{pmatrix} = \frac{(-1)^{j_1-j_2-m_3}}{\sqrt{2j_3+1}} (j_1\, m_1\, j_2\, m_2 \mid j_3 - m_3)$$

(A3.2) $$(j_1\, m_1\, j_2\, m_2 \mid j_3\, m_3) = (-1)^{j_2-j_1-m_3}\sqrt{2j_3+1}\begin{pmatrix} j_1 & j_2 & j_3 \\ m_1 & m_2 & -m_3 \end{pmatrix}$$

(A3.3) $$\begin{pmatrix} j_2 & j_1 & j_3 \\ m_2 & m_1 & m_3 \end{pmatrix} = (-1)^{j_1+j_2+j_3}\begin{pmatrix} j_1 & j_2 & j_3 \\ m_1 & m_2 & m_3 \end{pmatrix}$$

(A3.4) $$\begin{pmatrix} j_1 & j_2 & j_3 \\ -m_1 & -m_2 & -m_3 \end{pmatrix} = (-1)^{j_1+j_2+j_3}\begin{pmatrix} j_1 & j_2 & j_3 \\ m_1 & m_2 & m_3 \end{pmatrix}$$

(A3.5) $$(j_2\, m_2\, j_1\, m_1 \mid j_3\, m_3) = (-1)^{j_1+j_2-j_3}(j_1\, m_1\, j_2\, m_2 \mid j_3\, m_3)$$

(A3.6) $$(j_1 - m_1\; j_2 - m_2 \mid j_3 - m_3) = (-1)^{j_1+j_2-j_3}(j_1\, m_1\, j_2\, m_2 \mid j_3\, m_3)$$

(A3.7) $$(j_1\, m\, j_2 - m \mid 0\, 0) = \frac{(-1)^{j_1-m}}{\sqrt{2j_1+1}}\,\delta_{j_1 j_2} = \begin{pmatrix} j_1 & j_2 & 0 \\ m & -m & 0 \end{pmatrix}$$

(A3.8) $$(j_1\, 0\, j_2\, 0 \mid j_3\, 0) = 0 = \begin{pmatrix} j_1 & j_2 & j_3 \\ 0 & 0 & 0 \end{pmatrix}, \text{ if } j_1+j_2+j_3 = \text{odd}$$

CG orthogonality :

(A3.9) $$\sum_{m_1 m_2} (j_1\, m_1\, j_2\, m_2 \mid j'\, m')(j_1\, m_1\, j_2\, m_2 \mid j\, m) = \delta_{jj'}\delta_{mm'}$$

(A3.10) $$\sum_{jm} (j_1\, m_1'\, j_2\, m_2' \mid j\, m)(j_1\, m_1\, j_2\, m_2 \mid j\, m) = \delta_{m_1' m_1}\delta_{m_2' m_2}$$

3j orthogonality :

(A3.11) $$\sum_{m_1 m_2} \begin{pmatrix} j_1 & j_2 & j_3 \\ m_1 & m_2 & m_3 \end{pmatrix} \begin{pmatrix} j_1 & j_2 & j_3' \\ m_1 & m_2 & m_3' \end{pmatrix} = \frac{1}{2j_3+1} \delta_{j_3 j_3'} \delta_{m_3 m_3'}$$

(A3.12) $$\sum_{j_3 m_3} (2j_3+1) \begin{pmatrix} j_1 & j_2 & j_3 \\ m_1 & m_2 & m_3 \end{pmatrix} \begin{pmatrix} j_1 & j_2 & j_3 \\ m_1' & m_2' & m_3 \end{pmatrix} = \delta_{m_1 m_1'} \delta_{m_2 m_2'}$$

B. THE MODEL OF BOHR AND MOTTELSON

The Bohr and Mottelson model (=BMM) contains the spherical vibrators (spherical liquid drop model = SLDM) and deformed rotors (the deformed LDM, which for axially symmetric shapes is called the rotation-vibration model = RVM). More about this one can read from /Ri80/ and /Ei75/ .

In the LDM the nuclear surface is described by the quadrupole degrees of freedom (which is not,of course, the most general description):

$$(B.1) \qquad R = R(\theta,\phi) = R_0\left[1 + \sum_{m=-2}^{2} \alpha_m Y^*_{2m}(\theta,\phi)\right] \quad ,$$

where α_{00} and the α_{1m} have been dropped because of the conservation of the volume and to exclude the spurious centre-of-mass motion. Here the α's are classical time dependent coordinates of small vibrations around a spherical shape of radius R_0 /Ei75/ .

The startig point in the BMM is the harmonic, scalar(=rotationally invariant), time-reversal invariant collective laboratory Hamiltonian (isotropic)

$$(B.2) \qquad \hat{H} = \hat{T} + \hat{V} = \frac{1}{2}\sum_{m=-2}^{2}\left(B|\dot{\alpha}_m|^2 + C|\alpha_m|^2\right) \quad ,$$

where B and C are real constants (the inertia and stiffness

parameters) . In the case of SLDM the usual rules of canonical quantization lead to the following second-quantized form of $\hat{H}$ /Ei75/ :

$$\text{(B.3)} \qquad \hat{H} = \sum_{m=-2}^{2} \hbar\omega \left(b_m^{+} b_m + \tfrac{1}{2} \right) = \hbar\omega \hat{N} + \tfrac{5}{2}\hbar\omega \quad , \quad \omega \equiv \sqrt{C/B} \quad ,$$

where the b's are boson operators which are related to the first-quantized coordinates $\hat{\alpha}_m$ and their conjugate momenta $\hat{\Pi}_m$ by the relations

$$\text{(B.4)} \qquad \begin{aligned} \hat{\alpha}_m &= \sqrt{\frac{\hbar}{2\omega B}} \left(b_m^{+} + \bar{b}_m \right) \quad , \\ \hat{\Pi}_m &= i \sqrt{\frac{\hbar\omega B}{2}} \left((-1)^m b_{-m}^{+} - b_m \right) \quad . \end{aligned}$$

This gives the familiar phonon picture of harmonic quadrupole phonon oscillations around a spherical equilibrium shape.

In order to describe oscillations around a deformed shape and the resulting possibility of collective quantum mechanical rotations, a different way of approach to the Hamiltonian (B.2) must be taken. This leads to the deformed LDM or, in the special case of an axially symmetric droplet shape, to the RVM. The first thing to do is to try to separate the three rotational degrees of freedom described by the three Euler angles Ω from the intrinsic degrees of freedom (of which there must be two because the Hamiltonian (B.2) has five degrees of freedom). This may be achieved by the principal axis transformation to the intrinsic system

(also called the body-fixed or principal axis system, see appendix A2).

After this transformation one has, instead of the five laboratory variables α_m ($m=0,\pm1,\pm2$), the angles Ω and two intrinsic variables a_0, a_2, where the latter variables can be replaced by the more convenient Hill-Wheeler coordinates β and γ ($\beta>0$) :

$$a_0 = \beta\cdot\cos\gamma \quad ; \quad a_2 = a_{-2} = \frac{1}{\sqrt{2}}\beta\sin\gamma \tag{B.5}$$

The potential term of the Hamiltonian (B.2) is easy to handle because it has the same form in the laboratory system and in the principal axis system :

$$\sum_{m=-2}^{2}|\alpha_m|^2 \longrightarrow a_0^2 + 2a_2^2 = \beta^2 = V(\beta,\gamma=0) \tag{B.6}$$

In the deformed model, however, one wants to make a quadratic approximation in the vicinity of a deformed minimum β_0, γ_0 . Then the potential of (B.6) is replaced by

$$V(a_0,a_2) = \tfrac{1}{2}\left[C_0(a_0-\bar{a}_0)^2 + C_2(a_2-\bar{a}_2)^2\right], \tag{B.7}$$

where $\bar{a}_0$ and $\bar{a}_2$ correspond to the static deformed minimum (this model is called the Asymmetric Rotor Model =ARM /Ei75/). It is to be noted that the above potential is not an U(5)-scalar. When $\bar{a}_2=0$ one has the RVM, i.e. denoting $\bar{a}_0$ by β_0 :

(B.8) $$V_{RVM}(a_0, a_2) = \tfrac{1}{2}C_0(a_0 - \beta_0)^2 + C_2 a_2^2 \quad .$$

It is worth noting that in addition to the static deformation β_0 in the direction of the intrinsic z axis, an isotropy ingredient is introduced in the form of different C´s

The next step is to transform the kinetic energy in eq. (B.2) to the intrinsic system. This is done in /Ei75/ ch.5, and the result is the so called Bohr Hamiltonian /Bo52/

(B.9) $$\tfrac{1}{2}B\sum_m |\dot{\alpha}_m|^2 \longrightarrow \sum_{k=1}^{3} \frac{L'^2_k}{2\mathcal{I}_k(a_0, a_2)} + \tfrac{1}{2}B(\dot{a}_0^2 + 2\dot{a}_2^2),$$

where L'_k , k=1,2,3, are the components of the angular momentum $\vec{L}$ along the intrinsic axis and the

(B.10) $$\mathcal{I}_k(\beta, \gamma) = 4B\beta^2 \sin^2(\gamma - k\cdot\tfrac{2}{3}\pi) \, , \; k = 1,2,3$$

are the principal moments of inertia. The first term in (B.9) is clearly a rotational-like term, but because the $\mathcal{I}_k$ are functions of β and γ (i.e. a_0 and a_2) the intrinsic and rotational motion are intertwined, representing Coriolis and centrifugal effects in the system (this is why the model is called RVM). The second term in (B.9) represents an intrinsic kinetic energy term.

The next step is again the quantization of the classical Hamiltonian (B.8) and (B.9) . There is no unique way of doing this (freedom in ordering noncommutable operators), but commonly one adopts the Pauli prescription of quantiza-

tion in curvilinear coordinates, resulting in a form of $\hat{H}$ used by the Copenhagen school(/Ei75/ ch.6):

(B.11) $$\hat{H} = \hat{T}_{rot} + \hat{T}_{vib} + \hat{V} \quad ,$$

where

$$\hat{T}_{rot} = \hbar^2 \sum_{k=1}^{3} \frac{\hat{L}'^2_k(\Omega)}{2\mathcal{J}_k(a_0, a_2)} \quad ,$$

(B.12) $$\hat{T}_{vib} = -\frac{\hbar^2}{2B}\left[\frac{1}{\beta^4}\frac{\partial}{\partial\beta}\beta^4\frac{\partial}{\partial\beta} + \frac{1}{\beta^2}\frac{1}{\sin 3\gamma}\frac{\partial}{\partial\gamma}\sin 3\gamma\frac{\partial}{\partial\gamma}\right]$$

and $\hat{V}$ is of the form V_{RVM} in eq. (B.8). Here the $\mathcal{J}_k$ are given by (B.10) and the $\hat{L}'_k$ are the components of the angular momentum $\hat{\vec{L}}$ along the intrinsic axes expressed in terms of the Euler angles Ω (/Ei75/,ch.5,eq.(29)).

The eigenfunctions of $\hat{\vec{L}}^2, \hat{L}'_3$ and $\hat{L}_z$ are given by the rigid rotor or symmetric top eigenfunctions

(B.13) $$|L\,M\,K\rangle = \sqrt{\frac{2L+1}{8\pi^2}}\, D^{L\,*}_{MK}(\Omega) \quad ,$$

which satisfy

(B.13′) $$\hat{\vec{L}}^2|L\,M\,K\rangle = L(L+1)|L\,M\,K\rangle \; ; \; \hat{L}_z|L\,M\,K\rangle = M|L\,M\,K\rangle \; ; \; \hat{L}'_3|L\,M\,K\rangle = K|L\,M\,K\rangle \; .$$

Then, since $\hat{H}$, $\hat{\vec{L}}^2$ and $\hat{L}_z$ commute, the eigenfunctions of the collective Hamiltonian (B.11) have the general form

(B.14) $$|\Psi_{\alpha L M}\rangle = \sum_K \chi_{\alpha K}(\beta,\gamma)|L\,M\,K\rangle \quad ,$$

where α includes all the additional quantum numbers. In the case of weak rotation-vibration coupling one has a total

separation of the intrinsic and the rotational degrees of freedom, yielding the familiar BM-eigenfunctions /Bo75/

$$|\alpha L M K\rangle = \sqrt{\frac{2L+1}{16\pi^2(1+\delta_{K0})}}\left[D^{L*}_{MK}(\Omega) + (-1)^L D^{L*}_{M-K}(\Omega)\right] \chi_{\alpha K}(\beta,\gamma) \quad , \tag{B.15}$$

where the invariance of $\hat{H}$ under the point group D_2 /Ti64/ is taken into account.

The function $\chi_{\alpha K}(\beta,\gamma)$ is of the form (/Ei75/,ch.6)

$$\chi_{\alpha K}(\beta,\gamma) = \chi_{K,n_2}(a_2) Y_{n_0}(a_0) \quad , \tag{B.16}$$

where the a_0 and a_2 degrees of freedom are separated.

Any set of quantum numbers (K,n_2,n_0) is called a band because the rigid rotor part of the wavefunction gives a J(J+1) spectrum on top of the state $|\, L=K\ K\ n_2\ n_0\ \rangle$ (this is because of the term $\hat{T}_{rot}$ of eq. (B.12) in $\hat{H}$). The combination (0,0,0) gives the ground state, (0,0,1) gives the β vibrations, (i.e. deformations along the intrinsic z axis) and (2,1,0) gives the γ vibrations (deformations perpendicular to the intrinsic z axis).

The adiabatic wave functions (B.15) lead to an interesting rule for the quadrupole moments. This rule reads

$$eQ = (J\,K\,2\,0\,|\,J\,K)(J\,J\,2\,0\,|\,J\,J)\,eQ_0 = \frac{3K^2 - J(J+1)}{(J+1)(2J+3)}\,eQ_0 \quad , \tag{B.17}$$

where Q is the spectroscopic quadrupole moment and Q_0 is the intrinsic quadrupole moment,

$$eQ_0 \equiv \langle K | \int \rho(\vec{r}) r^2 (3\cos^2\theta - 1) d\tau | K \rangle =$$

(B.18)

$$= \sqrt{\frac{16\pi}{5}} \langle K | T^{(E2)}_{0,intr} | K \rangle \quad .$$

Specifying eq. (B.17) for the ground, β and γ band one obtains

(B.19)

$$eQ(\alpha, J) = -\frac{J}{2J+1} eQ_0 \quad , \quad \alpha = g, \beta$$

$$eQ(\gamma, J) = \frac{12 - J(J+1)}{(J+1)(2J+3)} eQ_0 \quad .$$

According to the formulas (B.19), the ground and β band states have negative quadrupole moments all the way, but the gamma band has positive quadrupole moments for the states 0^+_γ and 2^+_γ, a zero quadrupole moment for the state 3^+_γ and negative quadrupole moments for the rest of the gamma band states. All this naturally assumes a positive intrinsic quadrupole moment Q_0, which means a prolate intrinsic shape. The negative spectroscopic quadrupole moment may be interpreted to follow from the fact that when revolving around this prolate object generates, on the average, an oblate charge distribution.

C. SOME RELATIONS FOR A NON-ORTHOGONAL BASIS

In the EPM one has to face a generalized eigenvalue problem in the non-orthogonal basis $\{|g_0\rangle, |\beta_0\rangle, |\gamma_0\rangle\}$. Because of this, a short general discussion of this subject is given here.

Let $\mathcal{O}$ be a linear hermitean operator in a Hilbert space with non-orthogonal basis states $\{|i\rangle\}_{i\in I}$. Then let

(C.1) $$\mathcal{O}|\alpha\rangle = \alpha|\alpha\rangle \quad ,$$

where $|\alpha\rangle$ is an eigenstate of $\mathcal{O}$ corresponding to the eigenvalue α. Let the basis states be normalized, i.e.

(C.2) $$\langle i|j\rangle \neq \delta_{ij} \quad , \quad \langle i|i\rangle = 1 \qquad \forall\ i,j \in I$$

Then, owing to the completeness of the basis

(C.3) $$|\alpha\rangle = \sum_i C_i |i\rangle$$

and

$$\mathcal{O}\sum_i C_i|i\rangle = \mathcal{O}|\alpha\rangle = \alpha|\alpha\rangle = \alpha\sum_i C_i|i\rangle \ .$$

Then sandwiching with a state $\langle j| \in \{\langle i|\}_{i\in I}$ we get

$$\sum_i C_i\langle j|\mathcal{O}|i\rangle = \alpha\sum_i C_i\langle j|i\rangle$$

Denoting

(C.4) $$\langle j|\mathcal{O}|i\rangle \equiv \mathcal{O}_{ji} \ ; \quad \langle j|i\rangle = f_{ij} \quad (\text{real})$$

one gets

(C.5) $$\sum_i (\mathcal{O}_{ij} - \alpha f_{ij})C_i = 0 \quad ,$$

which is a linear homogenous equation for every j. Then, as in the usual eigenvalue problem, one gets a nontrivial solution of (C.5) if

(C.6) $$\det(\mathcal{O}_{ji} - \alpha f_{ji}) = 0 \quad ,$$

It is worth noting that the usual eigenvalue problem is recovered if $f_{ji} = \delta_{ij}$. In addition, because the basis is non-orthogonal, the matrix $\mathcal{O}_{ji}$ is not necessarily a Hermitean matrix.

Let α_k, $k \in J$ be the eigenvalues of the problem (C.1) and C_{ki}, $i \in I$ the corresponding eigenvectors. Then

(C.7) $$\sum_i (\mathcal{O}_{ji} - \alpha_k f_{ji}) C_{ki} = 0 \quad \forall j \quad ,$$

and as the solution to this set of equations one obtains

$$|\alpha\rangle_k = (C_{k1}, C_{k2}, \ldots, C_{ki}, \ldots)^T \quad ,$$

ie.

(C.8) $$|\alpha_k\rangle = \sum_i C_{ki} |i\rangle \quad ; \quad \langle\alpha_k| = \sum_i C^*_{ki} \langle i|$$

So, because $\mathcal{O}$ was Hermitean

(C.9) $$\delta_{kl} = \langle\alpha_k|\alpha_l\rangle = \sum_{ij} C^*_{ki} C_{lj} \langle i|j\rangle = \sum_{ij} f_{ij} C^*_{ki} C_{lj}$$

One can check the calculation in the following way :

$$\langle\alpha_k|\mathcal{O}|\alpha_l\rangle = \sum_{ij} C^*_{ki} C_{lj} \langle i|\mathcal{O}|j\rangle = \sum_i C^*_{ki} \sum_j \mathcal{O}_{ij} C_{lj} =$$

$$\overset{(C.7)}{=} \sum_i C^*_{ki} \sum_j \alpha_l f_{ij} C_{lj} = \alpha_l \sum_{ij} C^*_{ki} C_{lj} \overset{(C.9)}{=} \alpha_l \delta_{kl} \quad .$$

Then let us normalize the eigenstates :

$$1 = \langle\alpha_k|\alpha_k\rangle = \sum_{ij} C^*_{ki} C_{kj} f_{ij} = \sum_i |C_{ki}|^2 f_{ii} +$$

$$+ 2 \sum_{i<j} f_{ij} C^*_{ki} C_{kj} \quad .$$

So

(C.10) $$\sum_i C_{ki}^2 + 2\sum_{i<j} f_{ij} C_{ki} C_{kj} = 1 \quad .$$

Let us see what kind of closure relation one gets in the non-orthogonal basis $\{|i\rangle\}_{i\in I}$: if the basis $\{|\mu\rangle\}_{\mu\in J}$ is an orthonormal one in a Hilbert space $\mathcal{H}$, then

(C.11) $$\sum_{\mu\in J} |\mu\rangle\langle\mu| = \mathbb{1} \quad .$$

Now

(C.12) $$|i\rangle = \sum_{\mu\in J} K_{i\mu}|\mu\rangle \quad ; \quad |\mu\rangle = \sum_{i\in I} A_{\mu i}|i\rangle$$

where the coefficients $A_{\mu i}$ and $B_{\mu i}$ can be specified to to be real. So

$$\delta_{\mu\nu} = \langle\nu|\mu\rangle = \sum_{i\in I} A_{\mu i}\langle\nu|i\rangle = \sum_{i\in I} A_{\mu i} K_{i\mu} \quad ,$$

that is

(C.13) $$\mathbb{A}\mathbb{K} = \mathbb{1} \quad ; \mathbb{A} = \mathbb{K}^{-1} \quad ,$$

where the fat symbols denote matrices. It is easy to prove also the relation

(C.14) $$\sum_\mu K_{i\mu} K_{j\mu} = f_{ij} = \sum_{\mu\in J}\sum_{n,m\in I} A_{\mu n} A_{\mu m} f_{in} f_{mj}$$

i.e.

(C.14′) $$(\mathbb{K}\mathbb{K}^T)_{ij} = f_{ij} = \sum_{n,m\in I} (\mathbb{A}^T\mathbb{A})_{nm} f_{in} f_{mj}$$

From the above relation one sees clearly that the matrices $\mathbb{K}$ and $\mathbb{A}$ are not Hermitean. Further, it is easy to show that

(C.15) $$\mathbb{1} = \sum_{i,j\in I} (\mathbb{A}^T\mathbb{A})_{ij} |i\rangle\langle j|$$

Equation (C.15) goes back to the familiar expression (C.11) if $\mathbb{A}^T\mathbb{A} = \mathbb{1}$. So the calculation of the closure in non-orthogonal basis reduces to matrix inversion according to formulas (C.15) and (C.13). Let us take a two dimensional example: let $\{|1\rangle, |2\rangle\}$ be the orthonormal basis and $\{|1\rangle', |2\rangle'\}$ the normalized non-orthogonal one. Then

$$|1\rangle' = K_{11}|1\rangle + K_{12}|2\rangle$$

$$|2\rangle' = K_{21}|1\rangle + K_{22}|2\rangle$$

and so

$$\mathbb{1} = \frac{|1\rangle'\langle 1|' - '\langle 1|2\rangle'(|1\rangle'\langle 2|' + |2\rangle'\langle 1|') + |2\rangle'\langle 2|'}{(\langle 1|1\rangle'\langle 2|2\rangle' - \langle 1|2\rangle'\langle 2|1\rangle')^2} \tag{C.16}$$

D. MATRIX ELEMENTS OF THE ENERGY MATRIX

D1. Basic Integrals

Here are retabulated the integrals of ref. /Ha70/ in the original form and in a form suitable for computer calculation. The notations are

$\xi = d^2 D^2_{00}(\Omega) = d^2 P_2(\beta)$,

where P_1 is a Legendre polynomial (/Ar70/,/Ab65/)

$d\Omega = \sin\beta d\beta d\alpha d\gamma$

$\eta = 3d^2x^2/2$

$\mathcal{R} = \frac{1}{2}\exp(-d^2/2)$

The integrals are :

$$I_1(J) = \frac{1}{8\pi^2}\int d\Omega D^{J*}_{00}(\Omega) e^{\xi} = \mathcal{R}\int_{-1}^{1} d^J_{00}(x) e^{\eta} dx$$

$$I_2(J) = \frac{dI_1(J)}{d(d^2)} = \frac{1}{8\pi^2}\int d\Omega D^{J*}_{00}(\Omega) D^2_{00}(\Omega) e^{\xi} = \mathcal{R}\int_{-1}^{1} d^J_{00}(x) d^2_{00}(x) e^{\eta} dx$$

$$I_3(J) = \frac{d^2 I_1(J)}{d(d^2)^2} = \frac{1}{8\pi^2}\int d\Omega D^{J*}_{00}(\Omega)\left[D^2_{00}(\Omega)\right]^2 e^{\xi} = \mathcal{R}\int_{-1}^{1} d^J_{00}(x)\left[d^2_{00}(x)\right]^2 e^{\eta} dx$$

$$I_4(J) = \frac{d^3 I_1(J)}{d(d^2)^3} = \frac{1}{8\pi^2}\int d\Omega D^{J*}_{00}(\Omega)\left[D^2_{00}(\Omega)\right]^3 e^{\xi} = \mathcal{R}\int_{-1}^{1} d^J_{00}(x)\left[d^2_{00}(x)\right]^3 e^{\eta} dx$$

$$I_5(J) = \frac{1}{8\pi^2}\int d\Omega D^{J*}_{02}(\Omega) D^2_{02}(\Omega) e^{\xi} = \mathcal{R}\int_{-1}^{1} d^J_{02}(x) d^2_{02}(x) e^{\eta} dx$$

$$I_6(J) = \frac{dI_5(J)}{d(d^2)} = \frac{1}{8\pi^2}\int d\Omega D^{J*}_{02}(\Omega) D^2_{02}(\Omega) D^2_{00}(\Omega) e^{\xi} =$$

$$= \mathcal{R}\int_{-1}^{1} d^J_{02}(x) d^2_{02}(x) d^2_{02}(x) d^2_{00}(x) e^{\eta} dx$$

$$I_7(J) = \frac{d^2 I_5(J)}{d(d^2)^2} = \frac{1}{8\pi^2}\int d\Omega D^{J*}_{02}(\Omega) D^2_{02}(\Omega)\left[D^2_{00}(\Omega)\right]^2 e^{\xi}$$

$$= R\int_{-1}^{1} d^J_{02}(x) d^2_{02}(x)\left[d^2_{00}(x)\right]^2 e^{\eta} dx$$

$$I_8(J) = \frac{1}{8\pi^2}\int d\Omega D^{J*}_{22}(\Omega) D^2_{22}(\Omega) e^{\xi} = R\int_{-1}^{1} d^J_{22}(x) d^2_{22}(x) e^{\eta} dx$$

$$I_9(J) = \frac{1}{8\pi^2}\int d\Omega D^{J*}_{22}(\Omega) D^2_{02}(\Omega) D^2_{20}(\Omega) e^{\xi} =$$

$$= R\int_{-1}^{1} d^J_{22}(x) d^2_{02}(x) d^2_{20}(x) e^{\eta} dx$$

$$I_{10}(J) = \frac{dI_8(J)}{d(d^2)} = \frac{1}{8\pi^2}\int d\Omega D^{J*}_{22}(\Omega) D^2_{22}(\Omega) D^2_{00}(\Omega) e^{\xi} =$$

$$= R\int_{-1}^{1} d^J_{22}(x) d^2_{22}(x) d^2_{00}(x) e^{\eta} dx$$

$$I_{11}(J) = \frac{dI_9(J)}{d(d^2)} = \frac{1}{8\pi^2}\int d\Omega D^{J*}_{22}(\Omega) D^2_{02}(\Omega) D^2_{20}(\Omega) \times$$

$$\times D^2_{00}(\Omega) e^{\xi} = R\int_{-1}^{1} d^J_{22}(x) d^2_{02}(x) d^2_{20}(x) d^2_{00}(x) e^{\eta} dx$$

D2. Expressions for Normalization Constants and Energy Matrix Elements

$$|g_0\ J\rangle = N_{g_0}(J) P^J_{M0} |\tilde{0}\rangle$$
$$|\beta_0\ J\rangle = N_{\beta_0}(J) P^J_{M0} (b^\dagger_0 - d)|\tilde{0}\rangle$$
$$|\gamma_0\ J\rangle = N_{\gamma_0}(J) P^J_{M2} b^\dagger_2 |0\rangle$$
$$A = 2J+1\ ;\ \langle i_0 |\ \ |j_0\rangle_J = \langle j_0 |\ \ |i_0\rangle_J \quad \forall \quad i,j \in g,\beta,\gamma$$

The normalization constants read

$$N_{g_0}(J) = \left[A I_1(J)\right]^{-1/2}$$
$$N_{\beta_0}(J) = A^{-1/2}\left[d^2 I_1(J) + (1-2d^2) I_2(J) + d^2 I_3(J)\right]^{-1/2}$$
$$N_{\gamma_0}(J) = A^{-1/2}\left[I_8(J) + d^2 I_9(J)\right]^{-1/2}$$

The overlap functions read

$$\langle g_0 | \beta_0 \rangle_J = N_{g_0}(J) N_{\beta_0}(J) A d \left[I_2(J) - I_1(J)\right]$$
$$\langle g_0 | \gamma_0 \rangle_J = N_{g_0}(J) N_{\gamma_0}(J) A d I_5(J)$$
$$\langle \beta_0 | \gamma_0 \rangle_J = N_{\beta_0}(J) N_{\gamma_0}(J) A \left[(1-d^2) I_5(J) + d^2 I_6(J)\right]$$

The different matrix elements are :

$\hat{N}$:

$$\langle g_0 | \hat{N} | g_0 \rangle_J = d^2 I_2(J)/I_1(J)$$
$$\langle g_0 | \hat{N} | \beta_0 \rangle_J = N_{g_0}(J) N_{\beta_0}(J) A d \left[(1-d^2) I_2(J) + d^2 I_3(J)\right]$$
$$\langle g_0 | \hat{N} | \gamma_0 \rangle_J = N_{g_0}(J) N_{\gamma_0}(J) A d \left[I_5(J) + d^2 I_6(J)\right]$$
$$\langle \beta_0 | \hat{N} | \beta_0 \rangle_J = N^2_{\beta_0}(J) A \left[(1-d^2)^2 I_2(J) + d^2(3-2d^2) I_3(J) + d^4 I_4(J)\right]$$
$$\langle \beta_0 | \hat{N} | \gamma_0 \rangle_J = N_{\beta_0}(J) N_{\gamma_0}(J) A \left[(1-d^2) I_5(J) + d^2(3-d^2) I_6(J) + d^4 I_7(J)\right]$$
$$\langle \gamma_0 | N | \gamma_0 \rangle_J = N^2_{\gamma_0}(J) A \left[I_8(J) + 2d^2 I_9(J) + d^2 I_{10}(J) + d^4 I_{11}(J)\right]$$

B_{20} :

$$\langle g_0|B_{20}|g_0\rangle_J = 2d^2$$

$$\langle g_0|B_{20}|\beta_0\rangle_J = N_{g_0}(J)N_{\beta_0}(J)A\cdot 2d\left[(1-d^2)I_1(J)+d^2I_2(J)\right]$$

$$\langle g_0|B_{20}|\gamma_0\rangle_J = N_{g_0}(J)N_{\gamma_0}(J)A\cdot 2d^3I_5(J)$$

$$\langle \beta_0|B_{20}|\beta_0\rangle_J = N_{\beta_0}(J)A\cdot 2d^2\left[(d^2-2)I_1(J)+(3-2d^2)I_2(J)+d^2I_3(J)\right]$$

$$\langle \beta_0|B_{20}|\gamma_0\rangle_J = N_{\beta_0}(J)N_{\gamma_0}(J)A\cdot 2d^2\left[(2-d^2)I_5(J)+d^2I_6(J)\right]$$

$$\langle \gamma_0|B_{20}|\gamma_0\rangle_J = 2d^2$$

$B'_{21} = -\sqrt{7/8}\,d^{-1}B_{21} - \hat{N}$:

$$\langle g_0|B'_{21}|g_0\rangle_J = 0$$

$$\langle g_0|B'_{21}|\beta_0\rangle_J = N_{g_0}(J)N_{\beta_0}(J)A\cdot dI_2(J)/2$$

$$\langle g_0|B'_{21}|\gamma_0\rangle_J = -N_{g_0}(J)N_{\gamma_0}(J)A\cdot 3dI_5(J)/2$$

$$\langle \beta_0|B'_{21}|\beta_0\rangle_J = N^2_{\beta_0}(J)A\cdot\left[(1-d^2)I_2(J)+d^2I_3(J)\right]$$

$$\langle \beta_0|B'_{21}|\gamma_0\rangle_J = -N_{\beta_0}(J)N_{\gamma_0}(J)A\cdot\left[(1-3d^2/2)I_5(J)+d^2I_6(J)\right]$$

$$\langle \gamma_0|B'_{21}|\gamma_0\rangle_J = -3$$

$B'_{30} = -\sqrt{7/2}\,d^{-1}B_{30} - B_{20}$:

$$\langle g_0|B'_{30}|g_0\rangle_J = 0$$

$$\langle g_0|B'_{30}|\beta_0\rangle_J = N_{g_0}(J)N_{\beta_0}(J)A\cdot dI_1(J)$$

$$\langle g_0 | B'_{30} | \gamma_0 \rangle_J = 0$$

$$\langle \beta_0 | B'_{30} | \beta_0 \rangle_J = -2N^2_{\beta_0}(J) A \cdot d^2 \left[I_1(J) - I_2(J) \right]$$

$$\langle \beta_0 | B'_{30} | \gamma_0 \rangle_J = N_{\beta_0}(J) N_{\gamma_0}(J) A \cdot d^2 I_5(J)$$

$$\langle \gamma_0 | B'_{30} | \gamma_0 \rangle_J = 0$$

$$\underline{B^{(0)\prime}_{22} = 10 d^{-2} B^{(0)}_{22} + \sqrt{14}\, d^{-1} B_{30} + B_{20} :}$$

$$\langle \beta_0 | B^{(0)\prime}_{22} | \beta_0 \rangle_J = 8N^2_{\beta_0}(J) A I_1(J) \quad ,$$

all other $\langle \ \rangle$'s are zero .

$$\underline{B^{(2)\prime}_{22} = (7/2d^2) B^{(2)}_{22} + \sqrt{2/7}\, d^{-1} B_{21} + B_{11} \quad :}$$

$$\langle g_0 | B^{(2)\prime}_{22} | g_0, \beta_0, \gamma_0 \rangle_J = 0$$

$$\langle \beta_0 | B^{(2)\prime}_{22} | \beta_0 \rangle_J = 3N^2_{\beta_0}(J) A I_2(J)$$

$$\langle \beta_0 | B^{(2)\prime}_{22} | \gamma_0 \rangle_J = -3N_{\beta_0}(J) N_{\gamma_0}(J) A I_5(J)$$

$$\langle \gamma_0 | B^{(2)\prime}_{22} | \gamma_0 \rangle_J = 9N^2_{\gamma_0}(J) A I_8(J)$$

$$\underline{\vec{J}^2 = 6\hat{N} + 4B^{(4)}_{22} - 6B^{(0)}_{22} - 3B^{(2)}_{22} \quad :}$$

$$\langle i_0 | \vec{J}^2 | j_0 \rangle_J = J(J+1) \langle i_0 \ J | j_0 \ J \rangle$$

$$\forall \quad i_0, j_0 \in \{ g_0, \beta_0, \gamma_0 \}$$

E. INTEGRALS $I_i(J)$ IN THE SMALL-d AND LARGE-d LIMITS

E1. The Small-d Limit

In the small-d limit the integrals of appendix D1 can be expanded as a power series in d^2. This is done by expanding the exponent as

$$e^{d^2 D_{00}^2} = 1 + d^2 D_{00}^2 + \frac{1}{2} d^4 (D_{00}^2)^2 + \frac{1}{6} d^6 (D_{00}^2)^3 + \ldots$$

and using the formulas (A1.14),(A1.13),(A1.17) and the Clebsch-Gordan series (A1.15) to get rid of the integrals of one or more D-functions. After that, use of eq. (A3.1) gives the result in terms of the 3j symbols. It must be noted that these formulas are valid only for low J values because for sufficiently large angular momenta all the 3j symbols in the expressions vanish and it becomes necessary to go to higher orders in the expansion of the exponent. These few low angular momenta, however, suffice for the purpose of examining the behaviour of various quantities in the model at small deformations. The above behaviour of the integrals makes also their computer calculation increase in inaccuracy with increasing angular momentum.

The integrals are :

$$I_1(J) = \delta_{J0} + \frac{1}{5}\delta_{J2}\,d^2 + \frac{1}{2}\begin{pmatrix} 2 & 2 & J \\ 0 & 0 & 0 \end{pmatrix}^2 d^4 +$$
$$+ \frac{1}{6}\left[\frac{1}{25}\delta_{J2} + \frac{2}{7}\begin{pmatrix} J & 2 & 2 \\ 0 & 0 & 0 \end{pmatrix}^2 + \frac{18}{35}\begin{pmatrix} J & 2 & 4 \\ 0 & 0 & 0 \end{pmatrix}^2\right] d^6 + \mathcal{O}(d^8)$$

$$I_2(J) = \frac{1}{5}\delta_{J2} + \begin{pmatrix} 2 & 2 & J \\ 0 & 0 & 0 \end{pmatrix}^2 d^2 + \left[\frac{1}{50}\delta_{J2} + \frac{1}{7}\begin{pmatrix} J & 2 & 2 \\ 0 & 0 & 0 \end{pmatrix}^2 +\right.$$
$$\left. + \frac{9}{35}\begin{pmatrix} J & 2 & 4 \\ 0 & 0 & 0 \end{pmatrix}^2\right] d^4 + \mathcal{O}(d^6)$$

$$I_3(J) = \begin{pmatrix} 2 & 2 & J \\ 0 & 0 & 0 \end{pmatrix}^2 + \left[\frac{1}{25}\delta_{J2} + \frac{2}{7}\begin{pmatrix} J & 2 & 2 \\ 0 & 0 & 0 \end{pmatrix}^2 + \frac{18}{35}\begin{pmatrix} J & 2 & 4 \\ 0 & 0 & 0 \end{pmatrix}^2\right] d^2 +$$
$$+ \left\{\frac{1}{50}\delta_{J0} + \frac{2}{175}\delta_{J2} + \frac{2}{175}\delta_{J4} + \frac{36}{245}\begin{pmatrix} 2 & 4 & J \\ 0 & 0 & 0 \end{pmatrix}^2 +\right.$$
$$\left. + \frac{2}{49}\begin{pmatrix} 2 & 2 & J \\ 0 & 0 & 0 \end{pmatrix}^2 + \frac{162}{1225}\begin{pmatrix} 4 & 4 & J \\ 0 & 0 & 0 \end{pmatrix}^2\right\} d^4 + \mathcal{O}(d^6)$$

$$I_4(J) = \frac{d\,I_3(J)}{d(d^2)}$$

$$I_5(J) = \frac{1}{5}\delta_{J2} + \begin{pmatrix} 2 & 2 & J \\ 0 & 0 & 0 \end{pmatrix}\begin{pmatrix} 2 & 2 & J \\ 2 & 0 & -2 \end{pmatrix} d^2 + \left[\frac{1}{50}\delta_{J2} +\right.$$
$$\left. + \frac{1}{7}\begin{pmatrix} J & 2 & 2 \\ 0 & 0 & 0 \end{pmatrix}\begin{pmatrix} J & 2 & 2 \\ -2 & 2 & 0 \end{pmatrix} + \frac{9}{35}\begin{pmatrix} J & 2 & 4 \\ 0 & 0 & 0 \end{pmatrix}\begin{pmatrix} J & 2 & 4 \\ -2 & 2 & 0 \end{pmatrix}\right] d^4 + \mathcal{O}(d^6)$$

$$I_6(J) = d\,I_5(J)/d(d^2)$$

$$I_7(J) = \frac{1}{25}\delta_{J2} + \frac{2}{7}\begin{pmatrix} J & 2 & 2 \\ 0 & 0 & 0 \end{pmatrix}\begin{pmatrix} J & 2 & 2 \\ -2 & 2 & 0 \end{pmatrix} + \frac{18}{35}\begin{pmatrix} J & 2 & 4 \\ 0 & 0 & 0 \end{pmatrix}\begin{pmatrix} J & 2 & 4 \\ -2 & 2 & 0 \end{pmatrix} +$$
$$+ \left\{-\frac{2}{175}\delta_{J2} + \frac{1}{35}\frac{1}{\sqrt{15}}\delta_{J4} - \frac{4}{49}\begin{pmatrix} 2 & 2 & J \\ 0 & 0 & 0 \end{pmatrix}\begin{pmatrix} 2 & 2 & J \\ 2 & 0 & -2 \end{pmatrix} -\right.$$
$$- \frac{36}{245}\begin{pmatrix} 2 & 4 & J \\ 0 & 0 & 0 \end{pmatrix}\begin{pmatrix} 2 & 4 & J \\ 2 & 0 & -2 \end{pmatrix} + \frac{18}{49}\frac{1}{\sqrt{15}}\begin{pmatrix} 4 & 2 & J \\ 0 & 0 & 0 \end{pmatrix}\begin{pmatrix} 4 & 2 & J \\ 2 & 0 & -2 \end{pmatrix} +$$
$$\left. + \frac{162}{245}\frac{1}{\sqrt{15}}\begin{pmatrix} 4 & 4 & J \\ 0 & 0 & 0 \end{pmatrix}\begin{pmatrix} 4 & 4 & J \\ 2 & 0 & -2 \end{pmatrix}\right\} d^2 + \mathcal{O}(d^4)$$

$$I_8(J) = \frac{1}{5}\delta_{2J} + \begin{pmatrix} 2 & 2 & J \\ 2 & 0 & -2 \end{pmatrix} d^2 + \left[\frac{1}{50}\delta_{J2} + \frac{1}{7}\begin{pmatrix} 2 & 2 & J \\ 2 & 0 & -2 \end{pmatrix}^2 + \right.$$
$$\left. + \frac{9}{35}\begin{pmatrix} 2 & 4 & J \\ 2 & 0 & -2 \end{pmatrix}^2 \right] d^4 + \mathcal{O}(d^6)$$

$$I_9(J) = (-1)^J \begin{pmatrix} 2 & 2 & J \\ 0 & 2 & -2 \end{pmatrix}^2 + \left[\frac{2}{7}(-1)^{J+1} \begin{pmatrix} 2 & 2 & J \\ 0 & 2 & -2 \end{pmatrix}^2 + \right.$$
$$\left. + \frac{9}{7}\frac{1}{\sqrt{15}} \begin{pmatrix} 2 & 4 & J \\ 0 & 2 & -2 \end{pmatrix} \begin{pmatrix} 2 & 4 & J \\ 2 & 0 & -2 \end{pmatrix} \right] d^2 + \mathcal{O}(d^4)$$

$$I_{10}(J) = d\, I_8(J) / d(d^2)$$

$$I_{11}(J) = \frac{2}{7}(-1)^{J+1} \begin{pmatrix} 2 & 2 & J \\ 0 & 2 & -2 \end{pmatrix}^2 + \frac{9}{7}\frac{1}{\sqrt{15}} \begin{pmatrix} 2 & 4 & J \\ 0 & 2 & -2 \end{pmatrix} \begin{pmatrix} 2 & 4 & J \\ 2 & 0 & -2 \end{pmatrix} +$$
$$+ \left[\frac{2}{175}\delta_{J2} - \frac{1}{70}\delta_{J3} + \frac{1}{210}\delta_{J4} + \frac{4}{49}\begin{pmatrix} 2 & 2 & J \\ 2 & 0 & -2 \end{pmatrix}^2 + \right.$$
$$+ \frac{36}{245}\begin{pmatrix} 2 & 4 & J \\ 2 & 0 & -2 \end{pmatrix}^2 - \frac{1}{7}\begin{pmatrix} 3 & 2 & J \\ 2 & 0 & -2 \end{pmatrix}^2 - \frac{9}{35}\begin{pmatrix} 3 & 4 & J \\ 2 & 0 & -2 \end{pmatrix}^2 +$$
$$\left. + \frac{3}{49}\begin{pmatrix} 4 & 2 & J \\ 2 & 0 & -2 \end{pmatrix}^2 + \frac{27}{245}\begin{pmatrix} 4 & 4 & J \\ 2 & 0 & -2 \end{pmatrix}^2 \right] d^2 + \mathcal{O}(d^4)$$

E2. The Asymptotic Limit

The large-d limit of the integrals is somewhat more difficult to calculate and the result has quite a complicated look. The starting point is the formula (A1.18). For $d^J_{00}(\beta)$ one obtains

$$d^J_{00}(\beta) = \sum_\delta \binom{J}{\delta}^2 (-1)^\delta \left(\cos\tfrac{\beta}{2}\right)^{2\delta} \left(\sin\tfrac{\beta}{2}\right)^{2(J-\delta)} .$$

Using the relations /Sp68/

$$\cos\tfrac{\beta}{2} = \sqrt{\frac{1+\cos\beta}{2}} \quad ; \quad \sin\tfrac{\beta}{2} = \sqrt{\frac{1-\cos\beta}{2}} \quad , 0 \le \beta \le \pi$$

and the definition of the integral $I_1(J)$ of appendix D1, one obtains ($x=\cos\beta$)

$$I_1(J) = \tfrac{1}{2} \sum_\delta \binom{J}{\delta}^2 (-1)^\delta \int_{-1}^{1} \left(\frac{1+x}{2}\right)^\delta \left(\frac{1-x}{2}\right)^{J-\delta} e^{d^2(\frac{3}{2}x - \frac{1}{2})}\, dx .$$

Using the binomial series in the form

$$(1+x)^\delta = \sum_{m=0}^{\delta} \binom{\delta}{m} x^m$$

$$(1-x)^{J-\delta} = \sum_{n=0}^{J-\delta} \binom{J-\delta}{n} (-1)^n x^n$$

and substituting it in the above expression yields

$$I_1(J) = 2^{-J-1} e^{-d^2/2} \sum_{\delta,m,n} \binom{J}{\delta}^2 \binom{\delta}{m} \binom{J-\delta}{n} (-1)^{n+\delta} \int_{-1}^{1} x^{m+n} e^{\frac{3}{2}d^2x^2}\, dx$$

$$= 2^{-J} e^{-d^2/2} \sum_{\delta,s,n} \binom{J}{\delta}^2 \binom{\delta}{2s-n} \binom{J-\delta}{n} (-1)^{n+\delta} \int_{0}^{1} x^{2s} e^{\frac{3}{2}d^2x^2}\, dx$$

where the last form follows from applying parity arguments to the integrand. Now one can change the integration variable by $2\xi^2 = 3d^2x^2$ and use the formula (which is easy to prove by induction)

$$\int_0^{\sqrt{\frac{3}{2}}d} \xi^{2\varkappa} e^{\xi^2} d\xi = e^{\frac{3}{2}d^2}(1-\delta_{\varkappa 0})\sum_{k=0}^{\varkappa-1} \frac{(-1)^k}{2^{k+1}} \frac{(2\varkappa-1)!!}{(2\varkappa-2k-1)!!} \sqrt{\frac{2}{3}} \frac{1}{d} \times$$

$$\times \left(\frac{3}{2}d^2\right)^{\varkappa-k} + \frac{(-1)^{\varkappa}(2\varkappa-1+\delta_{\varkappa 0})!!}{2^{\varkappa}} \int_0^{\sqrt{\frac{3}{2}}d} e^{\xi^2} d\xi \quad .$$

The remaining integral one can expand according to the asymptotic formula /Ab65,page 298/

$$\int_0^{\sqrt{\frac{3}{2}}d} d\xi\, e^{\xi^2} = \sqrt{\frac{2}{3}} \frac{e^{\frac{3}{2}d^2}}{2d} \left(1 + \sum_{\ell=1}^{\infty} \frac{(2\ell-1)!!}{(3d^2)^{\ell}}\right)$$

Substituting all this to the last expression for $I_1(J)$ yields the result

(E2.1)
$$I_1(J) = \frac{e^{d^2}}{3d^2 2^J} \sum_{s=0}^{J/2} F_1(2s,J)\, A(s,J,d^2)$$

where

$$A(s,J,d^2) \equiv (1-\delta_{s0})\, \mathcal{F}(2s,d^2) + G(s,d^2)\, g(d^2)$$

(E2.2)
$$\mathcal{F}(2s,d^2) \equiv \sum_{k=0}^{s-1} (-1)^k \frac{(2s-1)!!}{(2s-2k-1)!!} \left(\frac{1}{3d^2}\right)^k$$

$$G(s,d^2) \equiv (-1)^s (2s-1+\delta_{s0})!! \left(\frac{1}{3d^2}\right)^s$$

and
$$g(d^2) = \sum_{m=0}^{\infty} \frac{(2m-1+\delta_{m0})!!}{(3d^2)^m} = 1 + \frac{1}{3d^2} + \frac{1}{3d^4} + \ldots$$

$$F_1(2s,J) \equiv \sum_{\delta=0}^{J} (-1)^{\delta} \binom{J}{\delta}^2 f_1(2s,\delta,J)$$

(E2.3)

$$f_1(2s,\delta,J) \equiv \sum_{n=0}^{J-\delta} (-1)^n \binom{\delta}{2s-n}\binom{J-\delta}{n}, \quad n \le 2s$$

The integrals $I_{2,3,4}(J)$ can be obtained from $I_1(J)$ by differentiation according to appendix D1.

In the same way as above, one can derive the following formula for the integral $I_5(J)$:

$$I_5(J) = \frac{e^{d^2}}{3d^2 \cdot 2^{J+2}} \sqrt{\frac{6J(J-1)}{(J+1)(J+2)}} \sum_{s=0}^{\frac{J}{2}+1} F_5(2s,J) A(s,J,d^2), \tag{E2.4}$$

where

$$F_5(2s,J) \equiv \sum_{\delta=0}^{J-2} (-1)^{\delta} \binom{J+2}{J-\delta}\binom{J-2}{\delta} f_5(2s,\delta,J)$$

(E2.5)

$$f_5(2s,\delta,J) \equiv \sum_{n=0}^{J-\delta} (-1)^n \binom{\delta+2}{2s-n}\binom{J-\delta}{n}, \quad n \le 2s$$

Again by defferentiation one obtains the integrals $I_6(J)$ and $I_7(J)$. For $I_8(J)$ one obtains

$$I_8(J) = \frac{(-1)^J e^{d^2}}{3d^2 \cdot 2^{J+2}} \sum_{s=0}^{[\frac{J}{2}]+1} F_8(2s,J) A(s,J,d^2) \tag{E2.6}$$

where

$$F_8(2s,J) \equiv \sum_{\delta=0}^{J-2} (-1)^{\delta} \binom{J+2}{J-2-\delta}\binom{J-2}{\delta} f_8(2s,\delta,J)$$

(E2.7)

$$f_8(2s,\delta,J) \equiv \sum_{n=0}^{J-\delta-2} (-1)^n \binom{\delta+4}{2s-n}\binom{J-\delta-2}{n}, \quad n \le 2s$$

and $I_{10}(J) = dI_8(J)/d(d^2)$. Here the notation $[x]$ means the integer part of x.

Now $I_{11}(J) = dI_g(J)/d(d^2)$, and for $I_g(J)$ one has

$$I_g(J) = \frac{(-1)^J e^{d^2}}{2^{J+3} d^2} \sum_{s=0}^{\left[\frac{J}{2}\right]+2} F_g(2s, J) A(s, J, d^2) \tag{E2.8}$$

where

$$F_g(2s, J) = \sum_{\delta=0}^{J-2} (-1)^{\delta} \binom{J+2}{J-2-\delta} \binom{J-2}{\delta} f_g(2s, \delta, J)$$

$$f_g(2s, \delta, J) = \sum_{n=0}^{J-\delta} (-1)^n \binom{\delta+4}{2s-n} \binom{J-\delta}{n}, \quad n \leq 2s \tag{E2.9}$$

F. THE BASIC TRANSITION MATRIX ELEMENTS

The transition operator is $T^{(E2)}_m \equiv e^*(b^\dagger_m + \bar{b}_m)$, and the N's below are the normalization constants of eq. (II.3.1). For the γ band there are two kinds of matrix element depending on the evenness or oddness of the angular momentum of the initial and final states. This is due to the fact that the denominator of eq. (II.6.6) goes to zero if $M = 0$ and one of the J's is odd. When both J and J' are even or odd the formula with $M = 0$ is the simplest to apply. Furthermore, the matrix elements $\langle J'=\text{odd}| \; |J=\text{even}\rangle$ are not tabulated. The transition probabilities

$$B(E2;\ J=\text{even} \dashrightarrow J'=\text{odd})$$

are calculated by noting that /Li66/

$$(J' \| T^{(\lambda)} \| J) = (-1)^{J-J'} (J \| T^{(\lambda)} \| J')^* \tag{F.1}$$

where λ is the degree of the spherical tensor T .

For $M_o = 0$ one has :

$$\langle J' | T^{(E2)} | J \rangle = \langle J | T^{(E2)} | J' \rangle \ .$$

So, the matrix elements needed in (II.6.9) are

$$\langle g_0\ J'\ 0 | T^{(E2)}_0 | g_0\ J\ 0 \rangle = e^* N_{g_0}(J) N_{g_0}(J') d(2J+1) \times$$
$$\times (2J'+1) \begin{pmatrix} 2 & J & J' \\ 0 & 0 & 0 \end{pmatrix}^2 \left[I_1(J) + I_1(J') \right]$$

$$\langle g_0\, J'\, 0 | T_0^{(E2)} | \beta_0\, J\, 0 \rangle = e^* N_{g_0}(J') N_{\beta_0}(J)(2J+1) \times$$
$$\times (2J'+1) \begin{pmatrix} 2 & J & J' \\ 0 & 0 & 0 \end{pmatrix}^2 \Big\{ I_1(J') + d^2 \big[-I_1(J) + I_2(J) -$$
$$- I_1(J') + I_2(J') \big] \Big\}$$

$$\langle g_0\, J'\, 0 | T_0^{(E2)} | \gamma_0\, J = \text{even}\ 0 \rangle = e^* N_{g_0}(J') N_{\gamma_0}(J) \times$$
$$\times (2J+1)(2J'+1) \begin{pmatrix} 2 & J & J' \\ 0 & 0 & 0 \end{pmatrix} \Big\{ d^2 \begin{pmatrix} 2 & J & J' \\ 0 & -2 & 2 \end{pmatrix} I_5(J') +$$
$$+ d^2 \begin{pmatrix} 2 & J & J' \\ 0 & 0 & 0 \end{pmatrix} I_5(J) + \begin{pmatrix} 2 & J & J' \\ 2 & -2 & 0 \end{pmatrix} I_1(J') \Big\}$$

$$\langle g_0\, J'\, 0 | T_{-2}^{(E2)} | \gamma_0\, J = \text{odd}\ 2 \rangle = e^* N_{g_0}(J') N_{\gamma_0}(J) \times$$
$$\times (2J+1)(2J'+1) \begin{pmatrix} 2 & J & J' \\ 2 & -2 & 0 \end{pmatrix} \Big\{ \begin{pmatrix} 2 & J & J' \\ 2 & -2 & 0 \end{pmatrix} I_1(J') +$$
$$+ d^2 \begin{pmatrix} 2 & J & J' \\ 0 & -2 & 2 \end{pmatrix} I_5(J') \Big\}$$

$$\langle \beta_0\, J'\, 0 | T_0^{(E2)} | \beta_0\, J\, 0 \rangle = e^* N_{\beta_0}(J') N_{\beta_0}(J) d(2J+1) \times$$
$$\times (2J'+1) \begin{pmatrix} 2 & J & J' \\ 0 & 0 & 0 \end{pmatrix} \Big\{ (d^2-1) \big[I_1(J) + I_1(J') \big] +$$
$$+ 2(1-d^2) \big[I_2(J) + I_2(J') \big] + d^2 \big[I_3(J) + I_3(J') \big] \Big\}$$

$$\langle \beta_0\, J'\, 0 | T_0^{(E2)} | \gamma_0\, J = \text{even}\ 0 \rangle = e^* N_{\beta_0}(J') N_{\gamma_0}(J) \times$$
$$\times d(2J+1)(2J'+1) \begin{pmatrix} 2 & J & J' \\ 0 & 0 & 0 \end{pmatrix} \Big\{ \begin{pmatrix} 2 & J & J' \\ 0 & 0 & 0 \end{pmatrix} \big[(2-d^2) I_5(J) +$$
$$+ d^2 I_6(J) \big] + \begin{pmatrix} 2 & J & J' \\ 2 & -2 & 0 \end{pmatrix} \big[I_2(J') - I_1(J') \big] +$$
$$+ \begin{pmatrix} 2 & J & J' \\ 0 & -2 & 2 \end{pmatrix} \big[(1-d^2) I_5(J') + d^2 I_6(J') \big] \Big\}$$

$$\langle \beta_0\, J'\, 0 \,|\, T^{(E2)}_{-2} \,|\, \gamma_0\, J = \text{odd}\ 2 \rangle = e^* N_{\beta_0}(J') N_{\gamma_0}(J) \times$$

$$d(2J+1)(2J'+1)\begin{pmatrix} 2 & J & J' \\ 2 & -2 & 0 \end{pmatrix}\left\{ \begin{pmatrix} 2 & J & J' \\ 2 & -2 & 0 \end{pmatrix}\left[I_2(J') - \right.\right.$$

$$\left.\left. - I_1(J') \right] + \begin{pmatrix} 2 & J & J' \\ 0 & -2 & 2 \end{pmatrix}\left[(1-d^2) I_5(J') + d^2 I_6(J') \right] \right\}$$

$$\langle \gamma_0\, J' = \begin{cases} \text{odd} \\ \text{even} \end{cases} 0 \,|\, T^{(E2)}_0 \,|\, \gamma_0\, J = \begin{cases} \text{odd} \\ \text{even} \end{cases} 0 \rangle =$$

$$= e^* N_{\gamma_0}(J') N_{\gamma_0}(J) d(2J+1)(2J'+1)\begin{pmatrix} 2 & J & J' \\ 0 & 0 & 0 \end{pmatrix} \times$$

$$\times \left\{ \begin{pmatrix} 2 & J & J' \\ 2 & 0 & -2 \end{pmatrix} I_5(J) + \begin{pmatrix} 2 & J & J' \\ 2 & -2 & 0 \end{pmatrix} I_5(J') + \right.$$

$$\left. \begin{pmatrix} 2 & J & J' \\ 0 & 2 & -2 \end{pmatrix}\left[I_8(J) + I_8(J') + d^2\left(I_9(J) + I_9(J') \right) \right] \right\}$$

$$\langle \gamma_0\, J' = \text{even}\ 0 \,|\, T^{(E2)}_{-2} \,|\, \gamma_0\, J = \text{odd}\ 2 \rangle =$$

$$= e^* N_{\gamma_0}(J') N_{\gamma_0}(J) d(2J+1)(2J'+1)\begin{pmatrix} 2 & J & J' \\ -2 & 2 & 0 \end{pmatrix} \times$$

$$\times \left\{ \begin{pmatrix} 2 & J & J' \\ -2 & 2 & 0 \end{pmatrix} I_5(J') + \begin{pmatrix} 2 & J & J' \\ 0 & 2 & -2 \end{pmatrix}\left[I_8(J) + I_8(J') + \right.\right.$$

$$\left.\left. + d^2\left(I_9(J) + I_9(J') \right) \right] \right\}$$

G. THE IBA-1 PARAMETERS OF THE FITS IN Sm, Gd, Er and Yb REGIONS

The phenomenological forms of the IBA Hamiltonian and the transition operator read

$$\hat{H}_{IBA} = EPS\cdot\hat{n}_d + 2\cdot PAIR\cdot P^{\dagger}P + \tfrac{1}{2}\cdot ELL\cdot L^2 + \tfrac{1}{2}\cdot QQ\cdot Q^2 + 5\cdot OCT\cdot T_3^2 + 5\cdot HEX\cdot T_4^2$$

$$T^{(E2)}_{IBA} = E2SD\cdot(d^{\dagger}s + s^{\dagger}\tilde{d}) + (5)^{-\frac{1}{2}} E2DD\cdot[d^{\dagger}\tilde{d}]_2$$

$A_{eff} = Z_{eff} + N$; $A = Z + N$, where

N is the neutron and Z the proton boson number.

$\hat{H}_{IBA}$ and $T^{(E2)}_{IBA}$ are taken from ref. /Li83d/

The energy parameters are all in keV and the transition probability parameters in eb .

ISOTP.	^{146}Sm	^{148}Sm	^{150}Sm	^{152}Sm	^{154}Gd	^{162}Er	^{164}Er	^{166}Er	^{168}Er	^{172}Yb	^{172}Yb
A_{eff}	A=6+1=7	3+2=5	3+3=6	3+4=7	3+4=7	3+6=9	3+7=10	A=7+18 = 15	3+9=12	4+10=14	A=6+10=16
EPS	725	2645	1000	96.6	0.0	100	83.92	100	105	80.0	0.0
PAIR	17	268.1	38.45	-2.36	-2.88	30.83	35.20	37.4	24.95	0.0	-1.00
ELL	-24	-57.5	-19.8	0.76	8.98	7.65	7.29	8.31	8.11	6.0	5.82
QQ	25	67.54	-28.9	-39.1	-38.6	-27.7	-27.2	-16.1	-22.7	-25.0	-23.0
OCT	13	-7.21	5.13	11.1	7.03	4.28	1.45	1.90	-0.55	8.0	7.55
HEX	-2	-104	-31.8	-4.04	-2.25	-11.9	-12.6	-12.0	-13.1	-3.0	-4.0
E2SD	—	—	0.111	0.214	0.239	—	—	—	—	0.135	0.132
-E2DD	—	—	1.008	0.215	0.182	—	—	—	—	0.203	0.154

H. TABLES FOR THE EPM ENERGY LEVELS IN THE Sm, Gd, Er AND Yb CHAINS

Tables H.1 - H.4 list the 4 and 5 parameter EPM energies for Sm, Gd, Er and Yb chains. The isotopes $^{142,144}Sm$ are not tabulated because of the lack of sufficient experimental data. The isotopes $^{146-152}Sm$ are tabulated in table IV.3.1., $^{162-168}Er$ in table IV.3.6 and ^{172}Yb in table IV.3.7 . An asterisk indicates a fitted level.

BAND	J	^{154}Sm			^{156}Sm			^{150}Gd			^{152}Gd		
		EXP.	EPM		EXP.	EPM		EXP.	EPM		EXP.	EPM	
			4	5		4	5		4	5		4	5
g	2	82	83	82	76	76*	76*	638	636*	618*	344	364*	347*
	4	267	269	267	(250)	249*	250*	1288	1241*	1338*	755	732*	741*
	6	544	545	546	(518)	508	513	1937	1816*	2001*	1227	1083*	1127
	8	903	897	904	(878)	837	857	2768	2371*	2631*	1747	1428*	1522
	10	1333	1311	1330	--	1224	1276	(3288)	2912	3267	2300	1774*	1934
β	0	1100	1099	1098	1068	1068*	1068*	1207	1230*	1176*	615	707*	634*
	2	1178	1183	1180	--	1138	1181	1518	1784*	1615*	931	928*	878*
	4	(1371)	1380	1371	--	1301	1440	1700	2011	2389	1282	1275*	1301*
	6	--	1686	1671	--	1557	1825	--	2585	3312	1668	1699*	1839
	8	--	2090	2075	--	1904	2297	--	3190	4329	2139	2168*	2424
	10	--	2576	2570	--	2333	2837	--	4404	5399	2691	2658*	3029
γ^2	2	1440	1442	1440	1441	1441*	1441*	1430	1404*	1435*	1109	1186*	1132*
	3	(1540)	1523	1520	--	1512	1532	1988	2014*	1899*	1434	1425*	1358*
	4	(1661)	1633	1627	--	1607	1657	(2080)	2447	2007	1550	1658*	1644*
	5	--	1764	1756	--	1723	1802	--	2653	2636	1861	1853*	1843*
	6	--	1932	1918	--	1867	2002	--	3103	2760	1998	2123*	2235
	7	--	2103	2091	--	2021	2184	--	3278	3441	(2394)	2293*	2374
RMS		--	8.4	1.6	--	0	0	--	195	240	--	167	176
		--	(12)	(12)	--	(17)	(8.8)	--	(237)	(218)	--	(164)	(171)

TABLE H.1

BAND	J	^{154}Gd			^{156}Gd			^{158}Gd			^{160}Gd		
		EXP.	EPM		EXP.	EPM		EXP.	EPM		EXP.	EPM	
			4	5		4	5		4	5		4	5
g	2	123	129*	123*	89	91*	89*	79	81*	79*	75	78*	78*
	4	371	381*	376*	288	293*	290*	261	266*	262*	252	252*	252*
	6	718	695*	711*	585	586*	589*	539	540*	541*	514	503*	508*
	8	1144	1044*	1089	965	945*	966*	904	888*	906*	868	814*	835*
	10	1637	1417*	1498	1416	1350*	1400*	1350	1293*	1347*	--	1174	1221
β	0	681	711*	718	1049	1056*	1059*	1196	1190*	1193*	--	876	847
	2	815	822*	816*	1129	1127*	1126*	1260	1261*	1259*	1010	957*	945*
	4	1048	1054*	1040*	1298	1290*	1282*	1407	1429*	1412*	(1185)	1173*	1203*
	6	1366	1386*	1380*	1540	1539*	1526*	--	1697	1657	--	1489	1573
	8	1757	1791*	1816	1848	1867*	1856*	--	2070	2002	--	1911	2071
	10	2194	2247*	2318	2220	2267*	2269*	--	2545	2454	--	2428	2681
γ	2	996	1012*	1017*	1154	1179*	1184*	1187	1190*	1194*	988	972*	980*
	3	1128	1122*	1119*	1248	1256*	1259*	1265	1264*	1264*	1058	1047*	1064*
	4	1264	1270*	1257*	1355	1362*	1359*	1358	1361*	1358*	1148	1128*	1150*
	5	1432	1420*	1410*	1507	1484*	1480*	1481	1483*	1474*	--	1274	1313
	6	1607	1641*	1622*	1644	1646*	1633*	--	1620	1612	--	1386	1442
	7	(1810)	1798*	1797*	(1850)	1798*	1792*	--	1791	1774	--	1589	1663
RMS		--	64	53	--	23	18	--	18	3.5	--	29	26
		--	(62)	(51)	--	(26)	(22)	--	--	--	--	(27)	(25)

TABLE H.2

BAND	J	^{156}Er			^{158}Er			^{160}Er			^{170}Er			^{174}Yb		
		EXP.	EPM		EXP.	EPM		EXP.	EPM		EXP.	EPM		EXP.	EPM	
			4	5		4	5		4	5		4	5		4	5
g	2	344	361*	341*	192	202*	189*	126	131*	125*	79	81*	79*	76	77*	76*
	4	797	772*	828*	527	523*	546*	390	394*	393*	260	260*	260*	253	254*	253*
	6	1340	1199*	1344*	970	893*	980*	767	739*	768*	541	518*	538*	526	524*	527*
	8	1959	1634*	1855*	1493	1289*	1448*	1228	1140*	1221*	913	833	899	889	877*	894*
	10	2633	2076	2367	2073	1707	1945	1760	1587	1739	1374	1192	1329	1336	1299	1349
	12	3315	2526	2886	2681	2144	2471	2339	2072	2315	--	1585	1813	--	1779	1882
	14	3837	2982	3417	3190	2597	3025	2931	2590	2945	--	2010	2343	--	2304	2483
β	0	930	948*	953*	806	818*	816*	894	892*	888*	891	891*	894*	1487	1494*	1495*
	2	1221	1249*	1170*	989	1007*	960*	1008	1042*	1015*	960	965*	957*	1561	1556*	1556*
	4	1546	1686*	1593*	1257	1368*	1298*	--	1378	1320	(1123)	1145	1106	1715	1700*	1700*
	6	--	2212	2204	--	1860	1832	--	1879	1811	--	1433	1335	1909	1926*	1927*
	8	--	2779	2920	--	2429	2511	--	2505	2477	--	1821	1656	--	2233	2238
	10	--	3365	3688	--	3043	3283	--	3217	3287	--	2298	2064	--	2617	2636
γ	2	930	943*	952*	820	853*	852*	855	861*	861*	932	934*	938*	1634	1643*	1644*
	3	1243	1235*	1180*	1043	1026*	1000*	987	991*	979*	1010	1008*	1007*	1709	1711*	1712*
	4	1351	1397*	1375*	1184	1175*	1163*	--	1144	1131	1101	1101*	1098*	1805	1803*	1802*
	5	1663	1711*	1674*	--	1417	1396	--	1348	1325	--	1228	1212	1926	1914*	1914*
	6	--	1845	1856	--	1565	1581	--	1537	1532	--	1347	1356	--	2051	2049
	7	--	2211	2240	--	1875	1901	--	1811	1801	--	1530	1507	--	2202	2204
RMS		--	345	180	--	254	86	--	144	11	--	63	15	--	13	9.2
		--	--	--	--	--	--	--	--	--	--	(61)	(15)	--	--	--

TABLE H.3

BAND	J	^{164}Yb			^{166}Yb			^{168}Yb			^{170}Yb		
		EXP.	EPM		EXP.	EPM		EXP.	EPM		EXP.	EPM	
			4	5		4	5		4	5		4	5
g	2	124	126*	123*	102	104*	102*	88	89*	88*	84	87*	84*
	4	386	386*	389*	330	331*	331*	286	287*	287*	277	281*	278*
	6	760	733*	758*	668	649*	666*	585	575*	584*	573	565*	574*
	8	1222	1137	1200	1098	1033	1084	970	932	963	963	922*	961*
	10	1752	1584	1700	1606	1466	1567	1424	1338	1404	1437	1336	1426
β	0	976	967*	966*	(1043)	1046*	1043*	(1156)	1154	1158	1069	1077*	1069*
	2	1074	1094*	1086*	--	1147	1139	(1233)	1228*	1228*	(1146)	1169	1139
	4	(1323)	1382	1370	--	1382	1365	1391	1401*	1393*	--	1390	1302
	6	--	1824	1824	--	1751	1730	--	1671	1655	--	1738	1560
	8	--	2397	2441	--	2249	2239	--	2041	2019	--	2208	1914
	10	--	3067	3193	--	2857	2888	--	2512	2492	--	2788	2363
γ	2	864	876*	876*	932	937*	940*	984	987*	988*	1139	1140*	1144*
	3	1004	994*	991*	1039	1035*	1034*	(1067)	1065*	1065*	1225	1227*	1219*
	4	1145	1142*	1140*	1163	1163*	1160*	(1171)	1170*	1167*	(1328)	1332	1320
	5	(1365)	1326	1324	1328	1319*	1315*	(1302)	1296	1291	--	1480	1443
	6	--	1519	1530	1482	1496*	1498*	(1445)	1449	1443	--	1621	1597
	7	--	1764	1781	1725	1706	1710	--	1616	1611	--	1834	1763
RMS		--	61	19	--	47	15	--	36	8.2	--	39	4.8
		--	(59)	(25)	--	(45)	(14)	--	(26)	(7.0)	--	(35)	(5.5)

TABLE H.4

I. Special References for the Experimental Energy and Electromagnetic Data

NDS≡Nuclear Data Sheets

^{142}Sm: J.K.Tuli, NDS 25 (1978)53
G.L.Struble et al. ,Phys.Rev.C23 (1981)2447

^{144}Sm: J.K.Tuli, NDS 27 (1979)97

^{146}Sm: T.W.Burrows, NDS 14 (1975)413
W.Oerlet et al., Phys.Rev.C12 (1975)417

^{148}Sm: B.Harmatz and J.R.Shepard, NDS 20 (1977)373

^{150}Sm: C.M.Baglin, NDS 18 (1976)223
D.R.Zolnowski et al., Phys.Rev.C21 (1980)2556

^{152}Sm: C.M.Baglin, NDS 30 (1980)1

^{154}Sm: B.Hermatz, NDS 26 (1979)281

^{156}Sm: T.W.Burrows ,NDS 18 (1976)553

^{150}Gd: C.M.Baglin, NDS 18 (1976)223
D.R.Haeni and T.T.Sugihara, Phys.Rev.C16(1977)120

^{152}Gd: C.M.Baglin, NDS 30 (1980)1

^{154}Gd: B.Hermatz, NDS 26 (1979)281

^{156}Gd: T.W.Burrows, NDS 18(1976)553
Jan Konijn et al., Nucl. Phys.A352 (1981) 191

^{158}Gd: M.A.Lee, NDS 31 (1980)381

^{160}Gd: J.K.Tuli, NDS 12 (1974)477

S.A.Elbakr et al., Phys. Rev.C10 (1974)1864

^{156}Er: See the references in section IV.3.C

^{158}Er: M.A.Lee, NDS 31 (1980)381

^{160}Er: See the references in section IV.3.C

^{162}Er: A.Buyrn, NDS 17 (1976)97

^{164}Er: F.W.N.DeBoer, Nucl.Phys.A169 (1971)577

^{166}Er: A.Buyrn, NDS 14 (1975)471

^{168}Er: L.R.Greenwood, NDS 11 (1974)385

^{170}Er: M.R.Schmorak and R.L.Auble, NDS 15 (1975)371

^{164}Yb: A.Buyrn, NDS 11(1974)327

^{166}Yb: A.Buyrn, NDS 14(1975)471

^{168}Yb: L.R.Greenwood, NDS 11 (1974)385

^{170}Yb: M.R.Schmorak and R.L.Auble,NDS 15(1975)371

^{172}Yb: L.R.Greenwood, NDS 15 (1975)497

^{174}Yb: M.M.Minor, NDS 10 (1973)515

REFERENCES

/Ab65/ M.Abramowitz and I.Stegun, Handbook of Mathematical Functions (Dover,New York 1965)

/Al55/ G.Alaga,K.Alder,A.Bohr and B.R.Mottelson, Mat.Fys. Medd.Dan.Vid.Selsk.29(1955)no.9

/Ar70/ G.Arfken,Mathematical Methods for Physicists (Academic Press 1970)

/Ar81/ A.Arima and F.Iachello, Ann. Rev. Nucl. Part.Sci.31 (1981)75

/Ar82/ A.Arima,J.Ginocchio and N.Yoshida, Nucl. Phys.A384 (1982)112

/Ay74/ F.Ayres,Matrices,Schaum´s Outline Series (McGraw-Hill 1984)

/Ba77/ N.S.Bakhvalov,Numerical Methods (Mir Publishers,Moscow 1977)

/Be78/ R.Bengtsson, I.Hamamoto and B.R.Mottelsson, Phys.Lett.73B (1978)259

/Be79/ R.Bengtsson and S.Frauendorf, Nucl.Phys.A327 (1979)139
R.Bengtsson and S.Frauendorf, Nucl.Phys.A314(1979)27

/Bl79/ J.Blatt and V. Weisskopf, Theoretical Nuclear Physics (Springer-Verlag 1979)

/Bo52/ A.Bohr, Mat.Fys.Medd.Dan.Vid.Selsk.26(1952)

/Bo75/ A.Bohr, B.Mottelsson, Nuclear Structure, volume 2 (Benjamin 1975)

/Bo82/ A.Bohr and B. Mottelson, Phys.Scripta22(1982)28

/Br68/ D.M.Brink and G.R.Satchler,Angular Momentum (2nd ed.Oxford U.P., London 1968)

/By81/ T.Byrski et. al. ,Phys. Lett.102B(1981)235

/Ca73/ R.F.Casten et.al , Phys. Rev.C8(1973)1035

/Ca79/ O.Castanos, A.Frank and P.Federman,Phys.Lett.88(1979)203

/Ca80a/ R.F.Casten, in Proc. of the International Conference on Band Structure and Nuclear Dynamics, New Orleans, Louisiana 1980

/Ca80b/ R.F.Casten, in Contemporary Research Topics in Nuclear Physics, ed. by D.H.Feng, M.Vallieres, M.V.Gui dry and L.L.Riedinger(Plenum Press 1980)369

/Ca81/ R.F.Casten, D.D. Warner, D.S.Brenner and R.L.Gill, Phys.Rev.Lett.47(1981)1433

/Ca82a/ R.F.Casten and D.D.Warner, Phys. Rev.Lett.48(1982)666

/Ca82b/ O.Castanos, P.Federman, A.Frank and S.Pittel, Nucl.Phys. A379(1982)61

/Ca83b/ R.F.Casten, D.D. Warner and A.Aprahamian, Phys.Rev. C28(1983)894

/Ca83b/ R.F.Casten and D.D. Warner, in Progress in Particle and Nuclear Physics, volume 9,ed. by D.Wilkinson (Pergamon Press 1983)311

/Co71a/ J.O.Corbett, Nucl.Phys.A169(1971)426

/Co71b/ B.L.Cohen, Consepts of Nuclear Physics (McGraw-Hill 1971)

/Da58/ A.S.Davydov and G.F.Fillipov, Nucl. Phys 8(1958)237

/Da60/ A.S.Davydov and A.A.Chaban, Nucl.Phys 20(1960)499

/Da68/ J.P.Davidson,Collective Models of the Nucleus(Academic Press 1968)

/Da70/ T.K.Das, R.M.Dreizler and A.Klein, Phys.Rev.Lett.25 (1970)1625

/Da72/ T.K.Das,R.M.Dreitzler and A.Klein,Phys.Rev.C2(1972)632

/Di82/ A.Dieperink and R.Bijker, Phys.Lett.116B(1982)77

/Di84/ A.Dieperink, in Nuclear Collective States,Conference held in Suzhou,China(1983)

/Ei75/ J.M.Eisenberg and W.Greiner, Nuclear Theory 1.Nuclear Models(North-Holland 1975)

/Ei76/ J.M.Eisenberg and W.Greiner, Nuclear Theory 3.Microscopic Theory of the Nucleus (North-Holland 1976)

/Fa74/ A.Faessler, F.Grummen,L.Lin and J.Urbano,Phys.Lett. 48(1974)87

/FI72/ R.Fletcher,Fortran Subroutines for Minimization by Quasi-Newton Methods, Report R7125 AERE, Herwell, England, June 1972

/Fr71/ S.Frauendorf et al.,Phys.Lett.34B(1971)469

/Ga74/ S.Gasiorowicz,Quantum Physics (Wiley, New York 1974)

/Gh78/ A.Gheorghe, A.A.Raduta and Ceausescu, Nucl.Phys. A296(1978)228

/Gi82/ R.L.Gill et al., Phys. Lett.118B(1982)251

/Gi83/ C.Girit, W.D.Hamilton and C.A.Kalfas,J.Phys.G.Nucl. Phys.9(1983)797

/Gn69/ G.Gneuss, U.Mosel and W.Greiner, Phys. Lett.30B (1969)397

/Gn70a/ G.Gneuss,U.Mosel and W.Greiner,Phys.Lett.31B (1979)269

/Gn70B/ G.Gneuss, W.Greiner and U.Mosel, Phys. Lett.32B(1970)161

/Gn71/ G.Gneuss and W. Greiner ,Nucl.Phys.A171(1971)449

/Go81a/ A.L.Goodman,Phys. Lett.103B(1981)163

/Go81b/ A.L.Goodman, Nucl.Phys.A369(1981)365

/Gr57/ J.J.Griffin and J.A.Wheeler,Phys.Rev.108(1957)311

/Ha70/ P.Haapakoski,Lic.Thesis,University of Helsinki 1970 (unpublished)

P.Haapakoski, T.Honkaranta and P.O.Lipas, Phys.Lett. 31B(1970)493

/Ha73/ P.Haapakoski,P.Holmberg and P.O.Lipas, Phys. Fennica 8(1973)33

/Ha73b/ A.J.Hartley et al., J. of Phys.A6(1973)L60

/Ha78/ E.Hammaren PhD thesis ,University of Jyväskylä 1978 (Department of Physics Research Report 3/1978)

/Ha79/ E.Hammaren et al., Nucl.Phys.A321(1979)71

/He77/ P.O.Hess and W.Greiner, in Nuclear Structure Physics ,ed. S.Hall and J.Irvine (Published by the Scottish Universities Summer School in Physics 1977)339

/He80/ P.O.Hess, M.Seiwert, J.Maruhn and W.Greiner, Z.Phys. A(1980)147

/Hi57/ D.L.Hill and J.A.Wheeler, Phys.Rev.108(1957)311

/Ho70/ G.Holzwarth, Nucl.Phys. 156(1970)511

/Ho72/ T.Honkaranta, Master´s Thesis, University of Helsinki 1972 (unpublished)

/Hu77/ R.C.Hunter et al.,Phys. Rev C16(1977)384

/Ia79/ Interacting Bosons in Nuclear Physics, ed. F.Iachello (Plenum, New York 1979)

/Ia81/ Interacting Bose-Fermi systems in Nuclei, ed. F.Iachello (Plenum,New York 1981) F.Iachello, An Introduction to the Interacting Boson Model, in Nuclear Structure, ed. K.Abrahams et al. (Plenum ,New York 1981), and references therein

/Ik73/ A.Ikeda,R.K.Sheline and N.Onishi, Phys.Lett.44B(1973)397

/IM80/ The ISML Library (International Mathematical &Statistical Libraries, Inc.1980) adapted to UNIVAC 1100 at the Computer Centre of Jyväskylä University

/Is80/ P.van Isacker and G.Puddu, Nucl.Phys.A348(1980)125

/Is82/ P.van Isacker, K.Heyde, M.Waroquier and G.Wenes, Nucl.Phys. A380(1982)383

/Ja75/ F.James, M.Roos;MINUIT, a CERN Packet for Optimization, Computer Physics Communications 19(1975)343

/Ja77/ R.Janssens et al., Nucl. Phys. A283(1977)493

/Jo78/ N.R Johnson et al. ,Phys.Rev.Lett. 40(1978)151

/Kr84a/ T.I.Kracíková et al., J.Phys. G.:Nucl. Phys. 10(1984)571

/Kr84b/ T.I.Kracíková et al., J.Phys.G:Nucl.Phys.10(1984)667

/Kr84c/ T.I.Kracíková et al. J.Phys. G:Nucl.Phys.(1984) to be published

/Ku67a/ K.Kumar and M.Baranger, Nucl. Phys. A92(1967)608

/Ku67b/ K.Kumar, Nucl. Phys.A92(1967)653

/Ku68/ K.Kumar and M.Baranger, Nucl.Phys.A122 (1968)273

/Ku73/ J.L.Kuester and J.H.Mize, Optimization Techniques with Fortran (McGraw-Hill 1973)

/Ku78/ K.Kumar, Nucl.Phys.A231(1974)189

/La78/ J.Larysz et al.,Nucl.Phys.A309(1978)128

/Li66/ P.O.Lipas, Nucl.Phys.82(1966)91

/Li69/ P.O.Lipas and J.Savolainen ,Nucl.Phys.A130 (1969)7

/Li72/ P.O.Lipas, in Arkhimedes n:o 1-2 (1972)11

/Li72/ S.G.Lie and G.Holzwarth,Phys.Rev.C12(1975)1035

/Li76/ P.O.Lipas, P.haapakoski and T.Honkaranta, Physica Scripta 13(1976)339

/Li82/ P.O.Lipas et al.,Research report 4/1982, University of Jyväskylä

/Li83a/ P.O.Lipas, private communication

/Li83b/ P.O.Lipas, Proceedings of the Nordic Winter School in Hemsedal, Norway 1983 (to be published)

/Li83c/ P.O.Lipas et al.,Phys.Scripta 27(1983)8

/Li83d/ P.O.Lipas, in Progress in Particle and Nuclear Physics volume 9,ed. by D.Wilkinson (Pergamon Press 1983) 511

/Li84a/ P.O.Lipas ,E.Hammaren and P.Toivonen, Phys.Lett. 139B(1984)10

/Li84b/ P.O.Lipas et al. to be published, P.O.Lipas, private communication

/Li84c/ P.O.Lipas, fits performed with effective boson numbers, private communication

/Li84d/ P.O.Lipas et al. ,IBA-1 perturbation theory calculations, to be published

/Li84e/ P.O.Lipas ,in the Internatinal Workshop on Interacting Boson-boson and Boson Fermion Systems, Gull Lake, USA(1984

P.O.Lipas ,in the 5th Nordic Meeting on Nuclear Physics Jyväskylä, Finland (1984)

/Me70/ E.Merzbacher, Quantum Mechanics (Wiley, New York 1961,1970

/Mo60/ B.R.Mottelson and J.G.Valatin ,Phys. Rev.Lett.5(1960)511

/Mo73/ C.B.Moler and G.W.Stewart, SIAM J. Numer.Anal.10(1973)241

/Mo81/ M.Moshinsky, Nucl. Phys.A354(1981)257C

/Na65/ O.Nathan and S.G.Nilsson, in Alpha-,Beta- and Gamma-ray Spectroscopy, ed. by K.Siegbahn (North-Holland 1965)

/Ni55/ S.G.Nilsson, Mat.Fys. Medd. Dan. Vid Selsk.29(1955)n:o 16

/No68/ C.C.Noack, Nucl. Phys. A108(1968)493

/Og78/ M.Ogawa, R.Broda, K.Zell, P.J.Daly and P.Kleinheinz, Phys. Rev.Lett. 41(1978)289

/Ol77/ C.Olmer et al.Phys.Rev.Lett.38(1977)476, and references therein

/On66/ N.Onishi and S.Yoshida, Nucl. Phys.80(1966)367

/Pe57/ R.E.Peierls and J.Yoccoz, Proc. of the Physical Society A70(1957)381

/Pe62/ R.E.Peierls and D.J.Thouless, Nucl.Phys.38(1962)154

/Pr75/ M.Preston and R.Bhaduri, Structure of the Nucleus (Addison-Wesley 1975)

/Ra76a/ A.A.Răduţă, Phys.Lett.63B(1976)14

/Ra76b/ A.A.Răduţă and M.Badea, Z.Physik A278(1976)51

/Ra76c/ A.A.Răduţă and R.M.Dreizler,Nucl.Phys.258(1976)109

/Ra76d/ A.A.Răduţă, V.Ceauşescu and R.M.Dreizler, Nucl.Phys. A272(1976)11

/Ra77/ A.A.Răduţă, A.Gheorghe and M.Badea, Z.Phys.A283(1977)79

/Ra78a/ A.A.Răduţă and C.Şabac, J.Phys. G:Nucl.Phys.4(1978)1563

/Ra78b/ A.A.Răduţă, V.Ceauşescu and A.Gheorghe,Nucl.Phys.A311 (1978)118

/Ra81/ A.A.Răduţă,V.Ceauşescu,A.Gheorghe and R.M.Dreizler, Phys. Lett.99B(1981)444

/Ra82/ A.A.Răduţă et al.,Nucl.Phys.A381(1982)253

/Ra83a/ A.A.Răduţă and C.Şabac, Ann. of Phys.148(1983)1

/Ra83b/ A.A.Răduţă et al. ,Z.Phys.A312(1983)233

/Ra83c/ A.A.Răduţă, Rev.Roum.Phys.28(1983)195

/Ra84/ A.A.Răduţă, S.Stoica and N.Săndulescu, Rev.Roum.Phys.29 (1984)55

/Ri80/ P.Ring and P.Schuck, The Nuclear Many-Body Problem (Springer Verlag 1980)

/Ro57/ M.E.Rose, Elementary Theory of Angular Momentum (John Wiley & Sons 1957)

/Ro59/ M.Rotenberg, R.Bivins, N.Metropolis, J.K.Wooten Jr.The 3-j and 6-j Symbols (The Technology Press Massachusetts 1959)

/Ro70/ D.J.Rowe, Nuclear Collective Motion ,Models and Theory (Methuen,London 1970)

/Ro78/ C.Roulet et al. Phys. Scripta 17(1978)487

/Ry73/ H.Ryde et al., Nucl.Phys. A207 (1973)513

/Sa67/ M.Sakai, Nucl.Phys. A104(1967)301

/Sa77/ K.Salonen. Master´s Thesis, University of Jyväskylä 1977 (unpublished)

/Sa79/ A.Saha, O.Scholten, D.Hageman and H.T.Fortune, Phys.Lett.85B(1979)215

/Sa81/ M.Sambataro and A. Dieperink, Phys. Lett. 107B(1981)249

/Sa82/ M.Sakai, Quasi-Bands, INS Report (Institute for Nuclear Study, University of Tokyo 1982)

/Sa84/ M Sambataro, O.Scholten, A.Dieperink and G.Piccitto, KVI preprint, n:o KVI-461 (1984)

/Sc68/ F.Scheid, Numerical Analysis, Schaum´s Outline Series (McGraw-Hill 1968)

/Sc78/ O.Scolten , F.Iachello and A.Arima, Ann.Phys.(N.Y) 115(1978)366

/Sc79a/ O.Scholten, in Interacting Bosons in Nuclear Physics, ed. by F.Iachello (Plenum Press 1979)17 and O.Scholten Thesis 1980

/Sc79b/ O.Scholten, The Program-package PHINT, KVI report n:o 63 (1979)

/Sc83/ O.Scholten, Phys.Lett.127B(1983)144

/Sh60/ R.K.Sheline, Rev.Mod. Phys.32(1960)1,301

/Sh63/ A.de-Shalit and I Talmi, Nuclear Shell Theory (Academic Press 1963)

/Sh74/ A.de-Shalit and H.Feshbach, Theoretical Nuclear Physics (John Wiley & Sons 1974)

/Sp68/ M.R.Spiegel, Mathematical Handbook, Schaum´s Outline Series (Mc.Graw-Hill1968)

/St72/ F.Stephens and R.Simon, Nucl.Phys.A183 (1972)257

/St75/ F.Stephens ,Rev.Mod.Phys.47(1975)43

/St81/ G.L.Struble et al., Phys.Rev.C23(1981)2447

/St83/ F.Stephens, In Progress in Particle and Nuclear Physics volume 9,ed. by D.Wilkinson (Pergamon Press 1983) pages 373 and 374

/Su77/ Z.Sujkowski et al. ,Nucl.Phys.,A291(1977)365

/Su79/ Z.Sujkowski, in Interacting Bosons in Nuclear Physics ed. by F.Iachello (Plenum Press 1979)55

/Su82/ J.Suhonen and P.O.Lipas ,JYFL Annual Report 1982 University of Jyväskylä 1982

/Su83a/ J.Suhonen and P.O.Lipas, in Proc. XVII Ann.Conf. Finnish Physical Society (1983)

/Su83b/ J.Suhonen, JYFL Annual Report 1983, University of of Jyväskylä 1983

/Su84/ J.Suhonen ,In Proc. XVIII Ann.Conf. Finnish Physical Society (1984)

/Th73/ P.Thieburger, Phys.Lett.45B (1973) 417

/Ti64/ M.Tinkham, Group Theory and Quantum Mechanics (McGraw-Hill 1964)

/To83/ P.Toivonen, Master's Thesis, University of Jyväskylä 1983 (unpublished)

/Wa76/ D.Ward et al., Nucl.Phys.A266(1976)194

/Wa80a/ D.D.Warner, R.F.Casten and W.F.Davidson,Phys.Rev.Lett45 (1980)176

/Wa80b/ P.M.Walker et al.,Nucl.Phys.A343(1980)45

/Wa81a/ D.D.Warner ,R.F.Casten and W.F.Davidson, Phys.Rev. C24 (1981)1713

/Wa81b/ P.M.Walker et al.,Nucl.Phys.A365(1981)61

/Wa82a/ D.D.Warner and R.F.Casten ,Phys.Rev.C25(1982)2019

/Wa82b/ D.D.Warner and R.F.Casten, Phys. Rev.Lett.48(1982)1385

/Wa83/ D.D.Warner and R.F.Casten, Phys.Rev.C28(1983)1798

/Ve83/ A.Vesterinen, Numerical tests of EPM,University of Jyväskylä 1983 (unpublished)

/We78/ M.Weissbluth, Atoms and Molecules (Academic Press 1978)

/Wi56/ L.Wilets and M.Jean ,Phys.Rev.102(1956)788

/Wi83/ Progress in Part. and Nucl.Phys.9,ed.D.Wilkinson (Pergamon 1983)

/Wo70/ G.F.Wolters, Nucl.Phys.B18(1970)625

/Wo83/ A.Wolf et al., Phys.Lett. 123B (1983)165

/Ya80/ S.W.Yates et al., Phys. Rev.C21(1980)2366

/Zo80/ D.R.Zolnowski et al.,Phys.Rew.C21(1980)2556